Title

Real World Characteristics of the Non-Tailpipe Brake Source During Near Road Environments and Onboard Sensing Activity

Author

Lopez Reyna, Brenda

Publication Date

2024

UNIVERSITY OF CALIFORNIA
RIVERSIDE

Characteristics of the Non-Tailpipe Emissions in the Near Road Environment and Real World Brake Activity

A Dissertation submitted in partial satisfaction
of the requirements for the degree of

Doctor of Philosophy

in

Mechanical Engineering

by

Brenda E. Lopez Reyna

June 2024

Dissertation Committee:
  Dr. Heejung Jung, Chairperson
  Dr. Bhargav Rallabandi
  Dr. Lorenzo Mangolini
  Dr. Don Collins

The Dissertation of Brenda E. Lopez Reyna is approved:

____

____

____

____

Committee Chairperson

University of California, Riverside

Acknowledgements

My research progress and academic achievement have been made possible thanks to the exceptional guidance and unwavering support from educators, industry professionals, friends, and family. I am deeply grateful and wish to express my heartfelt thanks to those who have been pivotal to my success.

First and foremost, I would like to express my deepest appreciation to my advisor, Dr. Heejung Jung, for always prioritizing my success and growth in the doctoral program. Your mentorship, guidance, and knowledge in research have immensely impacted my journey. I am forever grateful for the opportunity and honored to have your support.

I'm extremely grateful to Dr. Bhargav Rallabandi, Dr. Lorenzo Mangolini, and Dr. Don Collins for your valuable feedback and contribution to my advancement to candidacy and final defense committee.

I would like to extend my sincere gratitude to Dr. Xiaoliang Wang at the Desert Research Institute, Dr. Lung-Wen Anthony Chen at the University of Nevada Las Vegas, and Dr. Kent Johnson at the Center for Environmental Research and Technology, for your invaluable contribution and assistance in my research projects and papers. Your expertise and guidance have been essential to my education and the completion of my dissertation.

Many thanks to Dr. Seungjun Yoon, Dr. Sonya Collier, and Dr. Qi Yao at the California Air Resources Board for their excellence in managing every stage of the research progress and report.

I am also thankful to my research collaborators and publication co-authors. Dr. Manabu Shiraiwa, Dr. Brian Hwang, and Dr. Ting Fang at UC Irvine for their in-kind contribution of MOUDI samples. Dr. Kihong Park and Dr. Minhan Park at the Gwangju Institute of Science and Technology, Korea for their in-kind chemical analysis of MOUDI samples.

Special thanks to Mr. Yusuke Mizuno and Mr. Mitsuhiko Maeda from Horiba for your formal training and assistance in operating PX-375 instruments. I am also thankful to Mr. Tyler Beck from Particle Instruments, and the staff at Dekati for providing instruments and technical advice.

Many thanks to site owners of private companies and South Coast Air Quality Management District staff for providing access to measurement sites in my research campaign. I'd like to recognize the help from Dr. Chengguo Li, Mr. Jesse Stuart, Mr. Joshua Dailey, and Ms. Ling Cobb, for taking the time to transport and set up equipment to measurement sites.

I am also thankful to CE-CERT research staff Mr. Mark Villela, facilities manager Mr. Henry Gomez, and technical staff Mr. Daniel Hartnett for their involvement, support, and knowledge in field-testing projects.

I had the pleasure of working alongside former and current graduate students, Dr. Chas Frederickson, Dr. Tianyi Ma, Dr. Tiambo Tang, Mr. David Mendez-Jimenez, Mr. Evan Renck, and Mr. Lucas Brown. I am appreciative of the valuable opportunity to learn from your achievements and for the meaningful friendship you have extended to me.

This endeavor would not have been possible without support from funding agencies, fellowship awards, and scholarships: California Air Resources Board, National Center for Sustainable Transportation, Graduate Assistance in Areas of National Need fellowship, UC President's Pre-Professoriate Fellowship, and Hackett Graduate Research Award.

Dedication

This dissertation is dedicated to my life partner, Joshua Dailey, for being a constant source of support and encouragement throughout this entire journey. Words cannot express my gratitude for your unwavering patience, compassion, motivation, and most importantly, your love. Thank you for being my source of strength and for always celebrating my accomplishments with true bliss.

I also dedicate my work to those who have given me unconditional love and support. To my parents, Minerva Reyna de Lopez and Rene Lopez, who have endured many sacrifices that have allowed me to reach this achievement. To my sister and new family, Diana Lopez, Elena Dorben Lopez, and Brent Dorben for your genuine support and love. Lastly, I want to honor my grandparents, Celia Reyna, and the loving memory of my grandfather, Sinforiano Reyna, who could not see this journey through but always remained proud of me every single day.

ABSTRACT OF THE DISSERTATION

Real World Non-Tailpipe Emissions at Near-Road Environments and Brake Activity

by

Brenda E. Lopez Reyna

Doctor of Philosophy, Graduate Program in Mechanical Engineering
University of California, Riverside, June 2024
Dr. Heejung Jung, Chairperson

Brake and tire wear particulate matter (PM) represent a large fraction of road traffic pollution from vehicles. Road traffic pollution is often associated with tailpipe sources from diesel and gasoline-powered vehicles. Although this contribution has drastically decreased over the years due to the implementation of stringent regulations and technological advancements, it is not the sole source of traffic pollution. The non-tailpipe sources, brake and tire wear, generate particle emissions through abrasive wear during vehicle driving activity. These emissions are not actively regulated and are a concern to near-road communities as their contribution to traffic-related emissions has surpassed their tailpipe counterpart.

This dissertation investigates the real-world characteristics of the non-tailpipe brake source during near-road environments and onboard sensing activity. Non-tailpipe sources contribute to airborne particulate matter concentrations and are reported to contain traces of heavy metals. Emitted particles that settle onto road surfaces can be mixed and resuspended with road dust. Long-term exposure to particulate air pollution is known to cause adverse health effects due to their size and chemical composition toxicity. This dissertation provides results of metal contents and size distributions of brake and tire wear particles found in ambient PM2.5 and PM10 at near-road environments for two major highways in California. Prior research efforts have focused on measurement from laboratory tests to examine non-tailpipe source emissions. Findings show that brake wear PM is dynamic and dependent on brake activity such as braking intensity, temperature, brake lining materials, vehicle weight, and vehicle vocation. Therefore, it is important to characterize brake emissions by first understanding the real-world brake activity. This dissertation investigates strategies to establish a test method and analysis for brake activity measurements of heavy-duty vehicles. The brake fluid pressure and brake pad temperature were measured for a heavy-duty vehicle using chassis dynamometer test cycles and on-road driving tests.

Table of Contents

List of Figures

List of Tables

1 Chapter 1: Introduction

Road traffic pollution is often associated with tailpipe sources from diesel and gasoline powered vehicles. Although this contribution has drastically decreased over the years due to the implementation of stringent regulations and technological advancements, it is not the sole source of traffic pollution (Wallington et al. 2022). Non-tailpipe sources constitute particulate matter (PM) emissions in near-road environments and originate from brake wear, tire wear, and road dust resuspension (Harrison 2020; Pant and Harrison 2013; Thorpe and Harrison 2008; Grigoratos and Martini 2015). These airborne particles vary in chemical composition and sizes that predominately range in aerodynamic diameters smaller than 10 µm (PM10), 2.5 µm (PM2.5), and 0.1 µm (PM0.1). Non-tailpipe PM emissions are not actively regulated and are reported to have surpassed their tailpipe counterpart with reference to total PM2.5 vehicle emissions (Chen et al. 2023; Particle Measurement Programme 2021). The EMission FACtor (EMFAC) model from California Air Resources Board (CARB) predicts these non-tailpipe emissions to remain dominant contributors of on-road PM (CARB. 2021). Even with transitions towards newer technology that achieve zero tailpipe emissions, battery electric vehicles will still produce non-tailpipe emissions and are predicted to increase with weight due to their heavier components compared to internal combustion engine vehicles (Timmers and Achten 2018). Additionally, it is widely reported that PM2.5 and PM10 cause adverse health effects to exposed populations (Tong et al. 2020). Therefore, the investigation into non-exhaust sources is necessary to quantify their real-world contribution to ambient PM at near-road environments, to evaluate the elemental contents that distinguish tracer markers between each source, and to establish an accurate test method during in situ vehicle operation that is comparable to laboratory brake activity measurements.

This thesis explores and assesses the real-world characteristics of the non-tailpipe brake source during near-road environments and onboard sensing activity. The dissertation investigates metal contents and size distributions found in PM2.5 and PM10 measurements next to two major highways in California, USA. It also investigates strategies to establish a test method and analysis for brake activity measurements of heavy-duty vehicles.

Chapter 1 introduces a review of the non-tailpipe sources, brake and tire wear. Topics include a background understanding of brake wear particulate matter, review of prior laboratory and on road measurement methods, review of brake friction materials, review of brake and tire wear characteristics, review of tire war composition, and review of road wear composition.

Chapter 2 provides an investigation of metal contents and size distributions of brake and tire wear particles at the I-5 highway in Anaheim, CA and I-710 highway in Long Beach, CA. Results include elemental abundances, elemental correlations, real-time elemental concentrations, particle size distributions, and element mass size distributions from samples taken at both nominal upwind and downwind sites.

Chapter 3 is a continuation of the research in Chapter 1 and provides further results of PM2.5 and PM10 concentrations at the near road highways, analysis of meteorological data observing wind speed and direction, and comparison between laboratory versus real world XRF analysis.

Chapter 4 further continues results from source apportionment of non-tailpipe contributions to near-road PM2.5 and PM10 using an effective variance chemical mass balance model (EV-CMB). Methods include source profile categories considered for the EV-CMB model include geological (road dust), mobile (brake wear, tire wear, diesel exhaust, gasoline exhaust), and secondary (secondary sulfate, secondary nitrate). Results showed the source contribution of these source profiles.

Chapter 5 introduces a method for measuring real time brake temperature and pressure on board a heavy-duty vehicle. Methods include the use of laboratory experiments using chassis dynamometer test cycles and on-road experiments along two different California routes. Results include temperature and pressure profiles, along with estimated kinetic energy loss during braking activities.

Lastly, chapter 6 summarizes all conclusions found within each chapter of this dissertation.

1.1 Background of brake wear particulate matter emissions

On-road vehicles in urban environments are an important contributor to atmospheric aerosols because they directly emit both primary aerosols and secondary organic aerosol (SOA) precursors (Zhao et al. 2022). Particulate matter can be directly emitted as primary aerosols or formed in the atmosphere from gas-to-particle conversion processes (Piscitello et al. 2021; Hinds and Zhu 2022). The source of PM is associated with both anthropogenic sources (fuel combustion, industrial activity, agricultural activity, road dust, abrasion of brakes and tires) and natural sources (forest fires, volcanoes, vegetation, sea spray) (Srimuruganandam and Shiva Nagendra 2012; Hinds and Zhu 2022). The US

Environmental Protection Agency (EPA) considers PM one of the six criteria pollutants (ozone, particulate matter, nitrogen oxides, sulfur oxides, carbon monoxide, and lead) that are enforced through air quality standards to protect the public from adverse health effects (US EPA 2017). Particulate matter is classified based on its aerodynamic particle diameters. Coarse particles, or PM10, have aerodynamic diameters up to 10 µm, while fine particles, or PM2.5, have aerodynamic diameters up to 2.5 µm. Another category are ultrafine particles, or PM0.1, with aerodynamic diameters below 0.1µm (Thorpe and Harrison 2008). Health effects studies have identified a correlation between exposure to ambient PM and increase risk of developing a chronic respiratory or cardiovascular disease, premature mortality, and hospitalization (Ostro et al. 2015; Cohen et al. 2017; Tong et al. 2020; Yu et al. 2019; Suh et al. 2000). Exposure to the different sizes of PM fractions can also have adverse effects on human health (Breysse et al. 2013; Thompson 2018; Kim, Kabir, and Kabir 2015). For example, coarse particles can be inhaled through the nose or mouth and can lodge in the nasal passages, upper throat, and the upper lungs (Atkinson et al. 2010). Fine particles affect the thoracic function by penetrating the lungs and escape into the blood stream (Kim, Kabir, and Kabir 2015; Xing et al. 2016). Ultrafine particles have the potential to impact health by entering the microscopic air sacs in the lungs called alveoli, where oxygen and carbon dioxide exchange occurs during breathing (Kim, Kabir, and Kabir 2015). These particles can also move into the cell tissue or circulatory system (Valavanidis, Fiotakis, and Vlachogianni 2008; Schraufnagel 2020).

The particulate matter emitted from vehicles can be classified into two groups, tailpipe and non-tailpipe. The tailpipe contribution results from fuel oxidation and lubricant volatilization during combustion processes, whereas the non-tailpipe contribution is from brake, tire, road surface wear, and road dust resuspension (Pant and Harrison 2013; Abu-Allaban et al. 2003; Thorpe and Harrison 2008).

Generally, there are two types of brake systems, disc brakes and drum brakes. Brake systems in passenger vehicles incorporate two brake pads that are forced together on opposite sides of a rotating rotor, or disc, during deceleration events. The interaction between the brake pad and rotor system generates brake wear PM through mechanical abrasion of both surfaces and creates heat as a byproduct. The size and wear rate are dependent on a number of factors including braking pressure, vehicle speed, vehicle weight, and frequency of braking to name a few (Thorpe and Harrison 2008; Wahid 2018; Grigoratos and Martini 2015). In a drum brake system, the brake pads are enclosed inside a circular drum housing where brake shoes are pressed outward in a radial direction. Class 8 vehicles used for pickup and delivery, short haul, and long haul vocations, are typically equipped with drum brake systems on the steer, drive, and trailer axles, in conjunction with disc brake systems (Koupal et al. 2021).

There are three further classifications of brakes and are based on the brake pads. These classifications are low-metallic (LM), semi-metallic (SM), and non-asbestos organics (NAO) (Chan and Stachowiak 2004). It is expected that most passenger car and light truck Original Equipment Manufacturer (OEM) and Original Equipment Service (OES) brake pads in North America are made of non-asbestos organics (Stanard et al., 2021). The worn brake pads are often replaced by aftermarket low-metallic and semi-metallic materials as a cost-effective alternative (Stanard et al., 2021).

In prior studies, non-tailpipe PM is reported to contribute a larger fraction by mass in the coarse particle size range at 86%, while having 63% for PM2.5, and 33% PM0.1 (Garg et al. 2000). In a literature review of non-tailpipe emissions, Grigoratos and Martini (2014) state that 50% of PM_{10} brake wear particles become airborne while the rest are deposited on the road, whereas Stanard et al (2021) and Sanders (2003) report estimated airborne fractions between 50-70%. Studies conducted in urban environments report that brake wear contributes up to 55% by mass to the total non-exhaust traffic-related PM emissions and up to 21% by mass to total traffic-related PM emissions, however the former fraction is now reported to be larger (Grigoratos and Martini 2015; Bukowiecki et al. 2009; Chen et al. 2023). As technological advances lead to zero tailpipe emissions with electric vehicles, the non-tailpipe will remain unchanged as a positive relationship exists between vehicle weight and non-exhaust emissions (Wahlström et al. 2020). Electric vehicles weigh 25% more than internal combustion powered vehicles, and studies have indicated that non-exhaust particulate emissions are influenced by weight (Timmers and Achten 2016; Vasiljevic et al. 2022).

1.2 Review of laboratory and real-world experiments

Characterizing brake wear emissions can be achieved through various testing methods. Laboratory experiments include the use of brake or chassis dynamometer tests where either the brake system alone is tested or a vehicle with the brake system installed is tested as a whole. Another testing method is classified as real-world because it typically involves testing a vehicle or vehicle traffic in situ, either through onboard sampling equipment or by conducting tests on-road, near-road, or at nearby roads.

A variation of brake dynamometer tests includes a “pin-on-disc” method. This uses a motor rotating a brake disc while a pin is applying a load to vary the desired pressure (Feo et al. 2023). Österle et al. (2009) performed a pin-on-disk test by using a cylindrical pin cut out from a commercial brake pad material with a gray cast iron disc. The tests corresponded to moderate braking scenarios and used a thermocouple installed at 2 mm from the contact surface radius. Depending on the test cycle, sliding speeds can vary from 0.05 m/s to 13 m/s with contact pressures ranging from 0.5 MPa to 1.5 MPa (Feo et al. 2023). Cast iron discs are common while brake pad material can vary from low-metallic, semi-metallic, or NOA pads (Wahlström et al. 2010; Grigoratos and Martini 2015; Alemani et al. 2015; Verma et al. 2016). The pin-on-disc method is simple and low cost; however, it does not reproduce realistic braking conditions in terms of speed, braking intensity, or temperature which is reflected in the consistently similar properties of particles emitted (Philippe et al. 2019).

A commonly used testing method includes an inertia brake dynamometer test with a full brake assembly consisting of a disc and pair of brake pads are either in closed or open chamber systems. Garg, Cadle et al. (2000) used an enclosed brake dynamometer system to test seven preconditioned brake pads at four different temperatures (100 ºC, 200 ºC, 300 ºC, 400 ºC) with braking decelerations from 50 to 0 km/h. The braking temperature was generated through continuous braking intervals without any airflow past the brakes. During brake cooling events, the airflow was controlled from 714 m^3/hr to 48,240 m^3/hr and passed through High Efficiency Particulate Air (HEPA) filters. This method of pumping clean air into the chamber is a common practice to ensure collected particles are coming from brake activity and can be adjusted from 125 m^3/hr to 5000 m^3/hr (Perricone, Wahlström, and Olofsson 2016; Hagino, Oyama, and Sasaki 2016). The study by Hagino, Oyama et al. (2016) also used brake dynamometer tests, to mimic urban driving and braking patterns on non-asbestos organic friction materials and cast iron brake/drum assemblies. A chamber was used to enclose the brake assembly and used a constant flow that passed into a constant-volume sampling (CVS) tunnel (Hagino, Oyama, and Sasaki 2016). Their study followed a similar test method to that reported in Iijima, Sato et al. (2007) which incorporated three non-steel brake lining materials to produce brake particles at varying temperatures and braking intensities. Iijima, Sato et al. (2007) used a cast iron disk and was set to rotate at constant speed before being decelerated at 3.0 m/s^2. Particle measurements were taken at each temperature regime of 200, 300 and 400 ^{o}C that were produced through replicating urban driving, high-load, and extremely high-load conditions, respectively. The advantages of this method include the ability to reflect the real conditions of braking through recreating contact pressures to a degree, however this method is standardized and only accounts for extreme situations as it is complicated recreating the variation of brake events (Borawski 2019)

The third category involves using a vehicle through a chassis dynamometer or on a test track with sampling equipment on board. Kwak, Kim et al. (2013) used both of these methods to compare results as laboratory measurements are controlled environments and they alone cannot precisely represent the aspects of real world conditions (Camatini et al. 2001; Kreider et al. 2010). Their findings showed that brake wear particles concentrations are observed higher than those from tire wear particles from dynamometer tests and road wear particles form track testing.

Overall, previous research efforts have used diverse forms of controlled laboratory environments to develop prediction models and on-road testing to estimate non-tailpipe contributions. It is challenging replicating real world driving conditions as brake wear, tire wear, and road dust resuspension varies from factors such as driving conditions, road surface conditions, braking intensity, temperature, vehicle weight, vocation, and vehicle operation to name a few (Grigoratos and Martini 2014; Sanders et al. 2003; Stanard et al. 2021; Blau 2001; Wahlström, Olander, and Olofsson 2010; Garg et al. 2000). One of the main challenges of measuring brake wear emission comes from a lack of a standardized test procedure (Oliveira et al. 2022). Current initiatives involve the use of a fully-enclosed brake inertia dynamometer for better boundary controls including airflows, reducing contamination of particles from outside equipment, representative speed and temperature (PMP IWG 2020).

1.3 Brake pad and rotor friction materials in light and heavy duty vehicles

A comprehensive review of brake friction materials in lining materials is provided by Chan and Stachowiak 2004. Their review includes classifications of brake linings and is separated into low-metallic, semi-metallic, and non-asbestos organic pads. Brake components include subcomponents that are categorized as frictional additives, fillers, binders, and reinforcing fibers (Chan and Stachowiak 2004). The frictional additives consist of lubricants that stabilize the frictional coefficient and abrasives that increase the friction coefficient during braking events. Fillers improve the manufacturability, cost, and heat stability of brake components. Binders hold all the elements together to maintain the structural integrity during braking. Lastly, reinforcing fibers provides the overall mechanical strength of the friction material (Chan and Stachowiak 2004). Reinforcing fibers can also contain many metallic elements including steel, brass, and copper, with zinc also being used to reduce rusting (Hell et al. 2002; Chan and Stachowiak 2004).

Based on a market survey and review of common brake materials used in North America, Stanard et al. (2021) found that light duty vehicles are typically expected to be equipped with Original Equipment Manufacturer (OEM) pads made of non-organic asbestos, and after use, they are commonly replaced with low metallic and semi metallic pads as vehicle age increases. Another survey of two major suppliers of brake components for heavy-duty vehicles by Koupal et al. (2021) showed that they are typically equipped with 52% drum, 31% hydraulic disc, and 17% air disc brakes.

1.4 Brake and tire wear physical and chemical composition

PM from non-tailpipe have been reported to contain traces of heavy-metals and raise concerns about long term exposure to near road communities due to them being linked to adverse health effects (Tong et al. 2020; Cohen et al. 2017; Johansson, Norman, and Burman 2009; Adachi and Tainosho 2004). The size of brake and tire wear particles, especially fine particles, can be suspended in air for weeks or months ($PM_{2.5}$) or minutes to hours (PM_{10}) and have the capacity to be transported for hundreds of km from their source origin (Johansson, Norman, and Gidhagen 2007; Kim, Kabir, and Kabir 2015;

Srimuruganandam and Shiva Nagendra 2012; Cheung et al. 2011). Studies reviewed by Grigoratos and Martini (2015) report that around urban environments, brake wear particles to non-exhaust traffic related PM10 contribute between 16 to 55 % by mass, while near highways that percentage is around 3% by mass.

Particle mass size distributions of brake dust Iijima et al (2007) showed peaks between 3 and 6 µm. This led to an estimation of PM2.5 to fall between 74% and 92% of total particles by number and 12-36% of particle mass. PM2.5 was also found to be abundant at the lower temperatures which simulated urban driving conditions. Wahlstrom et al. (2010) showed that a disk brake assembly test stand, a pin-on-disc machine, and field tests using a passenger car had peaks in number concentration of about .41 µm and volume-weighted mean diameters of 3, 2, and 1.7 µm for the brake, pin, and field tests respectively. As stated by the authors, regardless of the difference in load, load conditions, sliding velocity, and pad temperature, all three test methods showed similar number distributions (Wahlström et al. 2010). This study was continued further to investigate the size, shape, and elemental composition of brake wear particles using a disc brake assembly stand on low-metallic and non-asbestos brake pads (Wahlström, Olander et al. 2010).

The braking pressure also influences particle size distributions as reported by Mohsen et al. (2004) in a laboratory investigation of low and high speed pin on disk friction tests. Their results show that pressures of 0.125, 0.375, and 0.625 MPa generate secondary peaks near the 2, 7 and 15 µm particle diameters. A peak near the 350 nm range was also consistent in brake particle size distributions, however, it did not change with varying pressures or speeds. In high speed tests the peak at 350 nm remained while the secondary peaks showed to be at 3, 5, and 6 μm with pressures of 0.75, 1.0, and 1.25 MPa, respectively. These results are supported by Sanders, Xu et al. (2003) as they suggest that higher pressures or harsher braking events can lead to larger sizes of wear particles between different brake lining materials. Brake dynamometer studies show that mass median diameters can be within the range of 0.6 μm and 2.5 μm with an average diameter at 1.5 μm (Garg et al. 2000). The average percent mass of airborne particles had an average of 86% PM10, 63% PM2.5, and 33% PM0.1 (Garg, Cadle et al. 2000).

A comparison between disc and drum brake systems showed particle mass size distributions to be dominated below the 10 μm size range and have unimodal profiles with a peak between 0.68 to 3.5 μm (Hagino, Oyama et al. 2016). Sanders, Xu et al. (2003) used an open system brake dynamometer test on low metallic, semi-metallic, and non-asbestos organic pads representing mid-size and full size vehicles. The number particle size distributions measured using MOUDI and ELPI instruments with average wear densities of 5, 4, and 3 g/cm^3 respectively, peaked in the range of 0.5-2 μm under urban driving conditions (Sanders et al. 2003). Their study also investigated harsher braking conditions leading to high brake temperatures. The findings suggest that particle size is not only a function of material type, but temperature as well. Under the harsh braking conditions, the number size distributions had modes in the ultrafine particle size range below 0.3 μm which likely occurs due chemical processes as the brakes reach temperatures of 500 - 600°C. The ultrafine particle range contributions can also occur due to volatilization of surface lining material from exposure to high temperatures (Sanderson, Delgado-Saborit, and Harrison

2014; Iijima et al. 2007; Thorpe and Harrison 2008; Habre et al. 2021; Wahlström, Olander, and Olofsson 2010).

Among the key tracers for brake wear includes, iron (Fe), copper (Cu), lead (Pb), manganese (Mn), titanium (Ti), antimony (Sb), zinc (Zn), and barium (Ba) (Thorpe and Harrison 2008; Wahlström, Olander, and Olofsson 2010; Bukowiecki et al. 2009; Hulskotte, Roskam, and Denier van der Gon 2014; Iijima et al. 2007; Grigoratos and Martini 2015) Compositions of brake wear particles vary depending on brake friction material parameters, brake assembly type, and vehicle operating conditions (Hagino, Oyama et al. 2016). Wahlström et al. (2010) performed laboratory tests on low metallic and non-asbestos organic brake pads against cast iron discs; they report that most of the coarse particles are mechanically generated and consist mainly of iron and iron oxide indicating an origin from the brake disc wear. There were also traces of titanium, zinc, barium, copper, and manganese, which are predicted to originate from the low-metallic and non-asbestos organic brake pad material (Wahlström, Olander, and Olofsson 2010; Grigoratos and Martini 2014). These results have been confirmed by Kwak, Kim et al. (2013) with elemental size distributions of on-road measurement, they found that Fe, Ca, and Zn contained the highest concentrations in the coarse fraction particles generated under constant speed driving and cornering conditions. During braking events the element concentrations from highest to lowest were Fe, Ba, Ti, and Sb. The emission factors of these elements were also high indicating they are produced by brake wear activity. The pin on disc laboratory test representing moderate braking events by Österle, Dörfel et al. (2009) showed most components in brake pad materials contribute to the formation of a “third body” produced from a mix of pad and disc constituents trapped between the two “first bodies”, disc and pads. XRF analysis showed small signals corresponding to pad constituents from Pb, Cr, Mn, Ti, Sn, and K but mass fractions were minor compared to Fe, Cu, and Zn.

1.5 Tire wear and composition

Tire wear is generated by the shear forces between the tire tread and road surface during driving activity (Pant and Harrison, 2013; Thorpe and Harrison, 2008). The particle composition and size of tire wear is influenced by the road surface conditions, type of vehicle, vehicle weight, and vehicle operation conditions (Thorpe and Harrison, 2008). Tread particles tend to mix and interact with existing particles already present in road dust, therefore leading to mixed compositions of tire and tire tread with road dust (Panko et al., 2018). Adachi and Tainosho (2004) detected 2288 heavy metal particles in 60 tire dust samples using a field emission scanning electron microscope with an energy dispersive X-ray spectrometer. Tire dust was found to have higher levels of mineral materials and heavy metal elements than tire tread. Brake dust was found to contain high levels of iron (Fe) with trace levels of Cu, Sb, and Ba. Yellow road paint particles were rich in Cr and Pb, while tire tread contained zinc oxide (ZnO) particles. Zinc (Zn) concentration, although seen in brake dust, is found to be approximately 15 times higher in tires than in brakes, while ZnO specifically is seen in tire tread (Apeagyei et al., 2011). Zinc in tires can originate from zinc oxide and organozinc compounds that are used in the vulcanization process (Pant and Harrison, 2013). Kwak et al. (2013), found that under braking conditions, the PM concentrations coming from road wear particles and tire wear particles were significantly less than those of brake wear particles. The brake wear particles had a broad size range from 1 μm to 10 μm, there were no particles larger than 10 μm recorded during braking.

1.6 Road wear and road dust

Other non-tailpipe sources include tire wear produce during interactions between tire and road surfaces creating particles with size distributions ranging from 10 nm to above 300 μm (Panko, Kreider, and Unice 2018; Cadle and Williams 1978; Dannis 1974; Gustafsson et al. 2008). Road dust is an important category of non-tailpipe sources because it not only includes background urban contribution but also includes previously emitted brake and tire wear. The particles can settle onto road surfaces and later resuspended through vehicle induced turbulence.

1.7 References

Abu-Allaban, Mahmoud, John A. Gillies, Alan W. Gertler, Russ Clayton, and David Proffitt. 2003. “Tailpipe, Resuspended Road Dust, and Brake-Wear Emission Factors from on-Road Vehicles.” *Atmospheric Environment* 37 (January):5283–93. https://doi.org/10.1016/j.atmosenv.2003.05.005.

Adachi, Kouji, and Yoshiaki Tainosho. 2004. “Characterization of Heavy Metal Particles Embedded in Tire Dust.” *Environment International* 30 (8): 1009–17. https://doi.org/10.1016/j.envint.2004.04.004.

Alemani, Mattia, Oleksii Nosko, Ibrahim Metinoz, and Ulf Olofsson. 2015. “A Study on Emission of Airborne Wear Particles from Car Brake Friction Pairs.” *SAE International Journal of Materials and Manufacturing* 9 (1): 147–57. https://doi.org/10.4271/2015-01-2665.

Apeagyei, Eric, Michael Bank, and John Spengler. 2011. “Distribution of Heavy Metals in Road Dust Along an Urban-Rural Gradient in Massachusetts.” *Atmospheric Environment - ATMOS ENVIRON* 45 (April):2310–23. https://doi.org/10.1016/j.atmosenv.2010.11.015.

Atkinson, Richard W., Gary W. Fuller, H. Ross Anderson, Roy M. Harrison, and Ben Armstrong. 2010. "Urban Ambient Particle Metrics and Health: A Time-Series Analysis." *Epidemiology* 21 (4): 501. https://doi.org/10.1097/EDE.0b013e3181debc88.

Blau, P. J. 2001. "Compositions, Functions, and Testing of Friction Brake Materials and Their Additives." ORNL/TM-2001/64. Oak Ridge National Lab. (ORNL), Oak Ridge, TN (United States). https://doi.org/10.2172/788356.

Borawski, Andrzej. 2019. "Common Methods in Analysing the Tribological Properties of Brake Pads and Discs – A Review." *Acta Mechanica et Automatica* 13 (3): 189–99. https://doi.org/10.2478/ama-2019-0025.

Breysse, Patrick N., Ralph J. Delfino, Francesca Dominici, Alison C. P. Elder, Mark W. Frampton, John R. Froines, Alison S. Geyh, et al. 2013. "US EPA Particulate Matter Research Centers: Summary of Research Results for 2005–2011." *Air Quality, Atmosphere & Health* 6 (2): 333–55. https://doi.org/10.1007/s11869-012-0181-8.

Bukowiecki, Nicolas, Peter Lienemann, Matthias Hill, Renato Figi, Agnes Richard, Markus Furger, Karen Rickers, et al. 2009. "Real-World Emission Factors for Antimony and Other Brake Wear Related Trace Elements: Size-Segregated Values for Light and Heavy Duty Vehicles." *Environmental Science & Technology* 43 (21): 8072–78. https://doi.org/10.1021/es9006096.

Cadle, S.H., and R.L. Williams. 1978. "Gas and Particle Emissions from Automobile Tires in Laboratory and Field Studies." *Journal of the Air Pollution Control Association* 28 (5): 502–7. https://doi.org/10.1080/00022470.1978.10470623.

Camatini, Marina, Giovanni F. Crosta, Tigran Dolukhanyan, Changmo Sung, GianPaolo Giuliani, Gaia M. Corbetta, Simone Cencetti, and Claudia Regazzoni. 2001. "Microcharacterization and Identification of Tire Debris in Heterogeneous Laboratory and Environmental Specimens." *Materials Characterization* 46 (4): 271–83. https://doi.org/10.1016/S1044-5803(00)00098-X.

CARB, California Air Resources Board. 2021. "EMFAC2021 Volume III Technical Document." https://ww2.arb.ca.gov/sites/default/files/2021-03/emfac2021_volume_3_technical_document.pdf.

Chan, D, and G W Stachowiak. 2004. "Review of Automotive Brake Friction Materials." *Proceedings of the Institution of Mechanical Engineers, Part D: Journal of Automobile Engineering* 218 (9): 953–66. https://doi.org/10.1243/0954407041856773.

Chen, L. -W. Antony, Xiaoliang Wang, Brenda Lopez, Guoyuan Wu, Steven Sai Hang Ho, Judith C. Chow, John G. Watson, Qi Yao, Seungju Yoon, and Heejung Jung. 2023. "Contributions of Non-Tailpipe Emissions to near-Road PM2.5 and PM10: A Chemical

Mass Balance Study." *Environmental Pollution* 335 (October):122283. https://doi.org/10.1016/j.envpol.2023.122283.

Cheung, Kalam, Nancy Daher, Winnie Kam, Martin M. Shafer, Zhi Ning, James J. Schauer, and Constantinos Sioutas. 2011. "Spatial and Temporal Variation of Chemical Composition and Mass Closure of Ambient Coarse Particulate Matter (PM10–2.5) in the Los Angeles Area." *Atmospheric Environment* 45 (16): 2651–62. https://doi.org/10.1016/j.atmosenv.2011.02.066.

Cohen, Aaron J., Michael Brauer, Richard Burnett, H. Ross Anderson, Joseph Frostad, Kara Estep, Kalpana Balakrishnan, et al. 2017. "Estimates and 25-Year Trends of the Global Burden of Disease Attributable to Ambient Air Pollution: An Analysis of Data from the Global Burden of Diseases Study 2015." *The Lancet* 389 (10082): 1907–18. https://doi.org/10.1016/S0140-6736(17)30505-6.

Dannis, M. L. 1974. "Rubber Dust from the Normal Wear of Tires." *Rubber Chemistry and Technology* 47 (4): 1011–37. https://doi.org/10.5254/1.3540458.

Feo, Maria Luisa, Marco Torre, Patrizio Tratzi, Francesca Battistelli, Laura Tomassetti, Francesco Petracchini, Ettore Guerriero, and Valerio Paolini. 2023. "Laboratory and On-Road Testing for Brake Wear Particle Emissions: A Review." *Environmental Science and Pollution Research* 30 (45): 100282–300. https://doi.org/10.1007/s11356-023-29229-7.

Garg, Bhagwan D., Steven H. Cadle, Patricia A. Mulawa, Peter J. Groblicki, Chris Laroo, and Graham A. Parr. 2000. "Brake Wear Particulate Matter Emissions." *Environmental Science & Technology* 34 (21): 4463–69. https://doi.org/10.1021/es001108h.

Grigoratos, Theodoros, and Giorgio Martini. 2014. "Non-Exhaust Traffic Related Emissions – Brake and Tyre Wear PM." JRC Publications Repository. June 17, 2014. https://doi.org/10.2790/22000.

———. 2015. "Brake Wear Particle Emissions: A Review." *Environmental Science and Pollution Research* 22 (4): 2491–2504. https://doi.org/10.1007/s11356-014-3696-8.

Gustafsson, Mats, Göran Blomqvist, Anders Gudmundsson, Andreas Dahl, Erik Swietlicki, Mats Bohgard, John Lindbom, and Anders Ljungman. 2008. "Properties and Toxicological Effects of Particles from the Interaction between Tyres, Road Pavement and Winter Traction Material." *The Science of the Total Environment* 393 (May):226–40. https://doi.org/10.1016/j.scitotenv.2007.12.030.

Habre, Rima, Mariam Girguis, Robert Urman, Scott Fruin, Fred Lurmann, Martin Shafer, Patrick Gorski, et al. 2021. "Contribution of Tailpipe and Non-Tailpipe Traffic Sources to Quasi-Ultrafine, Fine and Coarse Particulate Matter in Southern California." *Journal* *of the Air & Waste Management Association* 71 (2): 209–30. https://doi.org/10.1080/10962247.2020.1826366.

Hagino, Hiroyuki, Motoaki Oyama, and Sousuke Sasaki. 2016. "Laboratory Testing of Airborne Brake Wear Particle Emissions Using a Dynamometer System under Urban City Driving Cycles." *Atmospheric Environment* 131 (April):269–78. https://doi.org/10.1016/j.atmosenv.2016.02.014.

Harrison, Roy M. 2020. "Airborne Particulate Matter." *Philosophical Transactions of the Royal Society A: Mathematical, Physical and Engineering Sciences* 378 (2183): 20190319. https://doi.org/10.1098/rsta.2019.0319.

Hell, Manfred, Wilfried Jaworek, Werner Huppatz, and Dietrich Wieser. 2002. Friction lining, especially for brakes and clutches, and a method for producing a friction lining. United States US6481555B1, filed June 24, 1999, and issued November 19, 2002. https://patents.google.com/patent/US6481555B1/en.

Hinds, William C., and Yifang Zhu. 2022. *Aerosol Technology: Properties, Behavior, and Measurement of Airborne Particles*. John Wiley & Sons.

Hulskotte, J. H. J., G. D. Roskam, and H. A. C. Denier van der Gon. 2014. "Elemental Composition of Current Automotive Braking Materials and Derived Air Emission Factors." *Atmospheric Environment* 99 (December):436–45. https://doi.org/10.1016/j.atmosenv.2014.10.007.

Iijima, Akihiro, Keiichi Sato, Kiyoko Yano, Hiroshi Tago, Masahiko Kato, Hirokazu Kimura, and Naoki Furuta. 2007. "Particle Size and Composition Distribution Analysis of Automotive Brake Abrasion Dusts for the Evaluation of Antimony Sources of Airborne Particulate Matter." *Atmospheric Environment* 41 (23): 4908–19. https://doi.org/10.1016/j.atmosenv.2007.02.005.

Johansson, Christer, Michael Norman, and Lars Gidhagen. 2007. "Spatial & Temporal Variations of PM10 and Particle Number Concentrations in Urban Air." *Environmental Monitoring and Assessment* 127 (1): 477–87. https://doi.org/10.1007/s10661-006-9296-4.

Kim, Ki-Hyun, Ehsanul Kabir, and Shamin Kabir. 2015. "A Review on the Human Health Impact of Airborne Particulate Matter." *Environment International* 74 (January):136–43. https://doi.org/10.1016/j.envint.2014.10.005.

Koupal, John, Allison DenBleyker, Sandeep Kishan, Ravi Vedula, and Carlos Agudelo. 2021. "Brake Wear Particulate Matter Emissions Modeling." Final Report CA21-3232. Eastern Research Group, LINK Engineering.

Kreider, Marisa L., Julie M. Panko, Britt L. McAtee, Leonard I. Sweet, and Brent L. Finley. 2010. “Physical and Chemical Characterization of Tire-Related Particles: Comparison of Particles Generated Using Different Methodologies.” *The Science of the Total Environment* 408 (3): 652–59. https://doi.org/10.1016/j.scitotenv.2009.10.016.

Kwak, Ji-hyun, Hongsuk Kim, Janghee Lee, and Seokhwan Lee. 2013. “Characterization of Non-Exhaust Coarse and Fine Particles from on-Road Driving and Laboratory Measurements.” *Science of The Total Environment* 458–460 (August):273–82. https://doi.org/10.1016/j.scitotenv.2013.04.040.

Mosleh, Mohsen, Peter J Blau, and Delia Dumitrescu. 2004. “Characteristics and Morphology of Wear Particles from Laboratory Testing of Disk Brake Materials.” *Wear* 256 (11): 1128–34. https://doi.org/10.1016/j.wear.2003.07.007.

Oliveira, Pedro, RaviTeja Vedula, Carlos Agudelo, Pedro Oliveira, RaviTeja Vedula, and Carlos Agudelo. 2022. “Background, Technologies, and Standards for Brake Emissions Laboratory Measurements.” In . SAE International. https://doi.org/10.4271/2021-36-0427.

Österle, W., I. Dörfel, C. Prietzel, H. Rooch, A. -L. Cristol-Bulthé, G. Degallaix, and Y. Desplanques. 2009. “A Comprehensive Microscopic Study of Third Body Formation at the Interface between a Brake Pad and Brake Disc during the Final Stage of a Pin-on-Disc Test.” *Wear*, 17th International Conference on Wear of Materials, 267 (5): 781–88. https://doi.org/10.1016/j.wear.2008.11.023.

Ostro, Bart, Jianlin Hu, Debbie Goldberg, Peggy Reynolds, Andrew Hertz, Leslie Bernstein, and Michael J. Kleeman. 2015. “Associations of Mortality with Long-Term Exposures to Fine and Ultrafine Particles, Species and Sources: Results from the California Teachers Study Cohort.” *Environmental Health Perspectives* 123 (6): 549–56. https://doi.org/10.1289/ehp.1408565.

Panko, Julie, Marisa Kreider, and Kenneth Unice. 2018. “Chapter 7 - Review of Tire Wear Emissions: A Review of Tire Emission Measurement Studies: Identification of Gaps and Future Needs.” In *Non-Exhaust Emissions*, edited by Fulvio Amato, 147–60. Academic Press. https://doi.org/10.1016/B978-0-12-811770-5.00007-8.

Pant, Pallavi, and Roy Harrison. 2013. “Estimation of the Contribution of Road Traffic Emissions to Particulate Matter Concentrations from Field Measurements: A Review.” *Atmospheric Environment* 77 (October):78–97. https://doi.org/10.1016/j.atmosenv.2013.04.028.

Particle Measurement Programme. 2021. “PMP Workshop on Brake Emissions Regulation - Transport - Vehicle Regulations.” UNECE Wiki. January 13, 2021. https://wiki.unece.org/display/trans/PMP+Workshop+on+Brake+Emissions++Regulation.

Perricone, Guido, Jens Wahlström, and Ulf Olofsson. 2016. “Towards a Test Stand for Standardized Measurements of the Brake Emissions.” *Proceedings of the Institution of Mechanical Engineers, Part D: Journal of Automobile Engineering* 230 (11): 1521–28. https://doi.org/10.1177/0954407015616025.

Philippe, F., M. Xiang, C. Bressot, Y. Chen, F. Guingand, P. Charles, J. Loigerot, and M. Morgeneyer. 2019. “Relevance of Pin-on-Disc and Inertia Dynamometer Bench Experiments for Braking Emission Studies.” *Journal of Physics: Conference Series* 1323 (1): 012025. https://doi.org/10.1088/1742-6596/1323/1/012025.

Piscitello, Amelia, Carlo Bianco, Alessandro Casasso, and Rajandrea Sethi. 2021. “Non-Exhaust Traffic Emissions: Sources, Characterization, and Mitigation Measures.” *Science of The Total Environment* 766 (April):144440. https://doi.org/10.1016/j.scitotenv.2020.144440.

PMP IWG, Particle Measurement Programme Informal Working Group. 2020. “Non-Exhaust Brake Emissions — Laboratory Testing — Part 1: Inertia Dynamometer Protocol to Measure and Characterise Brake Emissions Using the WLTPBrake Cycle.” https://unece.org/DAM/trans/doc/2020/wp29grpe/GRPE-81-12e.pdf.

Sanders, Paul G., Ning Xu, Tom M. Dalka, and M. Matti Maricq. 2003. “Airborne Brake Wear Debris: Size Distributions, Composition, and a Comparison of Dynamometer and Vehicle Tests.” *Environmental Science & Technology* 37 (18): 4060–69. https://doi.org/10.1021/es034145s.

Sanderson, Paul, Juana Maria Delgado-Saborit, and Roy M. Harrison. 2014. “A Review of Chemical and Physical Characterisation of Atmospheric Metallic Nanoparticles.” *Atmospheric Environment* 94 (September):353–65. https://doi.org/10.1016/j.atmosenv.2014.05.023.

Schraufnagel, Dean E. 2020. “The Health Effects of Ultrafine Particles.” *Experimental & Molecular Medicine* 52 (3): 311–17. https://doi.org/10.1038/s12276-020-0403-3.

Srimuruganandam, B., and S. M. Shiva Nagendra. 2012. “Source Characterization of PM10 and PM2.5 Mass Using a Chemical Mass Balance Model at Urban Roadside.” *Science of The Total Environment* 433 (September):8–19. https://doi.org/10.1016/j.scitotenv.2012.05.082.

Stanard, Alan, Tim DeFries, Cindy Palacios, and Sandeep Kishan. 2021. “Brake and Tire Wear Emissions Project 17RD016 Prepared for the California Air Resources Board and the California Environmental Protection Agency.”

Suh, H. H., T. Bahadori, J. Vallarino, and J. D. Spengler. 2000. “Criteria Air Pollutants and Toxic Air Pollutants.” *Environmental Health Perspectives* 108 (suppl 4): 625–33. https://doi.org/10.1289/ehp.00108s4625.

Thompson, Jonathan E. 2018. “Airborne Particulate Matter: Human Exposure and Health Effects.” *Journal of Occupational and Environmental Medicine* 60 (5): 392. https://doi.org/10.1097/JOM.0000000000001277.

Thorpe, Alistair, and Roy M. Harrison. 2008. “Sources and Properties of Non-Exhaust Particulate Matter from Road Traffic: A Review.” *Science of The Total Environment* 400 (1): 270–82. https://doi.org/10.1016/j.scitotenv.2008.06.007.

Timmers, Victor R. J. H., and Peter A. J. Achten. 2016. “Non-Exhaust PM Emissions from Electric Vehicles.” *Atmospheric Environment* 134 (June):10–17. https://doi.org/10.1016/j.atmosenv.2016.03.017.

———. 2018. “Chapter 12 - Non-Exhaust PM Emissions From Battery Electric Vehicles.” In *Non-Exhaust Emissions*, edited by Fulvio Amato, 261–87. Academic Press. https://doi.org/10.1016/B978-0-12-811770-5.00012-1.

Tong, Ruipeng, Jiefeng Liu, Wei Wang, and Yingqian Fang. 2020. “Health Effects of PM2.5 Emissions from on-Road Vehicles during Weekdays and Weekends in Beijing, China.” *Atmospheric Environment* 223 (February):117258. https://doi.org/10.1016/j.atmosenv.2019.117258.

US EPA, OAR. 2017. “Criteria Air Pollutants.” Policies and Guidance. 2017. https://19january2017snapshot.epa.gov/criteria-air-pollutants.

Valavanidis, Athanasios, Konstantinos Fiotakis, and Thomais Vlachogianni. 2008. “Airborne Particulate Matter and Human Health: Toxicological Assessment and Importance of Size and Composition of Particles for Oxidative Damage and Carcinogenic Mechanisms.” *Journal of Environmental Science and Health, Part C* 26 (4): 339–62. https://doi.org/10.1080/10590500802494538.

Vasiljevic, Sasa, Jasna Glišović, Blaza Stojanovic, Nadica Stojanovic, and Ivan Grujic. 2022. “The Analysis of the Influential Parameters That Cause Particles Formation during the Braking Process: A Review.” *Proceedings of the Institution of Mechanical Engineers, Part J: Journal of Engineering Tribology* 236 (1): 31–48. https://doi.org/10.1177/13506501211004798.

Verma, Piyush Chandra, Mattia Alemani, Stefano Gialanella, Luca Lutterotti, Ulf Olofsson, and Giovanni Straffelini. 2016. “Wear Debris from Brake System Materials: A Multi-Analytical Characterization Approach.” *Tribology International* 94 (February):249–59. https://doi.org/10.1016/j.triboint.2015.08.011.

Wahid, Syed M. S. 2018. “Automotive Brake Wear: A Review.” *Environmental Science and Pollution Research* 25 (1): 174–80. https://doi.org/10.1007/s11356-017-0463-7.

Wahlström, J, A Söderberg, L Olander, U Olofsson, and A Jansson. 2010. "Airborne Wear Particles from Passenger Car Disc Brakes: A Comparison of Measurements from Field Tests, a Disc Brake Assembly Test Stand, and a Pin-on-Disc Machine." *Proceedings of the Institution of Mechanical Engineers, Part J: Journal of Engineering Tribology* 224 (2): 179–88. https://doi.org/10.1243/13506501JET633.

Wahlström, Jens, Mara Leonardi, Minghui Tu, Yezhe Lyu, Guido Perricone, Stefano Gialanella, and Ulf Olofsson. 2020. "A Study of the Effect of Brake Pad Scorching on Tribology and Airborne Particle Emissions." *Atmosphere* 11 (5): 488. https://doi.org/10.3390/atmos11050488.

Wahlström, Jens, Lars Olander, and Ulf Olofsson. 2010. "Size, Shape, and Elemental Composition of Airborne Wear Particles from Disc Brake Materials." *Tribology Letters* 38 (1): 15–24. https://doi.org/10.1007/s11249-009-9564-x.

Wahlström, Jens, Anders Söderberg, Lars Olander, Anders Jansson, and Ulf Olofsson. 2010. "A Pin-on-Disc Simulation of Airborne Wear Particles from Disc Brakes." *Wear* 268 (5): 763–69. https://doi.org/10.1016/j.wear.2009.11.014.

Wallington, Timothy J., James E. Anderson, Rachael H. Dolan, and Sandra L. Winkler. 2022. "Vehicle Emissions and Urban Air Quality: 60 Years of Progress." *Atmosphere* 13 (5): 650. https://doi.org/10.3390/atmos13050650.

Xing, Yu-Fei, Yue-Hua Xu, Min-Hua Shi, and Yi-Xin Lian. 2016. "The Impact of PM2.5 on the Human Respiratory System." *Journal of Thoracic Disease* 8 (1): E69–74. https://doi.org/10.3978/j.issn.2072-1439.2016.01.19.

Yu, Xin, Melissa Venecek, Anikender Kumar, Jianlin Hu, Saffet Tanrikulu, Su-Tzai Soon, Cuong Tran, David Fairley, and Michael J. Kleeman. 2019. "Regional Sources of Airborne Ultrafine Particle Number and Mass Concentrations in California." *Atmospheric Chemistry and Physics* 19 (23): 14677–702. https://doi.org/10.5194/acp-19-14677-2019.

Zhao, Yunliang, Daniel S. Tkacik, Andrew A. May, Neil M. Donahue, and Allen L. Robinson. 2022. "Mobile Sources Are Still an Important Source of Secondary Organic Aerosol and Fine Particulate Matter in the Los Angeles Region." *Environmental Science & Technology* 56 (22): 15328–36. https://doi.org/10.1021/acs.est.2c03317.

2 Chapter 2: Metal contents and size distribution of brake and tire wear particles dispersed in the near-road environment

2.1 Introduction

Brake and tire wear particulate matter (PM) represent a large fraction of traffic emissions from on-road vehicles. Over the past several decades, PM emissions from tailpipes have significantly decreased through technological innovations and legislative regulations (Wallington et al., 2022). However, many of these advancements have not extended to the non-tailpipe related PM emissions which have been suggested to surpass tailpipe emissions in their contributions to total traffic emissions in California (Yao, 2021). Non-tailpipe (or non-exhaust) sources include brake wear, tire wear, and road dust. With newer technologies approaching zero tailpipe emissions with heavier vehicle weights, traffic emissions will be dominated by these non-tailpipe sources (Timmers and Achten 2016). Non-tailpipe PM can contain traces of heavy-metals and long term exposure to these particles can lead to adverse health effects (Tong et al., 2020; Cohen et al., 2017; Johansson et al., 2009; Adachi and Tainosho, 2004).

The sources and chemical compositions of non-tailpipe particles need to be investigated to better understand their emissions. Chan and Stachowiak (2004) reviewed automotive brake friction materials present as frictional additives, fillers, binders, and reinforcing fibers. Three main classifications of brakes include low-metallic (LM), semi-metallic

(SM), and non-asbestos organics (NAO) (Chan and Stachowiak, 2004; Thorpe and Harrison, 2008). It is expected that most passenger car and light truck Original Equipment Manufacturer (OEM) and Original Equipment Service (OES) brake pads in North America are made of non-asbestos organics (Stanard et al., 2021). The worn brake pads are often replaced by aftermarket low-metallic and semi-metallic materials as a cost-effective alternative (Stanard et al., 2021). The metal content of brake pads is often difficult to characterize as it varies by manufacturer and application (Sanderson et al., 2014). Koupal et al. (2021) used a market share analysis to construct a brake wear mass balance representative of the heavy duty fleet in California. They estimated brake types for heavy duty vehicles were around 52 % drum brakes, 31 % hydraulic disc, and 17 % air disc (Koupal et al., 2021). The study provides insight into brake types and formulations that can be present on California roads and highways.

Tire wear, another non-tailpipe emission source, is generated by the shear forces between the tire tread and road surface (Pant and Harrison, 2013; Thorpe and Harrison, 2008). Some of the factors that influence the chemical composition, particle size, and quantity of emitted tire wear particles include road surface conditions, type of vehicle, vehicle weight, and vehicle operation conditions (Thorpe and Harrison, 2008). Tread particles can mix and interact with existing particles already present in road dust (Panko et al., 2018). To examine the metal characteristics of non-tailpipe sources, Adachi and Tainosho (2004) detected 2288 heavy metal particles in 60 tire dust samples using a field emission scanning electron microscope with an energy dispersive X-ray spectrometer. Tire dust was found to have higher levels of mineral materials and heavy metal elements than tire tread. Brake dust was rich in Fe with trace levels of Cu, Sb, and Ba. Yellow road paint particles were rich in Cr and Pb, while tire tread contained zinc oxide (ZnO) particles. Zinc (Zn) concentration, although seen in brake dust, is found to be approximately 15 times higher in tires than in brakes, while ZnO specifically is seen in tire tread (Apeagyei et al., 2011). Zinc in tires can originate from zinc oxide and organozinc compounds that are used in the vulcanization process (Pant and Harrison, 2013).

Previous studies have shown that non-tailpipe particles span from ultrafine to coarse size ranges (Habre et al., 2021; Garg et al., 2000; Thorpe and Harrison, 2008; Grigoratos and Martini, 2015). These studies typically used one or a combination of methods to measure non-tailpipe particles by performing laboratory experiments in controlled environments on dynamometer configurations, on-track tests with instrumentation mounted onto the test vehicle, or in-situ measurements of near road ambient air. Brake wear particles can exist from ultrafine to large coarse size ranges. Several studies showed that ~55–70 % and 80–98 % of brake wear particles are in the PM2.5 and PM10 size fractions, respectively (Garg et al., 2000; Grigoratos and Martini, 2015; Iijima et al., 2008; Thorpe and Harrison, 2008). Most studies showed that PM10 brake wear particles having unimodal mass distributions with the peak ranging 1–6 μm. Number distributions are more variable by testing conditions and instruments used. Both unimodal and bimodal distributions were observed, with peaks variating from 10 nm to 2 μm (Grigoratos and Martini, 2015). Both particle size and emission factors may vary depending on factors such as braking intensity, temperature, brake lining materials, vehicle weight, driving conditions (Garg et al., 2000; Sanders et al., 2003; Wahlström et al., 2010).

Size distributions for tire wear have been reported to range from 10 nm to above 300 μm (Panko et al., 2018; Cadle and Williams, 1978; Dannis, 1974; Gustafsson et al., 2008). A study by Kreider et al. (2010) provides insight into the physical and chemical characteristics of the particles generated during interaction between the tire and road surface. They used transmission optical microscopy to examine tire wear particles collected from on-road and laboratory experiments and found that tire wear particles in the 4–350 μm size range had a bimodal number size distribution with peaks occurring at approximately 5 μm and 25 μm. Some studies observed submicron particle emissions from tire wear and attributed them to volatilization and re-condensation of tire materials (Cadle and Williams, 1978; Thorpe and Harrison, 2008). Given that the quantity of particles emitted is based on driving conditions, it is predicted that tires can lose up to 10 % of their mass during their operational lifetime under normal driving conditions (Grigoratos and Martini, 2014). Reported PM10 tire wear emission rates ranged between 2.4 and 13 mg km^{-1} $vehicle^{-1}$ with an average of 6.3 mg km^{-1} $vehicle^{-1}$ for the light duty fleet (Panko et al., 2018; Grigoratos and Martini, 2014).

Stanard et al. (2021) used six light duty vehicles representative of California fleets to update brake wear emission factors based on speed and other conditions. They used brake temperature behavior from track tests to model and developed a new dynamometer cycle aimed to replicate realistic speeds, decelerations, brake time, and brake temperatures. Particle sizes in the two ranges, 5.6 to 560 nm and 0.5 to 18 μm, were measured. All vehicles tested showed multimodal size distributions. While submicron particle distributions varied with brake pad materials, peaking at around 10 nm, 25 nm, or 50 nm, fine particles consistently peaked at around 2 µm. Koupal et al. (2021) followed up a lab study for HDV (Heavy Duty Vehicle) and reported the mode diameter of brake wear particle distribution at about 1.4 µm.

In-use and near road studies are often used to evaluate non-exhaust sources and compare their contribution to controlled laboratory tests. Wang et al. (2021) measured metal content of PM2.5 using hourly x-ray fluorescence (XRF) from 2015 to 2018 near an urban roadway and busy highway in Toronto, Ontario. Each near road sampling site was paired with a corresponding background measurement location intended for subtraction of representative background concentrations. Emission factors for selected elements were obtained by screening data for instrumentation detection limits, clear distinction between the sampling site and its background site, and diurnal trends. Ba, Ti, Fe, and Cu had near-road concentrations that were 3.5, 2.8, 2.3, and 1.6 times higher than those observed at the urban background site. Elements such as Fe, Cu, and Ba have been identified in laboratory controlled studies to be indicative of wear from low-metallic brake pads (Sanders et al., 2003). A previous review by Thorpe and Harrison (2008) states that elements such as Al, Ba, Ca, Cr, Cu, Fe, K, Mn, Mo, Sb, Sr, and Zn are also representative of metals present in brake linings and emitted brake dust. Other elements such as Si, Ti, and Zr are typically found in brake fillers, fibers, and abrasives, respectively (Chan and Stachowiak, 2004; Grigoratos and Martini, 2015). These elements are commonly representative of key tracers for non-exhaust PM (Garg et al., 2000; Pant and Harrison, 2013). However, California has passed Senate Bill 346 (2010), which prohibits the sale of brake friction materials that contain >5 % copper by weight starting in 2021. By 2025 the percentage of copper by weight is required to fall below 0.5 %. It is expected copper content in brake pad materials has been declining in California fleets since 2021.

This study is a part of Real-World Tire and Brake Wear Emissions Project funded by California Air Resources Board. The study aimed to assess the level of exposure to non-tailpipe emissions at near-road environment. Different from other studies that often used an urban background site that is far from the near-road site for background subtraction, this study measured PM concentration at the proximity of both sides of the highways to subtract urban background at the measurement location. This study investigates metal composition and size distribution of ambient PM2.5 and PM10 near I-5 freeway in Anaheim and I-710 highway in Long Beach and urban background location in Irvine in Southern California. We hypothesized non-tailpipe emissions to be distinguishable from particle size distributions measurement at near-road environments. We also hypothesized non-tailpipe emissions originated from the traffic may dominate metal emission in near-road environment and can be distinguishable by chemical composition. This is a companion research effort with Wang et al. (2023), Chen et al. (2023) and Hwang et al. (2021), which presented chemical analysis, source apportionment, and health effects of the particles in the near road environment, respectively.

2.2 Experimental

2.2.1 Monitoring sites and traffic data

Measurement took place during two weeks in the winter months of 2020 from January 28th to February 10th. Two major freeways in Southern California were selected based on their traffic mix between light-duty vehicles (LDV) and heavy-duty vehicles (HDV).

Measurement occurred within the existing South Coast Air Quality Management District (SCAQMD) near road (NR) sampling sites located adjacent to the I-5 freeway in Anaheim, CA (33°49'14.22"N, 117°55'12.34"W) and the I-710 highway in Long Beach, CA (33°51'34.98"N, 118°12'2.44"W). Testing occurred from January 28th, 2020, to February 3rd, 2020, in Anaheim and from February 4th, 2020, to February 10th, 2020, in Long Beach. Both highways were selected to incorporate distinct traffic and vehicle profiles while occupying existing SCAQMD sampling infrastructure for accessibility. Highway I-5 crosses the suburbs of Orange County, while Highway I-710 connects to the Port of Los Angeles and is known to be a HDV corridor. Real-world traffic data of these two freeways in California was obtained using the California Department of Transportation Performance Measurement System (PeMs) system (Caltrans 2021). PeMS utilizes data from vehicle detecting stations that use inductive loops to collect real time 30-second measurements of vehicle flow and occupancy. Traffic speed is estimated at each loop detector using the g-factor algorithm (Jia et al. 2001). Figure 2-1and Figure 2-2 shows the traffic flow, truck flow, and speed from January 28th to February 3rd at the I-5 Northbound and Southbound lanes, respectively. The I-710 Northbound and Southbound traffic profiles are shown in Figure 2-3 and Figure 2-4 respectively. The I-5 has a traffic mix of approximately 95% light duty vehicles (LDVs) while the I-710 is a heavy duty corridor with a higher percentage of heavy duty vehicles (HDVs) accounting for 10% of its traffic mix. Note data obtained is representative of regular traffic patterns prior to the occurrence of the Covid-19 pandemic. Measurements were recorded daily during the hours of 0600 to 1800 LST to include traffic during morning and afternoon rush hours.

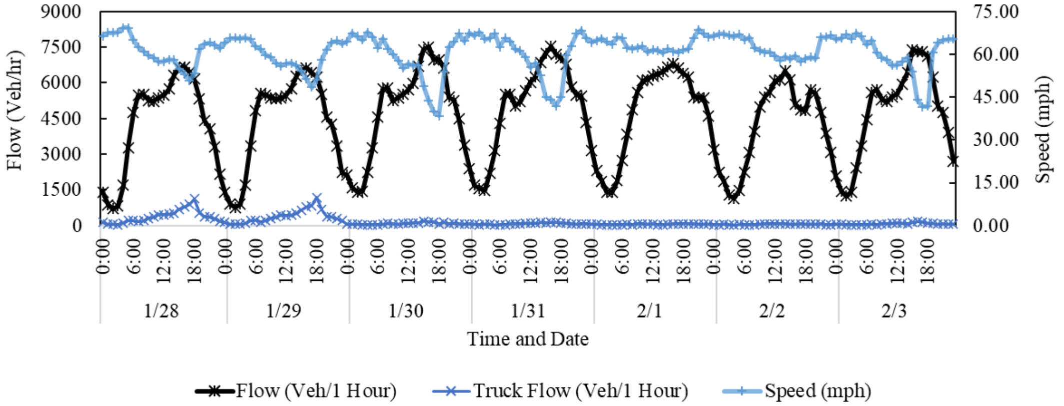

Figure 2-1: Traffic flow and speed of vehicles at the I-5 Northbound freeway per hour from Jan 28, 2020, through Feb 3, 2020.

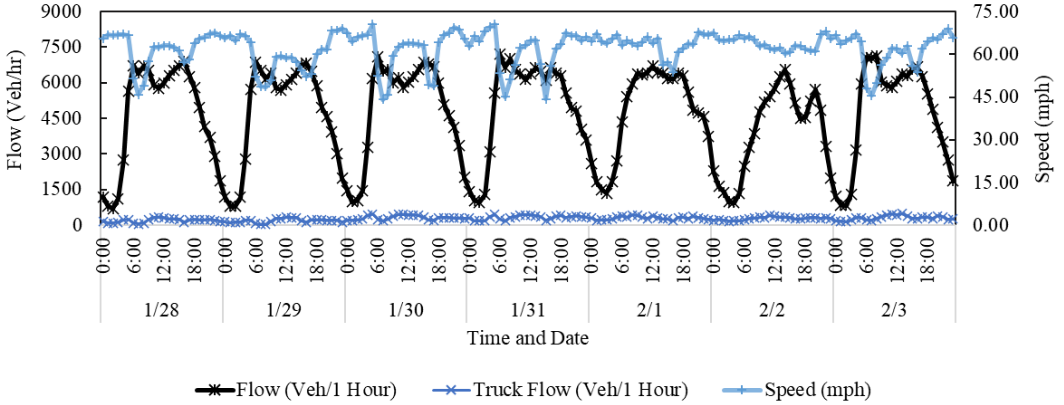

Figure 2-2: Traffic flow and speed of vehicles at the I-5 Southbound freeway per hour from Jan 28, 2020, through Feb 3, 2020.

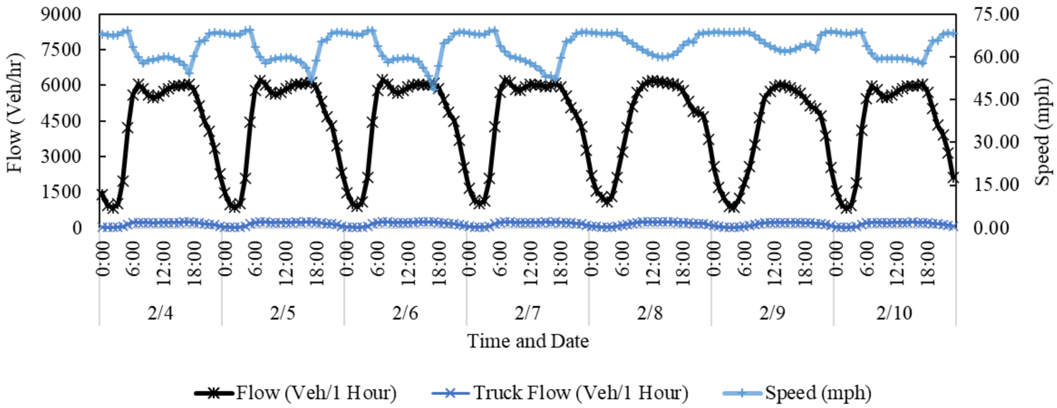

Figure 2-3: Traffic flow and speed of vehicles at the I-710 Northbound freeway per hour from Feb 04, 2020, through Feb 10, 2020.

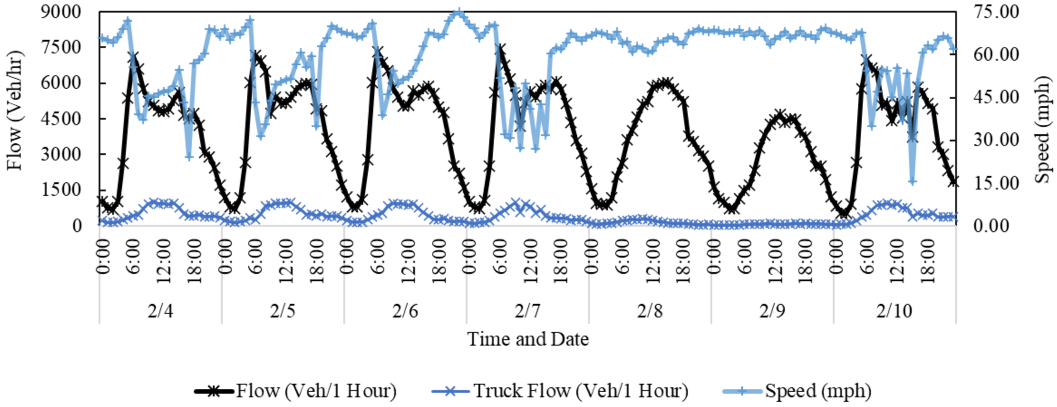

Figure 2-4: Traffic flow and speed of vehicles at the I-710 Southbound freeway per hour from Feb 04, 2020, through Feb 10, 2020.

Testing setup at each location included measurements from a nominal downwind site and one nominal upwind site across the highway, as shown in Figure 2-5. During the sampling periods, the wind direction was dominantly from south and southwest at the I-5 sampling location and from south to west at the I-710 sampling location (Wang et al. 2023). Note that as wind direction changed throughout the day, the nominal downwind sites were not always downwind.

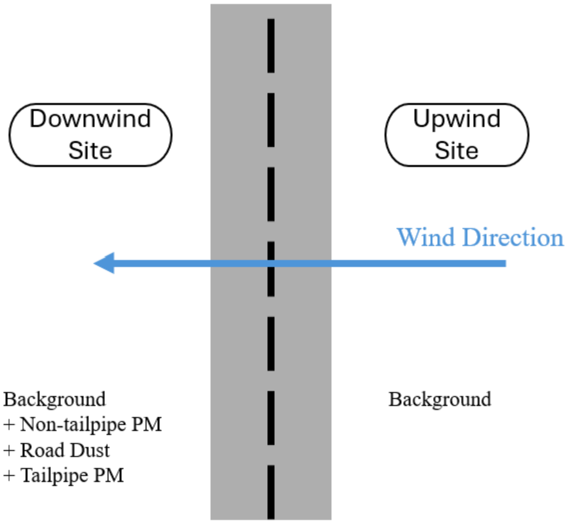

Figure 2-5: Measurement set up with a downwind and upwind site along opposite sides of the road.

2.2.2 Sampling instruments

MOUDI (Micro Orifice Uniform Deposit Impactor) sample was taken at both nominal downwind sites of Anaheim and Long Beach location. The MOUDI sample was taken at an urban background site which was located on the rooftop of a campus building at the University of California, Irvine. Particle filter samples were collected for 4–12 h daily from 1/28/2020 to 2/3/2020 at the Anaheim site, for 6–12 h per day from 2/4/2020 to 2/ 10/2020 (except on 2/9/2020) at the Long beach site, and for 8–11 h at the urban site from 2/23/2020 to 2/29/2020 (except on 2/28/2020). The details on the background sampling site and duration can be found in Hwang et al. (2021) and Fang et al. (2023).

Integrated PM2.5 and PM10 samples were collected using the Desert Research Institute (DRI) medium-volume (medvol) PM samplers with a Bendix Model 240 PM2.5 cyclone and a Sierra-Andersen 254 PM10 inlet, respectively (Wang et al., 2023). Two samplers were set up at each upwind and downwind site. PM2.5 and PM10 samples were collected on Teflonmembrane and quartz-fiber filters over four-hour intervals (0600–1000, 1000–1400, and 1400–1800 LST) during the two-week period. The Teflon-membrane filters were weighed to obtain gravimetric mass, followed by quantification of 51 elements using XRF. A statistical summary and minimum limit of detection of elements are shown in Table 2-8 and Table 2-9 in the appendix section. The 50 % cut off aerodynamic diameters of the MOUDI used for the collection are 18, 10, 3.2, 1, 0.56, and 0.056 μm. The size-segregated particles were collected using MOUDI in a non-rotating mode without a back-up filter at a flow rate of 30 L min^{-1}. The particles were collected on a 47 mm Teflon-membrane filter. After the collection, all filter samples were immediately sealed in Petri dishes and stored at −18 °C. The filter samples collected on 1/29/20, 1/30/20, 2/3/20, 2/4/20, 2/10/20, 2/19/20, 2/27/ 20, and 2/29/20 were cut in half for PM metal analysis for this study and ROS/DTT analysis for other studies (Fang et al., 2023; Hwang et al., 2021).

To determine the elements present, MOUDI filter samples were digested in Teflon-lined vessels by adding nitric acid (HNO3) (electronic high purity grade, Duksan Pure Chemical Co., Ansan-si, Korea), hydrofluoric acid (HF) (microelectronic grade, J. T. Baker, Phillipsburg, NJ, USA), and boric acid (H3BO3) (trace metals basis grade, Sigma Aldrich, St. Louis, MO, USA) in a closed microwave digestion system (multiwave 7000, Anton Paar, Graz, Austria) with dual-stage digestion method following a validated protocol (Kulkarni et al., 2007). The digested samples were then diluted with deionized water to a final volume of 10 mL with dilution factor of 3.3. The solution was subsequently filtered using a 0.45 μm PTFE (polytetrafluoroethylene) syringe filter (Advantec Co. Ltd., Tokyo, Japan). Then, 16 elements (Al, Si, K, Ca, Ti, Mn, Fe, Cu, Zn, Ga, Rb, Sr, Zr, Mo, Sb, and Ba) in the solution were analyzed by inductively coupled plasma-mass spectrometry (ICP-MS) (Elan 6000, Perkin-Elmer, Waltham, MA, USA) and inductively coupled plasma-optical emission spectroscopy (ICP-OES) (iCAP7400DUO, Thermo Scientific, Waltham,MA, USA). Recovery was determined in the range of 82–100% except for Si (35%) and Ti (68%) based on SRM 1648a (NIST, Gaithersburg, MD, USA). Limit of detection (LOD) was from 0.2 ppt (Zr) ~ 2.2 ppb (K).

Horiba PX-375 Continuous Particulate Monitor with XRF systems were used in conjunction with medvol PM samplers to measure ambient PM and to quantify real-time elemental concentrations on an hourly basis. The PX-375measures PM2.5 or PM10 mass concentration using beta-ray attenuation and elemental concentration using XRF. Aerosols are sampled through inlets located at the top of the instrument which then pass through either a PM10 impactor or a PM2.5 cyclone, while the air relative humidity is adjusted by a heater. Particles are collected on a glassfiber/PTFE filter tape where the mass concentration is measured by beta-ray attenuation (Erika, 2018). Next, the filter advances into an XRF analyzer to quantify the concentrations of the following 15 elements: Al, Si, S, K, Ca, Ti, V, Cr, Mn, Fe, Ni, Cu, Zn, As, and Pb. At the I-5 sampling location, a PX-375 measured hourly PM2.5 for 24 hours a day at the downwind site, while a second PX-375 measured PM2.5 during 0600–1800 LST at the upwind site. PM10 data was not available with the PX-375 systems at I-5 sites. The I-710 downwind site had one PX-375 unit measuring PM2.5 continuously between February 4th, 2020, and February 7th, 2020, and a second unit measuring PM10 during 0600–1800 LST. The upwind site measured both

PM2.5 and PM10 during 0600–1800 LST with few interruptions throughout the sampling periods. All sampling inlets were maintained at a height of approximately 3 m above ground to clear wall or container obstructions. Calibration of PX375 units was conducted by manufacturers using SRM2783 before the beginning of the field testing. QA/QC and limit of detection was determined following Method I.O.-3.2.

Real-time aerodynamic particle size distributions were measured using a Dekati High Resolution Electrical Low Pressure Impactor (HRELPI+). Measured particle size distributions range from 6 nm to 10 μmat10Hz sampling rate (Keskinen et al., 1992). The HRELPI+ obtains measurements by charging airborne particles before passing them through a series of 13 impactor stages acting as size classifiers and a final filter stage. The data inversion algorithm provides size distributions up to 500 size classes (Saari et al., 2018). One HRELPI+ unit was set for sampling at the downwind sites for both the I-5 and I-710 locations. The second-by-second size distribution data was averaged to every hour time resolution to match with the PX-375 time stamps.

SCAQMD NR sites monitor PM2.5, wind speed, and wind directions that were used in the analysis of this study in addition to CARB's Air Quality and Meteorological Information System (AQMIS) tool. The minute by minute time resolution wind speed and wind direction were used to evaluate cross wind magnitudes. Vehicle traffic count and speed were obtained from inductive loop detector measurement at two closest vehicle detection stations (VDS) of the California Department of Transportation Performance Measurement System (PeMS) at both highways. The data showed regular traffic patterns with morning and afternoon rush hours on weekdays and lower vehicle flows in early morning hours. See Wang et al. (2023) for detailed traffic analysis.

To assess statistical relationships between the selected elements, the squared Pearson correlation coefficient (r^2) was obtained through Eq. (1). The value r^2, commonly referred to as the coefficient of determination, explains the variability of the dependent variable, y, by the variation of the independent variable, x. Values of x_m and y_m are the averages of each respective data set. Resulting values range between 0 and 1, for a linear regression model.

$$r^2 = \left(\frac{\sum[(x-x_m)\cdot(y-y_m)]}{\sqrt{[\sum(x-x_m)^2\cdot\sum(y-y_m)^2]}}\right)^2 \tag{1}$$

Two sets of r^2 values were computed for each size range, PM2.5 and PM10, at each testing location. The first set evaluated r^2 values using element concentrations measured at the nominal downwind site and the upwind site separately. The second set removed background influence by subtracting the nominal upwind element concentration from the corresponding nominal downwind element concentration prior to evaluating r^2 values. Note that when the wind is different from the prevailing wind direction, the concentration differences between nominal downwind and upwind sites could be negative.

2.3 Results and Discussions

2.3.1 Elemental Abundances and correlations

The downwind and upwind PM (i.e., ΔPM2.5 and ΔPM10) and elemental concentration differences elucidate the traffic emissions from the highways. Figure 2-6 shows the fractions of each element (Fe, Si, Ca, S, Al, K, Zn, Cl, Ti, and Cu) relative to the total elemental concentrations measured by XRF on integrated PM2.5 filter samples at both the I-5 and I-710 locations. The remaining 41 elements were grouped as “other” because many had low concentrations near or below detection limit, and most are not prominent non-tailpipe markers except for Ba. Two elements, Fe and Si, were the most abundant in both PM2.5 and PM10. Figure 2-7 shows that Fe was 30 % and 24 % of total elements measured by XRF from ΔPM10 at the I-5 and I-710 sites, respectively, while the relative abundances of Si was 21 % at both locations. Both elements are abundant in crustal materials and therefore are related to road dust in the coarse particle size range. Additionally, Fe can be emitted from fresh wear of vehicle components including brakes or resuspension after they are deposited on road surface in fine particle size ranges (Garg et al., 2000; Thorpe and Harrison, 2008; Abu-Allaban et al., 2003). High Fe content can be found in road dust samples but is also often seen in studies for cast iron brake discs or drums. Mosleh et al. (2004) used a pin-on-disc friction and wear test configuration between a grey cast iron disc and semi-metallic brake pad material for the pins. They varied pressures from 0.125 and 1.25 MPa while maintaining speeds of 0.275 and 5 m/s. Submicron to few-micron sized particles from brake debris had high concentrations of Fe, Si, C, Al, O, and Mo. Similar results were shown by Iijima et al. (2007) by testing NAO pads on cast iron discs at various braking temperatures. The large amounts of Fe were concluded to originate from the cast iron discs as the bulk material of the brake pad contained trace amounts of K, Ti, Cu, Zn, Sb, and Ba. Barium had a 5 - 6% contribution at I-5 and 3% contribution at I-710 for both ΔPM2.5 and ΔPM10 size ranges. Zinc, a common marker for tire wear, consistently makes up between 1 and 2 % of elemental fractions in both ΔPM2.5 and ΔPM10 at both locations. Details of elemental fractions without background subtraction are shown in Figure 2-8.

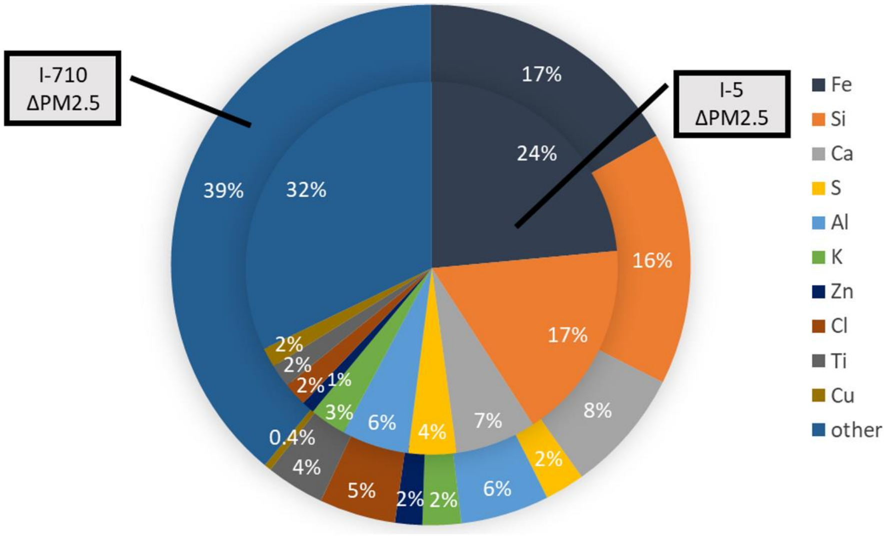

Figure 2-6: Elemental fractions measured by XRF on integrated filter samples of ΔPM2.5 at the I-5 highway location in Anaheim (inner) and the I-710 highway in Long Beach (outer).

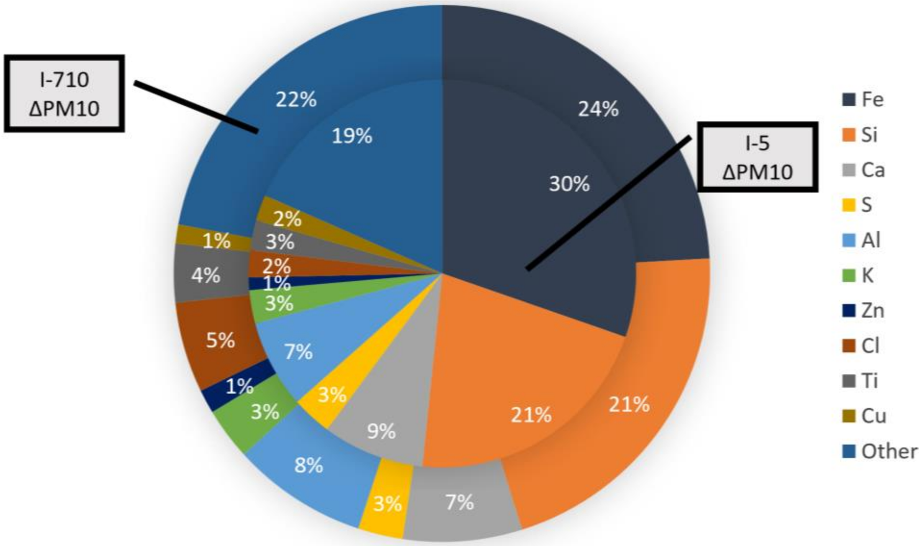

Figure 2-7: Elemental fractions measured by XRF on integrated filter samples of ΔPM10 at the I-5 highway location in Anaheim (inner) and the I-710 highway in Long Beach (outer).

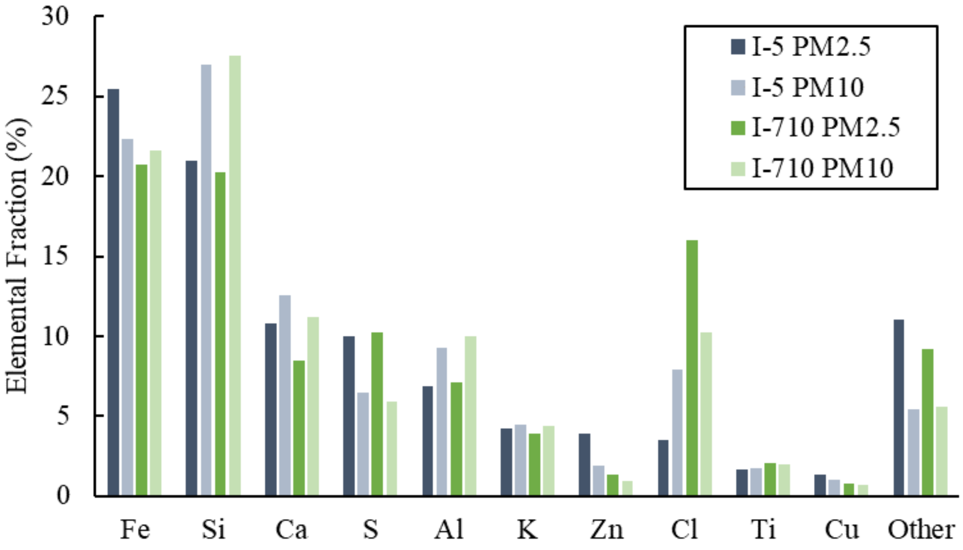

Figure 2-8: Elemental fractions of PM2.5 and PM10 elements at the downwind sites of I-5 in Anaheim, CA and I-710 in Long Beach, CA.

Pearson correlations among elements from XRF results were examined to infer their source commonalities. This analysis is similar to that by Wang et al. (2021) except the current study examined correlations with and without background subtraction. It should be noted that negative ΔPM due to wind direction change does not affect this analysis because the correlation extends from first quadrant to third quadrant linearly in a correlation graph. Table 2-1 and Table 2-2 show high correlations among main crustal elements of Si, Ca, and Al with $r^2 \gtrapprox 0.9$ before background subtraction at the I-5 downwind site, and the correlations were higher for PM10 than PM2.5. This is expected due to the abundant mineral dust at these near road sampling sites and PM10 contains more coarse dust than PM2.5. Fe and K are also important crustal elements; however, other sources, such as brake and vehicle wear for Fe and biomass burning for K, can contribute to these elements. Therefore, Fe and K show moderate correlations ($r^2 = 0.54$–0.93) with Si, Ca, and Al. Brake discs of light-duty fleets are shown to contain approximately 2.0–2.4 % of Si, with concentrations typically an order of magnitude less than Fe (Hulskotte et al., 2014; Blau, 2001). In this result, Si has high correlations ($r^2 > 0.78$) with Ca and Al, the most abundant elements found in the Earth's upper continental crust (UCC). Therefore, Si is assumed to be predominantly originated from road dust. Fe also shows moderate correlations with Ti, Cu, Ba, Mn, and Zr, confirming its partial origin from wear particles. Brake wear elements (i.e., Fe, Ti, Cu, Ba, Mn, and Zr) show moderate to high correlations, especially in PM10 (Table 2-2).

Table 2-1: Squared Pearson correlation coefficient (r^2) among PM2.5 elements at the I-5 downwind site. Note dark green color denotes high correlations and light green color denote intermedia correlations.

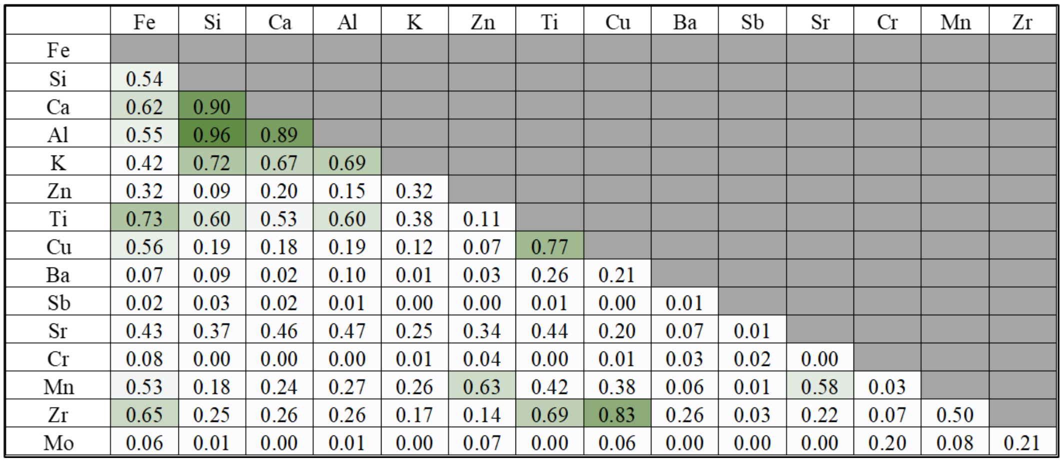

	Fe	Si	Ca	Al	K	Zn	Ti	Cu	Ba	Sb	Sr	Cr	Mn	Zr
Fe														
Si	0.54													
Ca	0.62	0.90												
Al	0.55	0.96	0.89											
K	0.42	0.72	0.67	0.69										
Zn	0.32	0.09	0.20	0.15	0.32									
Ti	0.73	0.60	0.53	0.60	0.38	0.11								
Cu	0.56	0.19	0.18	0.19	0.12	0.07	0.77							
Ba	0.07	0.09	0.02	0.10	0.01	0.03	0.26	0.21						
Sb	0.02	0.03	0.02	0.01	0.00	0.00	0.01	0.00	0.01					
Sr	0.43	0.37	0.46	0.47	0.25	0.34	0.44	0.20	0.07	0.01				
Cr	0.08	0.00	0.00	0.00	0.01	0.04	0.00	0.01	0.03	0.02	0.00			
Mn	0.53	0.18	0.24	0.27	0.26	0.63	0.42	0.38	0.06	0.01	0.58	0.03		
Zr	0.65	0.25	0.26	0.26	0.17	0.14	0.69	0.83	0.26	0.03	0.22	0.07	0.50	
Mo	0.06	0.01	0.00	0.01	0.00	0.07	0.00	0.06	0.00	0.00	0.00	0.20	0.08	0.21

Table 2-2: Squared Pearson correlation coefficient (r^2) among PM10 elements at the I-5 downwind site. Note dark green color denotes high correlations and light green color denote intermedia correlations.

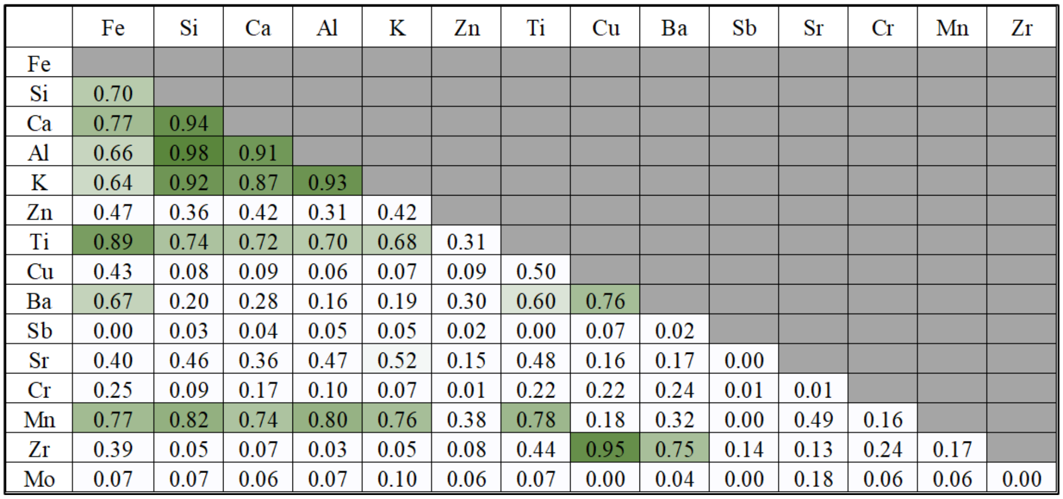

	Fe	Si	Ca	Al	K	Zn	Ti	Cu	Ba	Sb	Sr	Cr	Mn	Zr
Fe														
Si	0.70													
Ca	0.77	0.94												
Al	0.66	0.98	0.91											
K	0.64	0.92	0.87	0.93										
Zn	0.47	0.36	0.42	0.31	0.42									
Ti	0.89	0.74	0.72	0.70	0.68	0.31								
Cu	0.43	0.08	0.09	0.06	0.07	0.09	0.50							
Ba	0.67	0.20	0.28	0.16	0.19	0.30	0.60	0.76						
Sb	0.00	0.03	0.04	0.05	0.05	0.02	0.00	0.07	0.02					
Sr	0.40	0.46	0.36	0.47	0.52	0.15	0.48	0.16	0.17	0.00				
Cr	0.25	0.09	0.17	0.10	0.07	0.01	0.22	0.22	0.24	0.01	0.01			
Mn	0.77	0.82	0.74	0.80	0.76	0.38	0.78	0.18	0.32	0.00	0.49	0.16		
Zr	0.39	0.05	0.07	0.03	0.05	0.08	0.44	0.95	0.75	0.14	0.13	0.24	0.17	
Mo	0.07	0.07	0.06	0.07	0.10	0.06	0.07	0.00	0.04	0.00	0.18	0.06	0.06	0.00

Zn is a tire wear marker but can also originate from other sources such as tailpipe and industrial emissions. Therefore, Table 2-1 and Table 2-2 show that Zn was only moderately to weakly ($r^2 < 0.63$) correlated with wear elements Fe, Ba, and Mn. Similar correlations were also found in I-710 downwind samples without background subtraction in Table 2-3 and Table 2-4 except that Fe and Zn show higher correlations with more elements.

Table 2-3: Squared Pearson correlation coefficient (r^2) among PM2.5 elements at the I-710 downwind site. Note dark green color denotes high correlations and light green color denote intermedia correlations.

	Fe	Si	Ca	Al	K	Zn	Ti	Cu	Ba	Sb	Sr	Cr	Mn	Zr
Fe														
Si	0.80													
Ca	0.78	0.92												
Al	0.84	0.88	0.79											
K	0.81	0.64	0.64	0.58										
Zn	0.57	0.44	0.47	0.42	0.73									
Ti	0.61	0.49	0.41	0.68	0.40	0.26								
Cu	0.90	0.67	0.65	0.81	0.80	0.58	0.65							
Ba	0.58	0.30	0.26	0.53	0.36	0.35	0.35	0.58						
Sb	0.42	0.29	0.31	0.27	0.60	0.33	0.54	0.47	0.07					
Sr	0.63	0.67	0.65	0.80	0.38	0.23	0.72	0.64	0.36	0.33				
Cr	0.41	0.38	0.30	0.43	0.31	0.57	0.44	0.38	0.35	0.16	0.43			
Mn	0.67	0.51	0.37	0.45	0.71	0.47	0.37	0.54	0.39	0.38	0.25	0.36		
Zr	0.75	0.63	0.45	0.72	0.54	0.31	0.73	0.68	0.42	0.35	0.56	0.45	0.72	
Mo	0.24	0.14	0.16	0.09	0.40	0.55	0.00	0.16	0.29	0.04	0.01	0.19	0.33	0.07

Table 2-4: Squared Pearson correlation coefficient (r^2) among PM10 elements at the I-170 downwind site. Note dark green color denotes high correlations and light green color denote intermedia correlations.

	Fe	Si	Ca	Al	K	Zn	Ti	Cu	Ba	Sb	Sr	Cr	Mn	Zr
Fe														
Si	0.86													
Ca	0.88	0.98												
Al	0.88	0.98	0.98											
K	0.89	0.96	0.94	0.92										
Zn	0.85	0.71	0.78	0.74	0.79									
Ti	0.75	0.65	0.68	0.75	0.61	0.67								
Cu	0.88	0.58	0.61	0.61	0.67	0.78	0.66							
Ba	0.61	0.29	0.30	0.30	0.36	0.47	0.46	0.79						
Sb	0.17	0.19	0.17	0.16	0.27	0.13	0.02	0.15	0.04					
Sr	0.78	0.80	0.78	0.79	0.77	0.58	0.78	0.60	0.48	0.04				
Cr	0.67	0.54	0.61	0.61	0.58	0.88	0.58	0.61	0.32	0.13	0.38			
Mn	0.84	0.84	0.88	0.85	0.86	0.81	0.73	0.65	0.37	0.20	0.78	0.67		
Zr	0.86	0.59	0.61	0.62	0.69	0.80	0.62	0.97	0.72	0.23	0.57	0.67	0.68	
Mo	0.32	0.16	0.21	0.15	0.26	0.42	0.08	0.33	0.29	0.15	0.08	0.33	0.30	0.31

The ΔPM10 elemental correlations after background subtraction are shown in Table 2-5 and Table 2-6, while the corresponding ΔPM2.5 elemental correlations are shown in Table 2-7 and Table 2-8. The ΔPM10 crustal elements Si, Ca, and Al are still correlated, but the r^2 values decreased to 0.68–0.81 at I-5 and 0.35–0.70 at I-710. This is probably because the background dust particles were contributing significantly to the high correlations and the road dust particles deviated from crustal composition due to additional elements from brake, tire, and pavement wear deposition. Additionally, subtracting upwind concentrations from downwind concentrations introduced additional uncertainties in the elemental concentration differences, which could also reduce the correlations. On the other hand, some correlations were enhanced after background subtraction. Table 2-5 shows that brake wear elements Fe, Ti, Cu, Ba, Mn, and Zr mostly increased their paired r^2 values to 0.67–0.90 after the background removal, unmasking the interference due to background particles. Correlation values between Ti-Cu, Fe-Ti, and Fe-Cu are similar with $r^2 = 0.90$. Moderate correlations can be seen between these three elements and both Ba and Zr ($r^2 > 0.69$). The correlation of the potential tire marker Zn with brake markers such as Ti, Zr, Ba, and Cu also significantly increased to $r^2 \sim 0.6–0.7$ after background removal as brake and tire wears covary with traffic volume and braking events. The ΔPM10 elemental correlations at I-710 (Table 2-6) were mostly lower than those before background removal (Table 2-4) and also lower than those at I-5 (Table 2-5). This is probably because of the relatively long distance (1.05 km) between the upwind and downwind sites of I-710, making the upwind concentrations not representative of the background at the downwind site.

Table 2-5: Squared Pearson correlation coefficient (r^2) among ΔPM10 elements at the I-5 location. Note dark green color denotes high correlations and light green color denote intermedia correlations.

	Fe	Si	Ca	Al	K	Zn	Ti	Cu	Ba	Sb	Sr	Cr	Mn	Zr
Fe														
Si	0.31													
Ca	0.41	0.79												
Al	0.26	0.81	0.68											
K	0.56	0.33	0.22	0.24										
Zn	0.69	0.32	0.46	0.39	0.29									
Ti	0.90	0.27	0.30	0.21	0.49	0.70								
Cu	0.90	0.14	0.23	0.13	0.39	0.69	0.90							
Ba	0.69	0.07	0.17	0.07	0.32	0.63	0.76	0.80						
Sb	0.01	0.17	0.09	0.30	0.01	0.00	0.01	0.04	0.02					
Sr	0.53	0.22	0.23	0.12	0.27	0.38	0.43	0.46	0.28	0.00				
Cr	0.29	0.02	0.08	0.11	0.26	0.21	0.20	0.29	0.22	0.01	0.03			
Mn	0.67	0.25	0.34	0.12	0.43	0.26	0.48	0.49	0.26	0.07	0.50	0.08		
Zr	0.87	0.15	0.25	0.13	0.35	0.70	0.89	0.94	0.81	0.04	0.37	0.28	0.43	
Mo	0.01	0.03	0.01	0.00	0.01	0.01	0.01	0.06	0.00	0.02	0.00	0.25	0.00	0.04

Table 2-6: Squared Pearson correlation coefficient (r^2) among ΔPM10 elements at the I-710 location. Note dark green color denotes high correlations and light green color denote intermedia correlations.

	Fe	Si	Ca	Al	K	Zn	Ti	Cu	Ba	Sb	Sr	Cr	Mn	Zr
Fe														
Si	0.40													
Ca	0.64	0.38												
Al	0.34	0.70	0.35											
K	0.46	0.94	0.32	0.61										
Zn	0.42	0.74	0.43	0.64	0.62									
Ti	0.08	0.20	0.39	0.49	0.10	0.38								
Cu	0.75	0.07	0.32	0.11	0.14	0.08	0.01							
Ba	0.44	0.03	0.38	0.10	0.04	0.11	0.15	0.40						
Sb	0.15	0.31	0.27	0.26	0.30	0.33	0.17	0.01	0.05					
Sr	0.19	0.07	0.35	0.13	0.04	0.11	0.22	0.12	0.01	0.14				
Cr	0.35	0.30	0.07	0.29	0.30	0.45	0.00	0.15	0.09	0.07	0.02			
Mn	0.37	0.38	0.23	0.29	0.34	0.24	0.05	0.14	0.17	0.19	0.00	0.09		
Zr	0.50	0.01	0.16	0.02	0.04	0.05	0.00	0.76	0.31	0.04	0.03	0.12	0.07	
Mo	0.01	0.10	0.02	0.13	0.09	0.07	0.01	0.01	0.03	0.23	0.07	0.17	0.30	0.05

Table 2-7: Squared Pearson correlation coefficient (r^2) among ΔPM2.5 elements at the I-5 location. Note dark green color denotes high correlations and light green color denote intermedia correlations.

	Fe	Si	Ca	Al	K	Zn	Ti	Cu	Ba	Sb	Sr	Cr	Mn	Zr
Fe														
Si	0.28													
Ca	0.23	0.83												
Al	0.25	0.78	0.57											
K	0.36	0.67	0.73	0.37										
Zn	0.38	0.17	0.06	0.17	0.06									
Ti	0.87	0.17	0.16	0.17	0.28	0.29								
Cu	0.81	0.06	0.07	0.07	0.13	0.43	0.81							
Ba	0.47	0.04	0.03	0.06	0.04	0.29	0.60	0.50						
Sb	0.01	0.03	0.01	0.02	0.05	0.05	0.01	0.03	0.00					
Sr	0.01	0.13	0.13	0.19	0.04	0.03	0.00	0.00	0.00	0.00				
Cr	0.01	0.01	0.02	0.06	0.00	0.02	0.03	0.01	0.00	0.02	0.04			
Mn	0.19	0.00	0.01	0.04	0.02	0.17	0.35	0.31	0.23	0.00	0.00	0.04		
Zr	0.52	0.00	0.01	0.00	0.03	0.22	0.48	0.65	0.21	0.06	0.01	0.05	0.30	
Mo	0.02	0.13	0.09	0.21	0.09	0.04	0.03	0.00	0.01	0.02	0.00	0.02	0.05	0.14

Table 2-8: Squared Pearson correlation coefficient (r^2) among ΔPM2.5 elements at the I-710 location. Note dark green color denotes high correlations and light green color denote intermedia correlations.

	Fe	Si	Ca	Al	K	Zn	Ti	Cu	Ba	Sb	Sr	Cr	Mn	Zr
Fe														
Si	0.55													
Ca	0.55	0.54												
Al	0.45	0.34	0.61											
K	0.62	0.89	0.69	0.49										
Zn	0.20	0.23	0.26	0.06	0.25									
Ti	0.02	0.00	0.09	0.18	0.02	0.33								
Cu	0.34	0.31	0.17	0.18	0.25	0.01	0.14							
Ba	0.15	0.07	0.02	0.01	0.03	0.00	0.42	0.39						
Sb	0.08	0.17	0.25	0.33	0.23	0.03	0.00	0.28	0.04					
Sr	0.03	0.03	0.06	0.04	0.03	0.18	0.30	0.15	0.13	0.05				
Cr	0.32	0.33	0.37	0.22	0.41	0.32	0.13	0.10	0.01	0.09	0.09			
Mn	0.09	0.31	0.00	0.01	0.26	0.11	0.01	0.06	0.00	0.03	0.17	0.19		
Zr	0.00	0.04	0.12	0.03	0.06	0.34	0.05	0.00	0.02	0.02	0.05	0.06	0.00	
Mo	0.12	0.57	0.11	0.03	0.35	0.32	0.00	0.10	0.03	0.04	0.08	0.33	0.44	0.12

The temporal correlation causes difficulty in differentiating between brake and tire wear particles even after background subtraction. However, the fact that Ba having the lowest correlation with Zn among the brake wear indicators might help separate brake and tire wear contributions. Previous work by Wang et al. (2021) reported hourly resolution metal correlations for near road environments where Ti and Fe were shown to correlate with wind speed and relative humidity indicating influence of road dust resuspension. These elements were also correlated with brake wear markers Ba, Cu, and Sr, which indicates that they can originate from road dust resuspension in addition to direct emission from vehicles. Wang et al. (2021) suggested that Ba can be a better indicator for diesel vehicles based on a weak positive correlation to heavy duty vehicles as compared to weak negative correlations with copper observed at their high-traffic highway sampling location. In this study, moderate correlations ($r^2 \approx 0.7$) were observed between brake wear markers and the tire wear marker Zn. However, Ba had the lowest correlation with Zn among the brake wear elements. Ba is reported to comprise a large increment of measured roadside concentrations in London by Gietl et al. (2010). The size range of Ba is stated to be between 2.2 and 3.7 μm; however, different driving patterns and brake temperatures are suspected to change the existing modes to 1.2–2.2 μm and 3.7–7.2 μm. The fine particle sizes could occur due to volatilization of metals under high brake temperatures while larger sizes are generated through the mechanical abrasion (Garg et al., 2000; Thorpe and Harrison, 2008).

In this study, the ΔPM2.5 Ba concentrations were examined in relation to crosswind speeds during the sampling period. Crosswind direction vectors perpendicular to the highway were calculated to obtain wind speeds flowing from the upwind to the downwind sites. Figure 2-9a shows ΔPM2.5 Ba concentration against crosswind speeds at the I-5 location in Anaheim. Ba concentrations tracked the crosswind speed on 1/28, 1/29, 1/30, and 2/1. Opposing trends, however, occurred on 1/31, 2/2, and 2/3. The crosswind speeds varied and changed directions during the 1000–1400 LST period on each test date except for 2/6. The crosswind speeds had a weak correlation (r^2 = 0.3) with ΔPM2.5 Ba concentration at the I-5 location (Figure 2-10b). Except for two data points, the ΔPM2.5 Ba concentrations were positive (downwind concentrations higher than upwind concentrations) when crosswind speed was positive (wind blowing from upwind to downwind sites), and negative when wind speed was negative. An even lower correlation between crosswind speeds and ΔPM2.5 concentration (r^2 =0.14) was observed at the I-5 location (Figure 2-10a). A higher wind speed may increase road dust emission rates, but it enhances dispersion simultaneously that lowers ambient PM levels. The two competing mechanisms explain the low correlations between crosswind speeds and ΔPM2.5 Ba or mass concentrations. The I-710 location showed slightly higher concentrations of Ba in the downwind measurement site resulting in only positive ΔPM2.5 Ba concentrations throughout the monitoring period (Figure 2-9b). The impact of wind speed on exposure concentrations at an urban street environment has been studied by Hu et al. (2022). They analyzed ambient PM2.5 and PM10 exposure with background correction under different wind directions and found the highest exposure concentrations occurring during calm/light air wind speed <1.5 m/s. At medium and high wind speeds, decreased exposure concentrations occurred possibly due to wind-dilution effects.

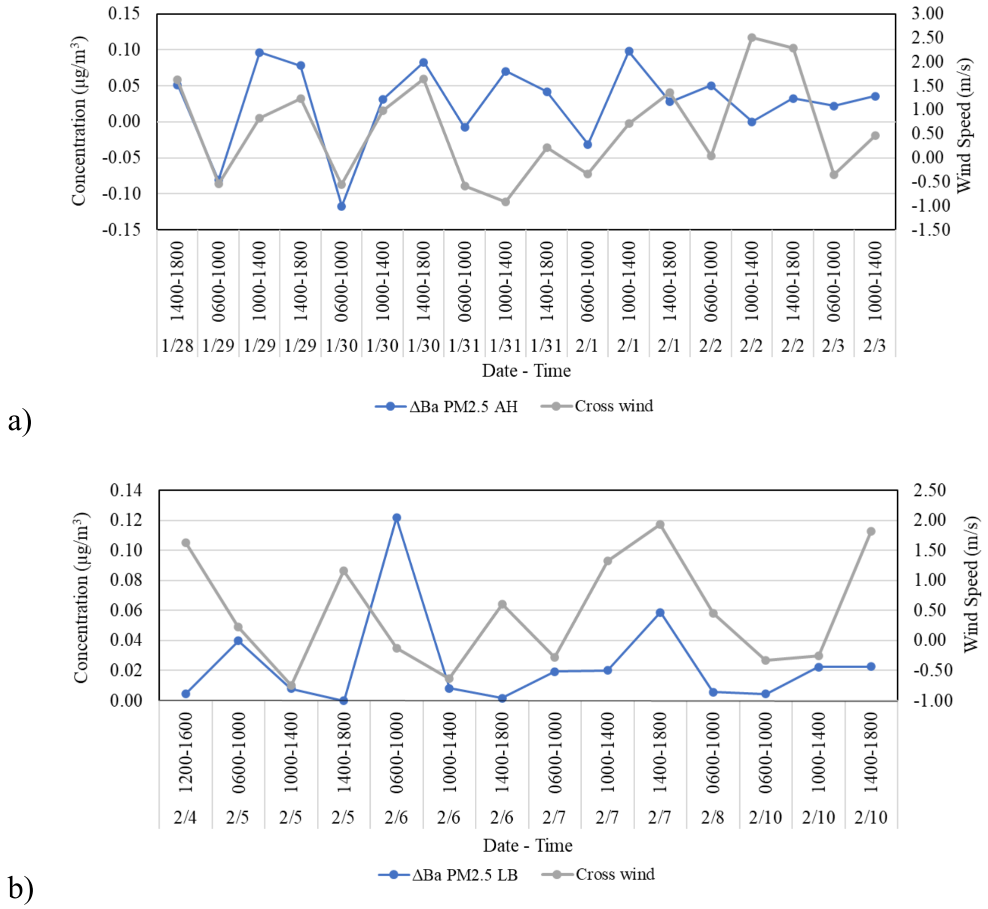

Figure 2-9: Four-hour average ΔPM2.5 concentration of Barium and cross wind speed at (a) I-5 Anaheim and (b) I-710 Long Beach.

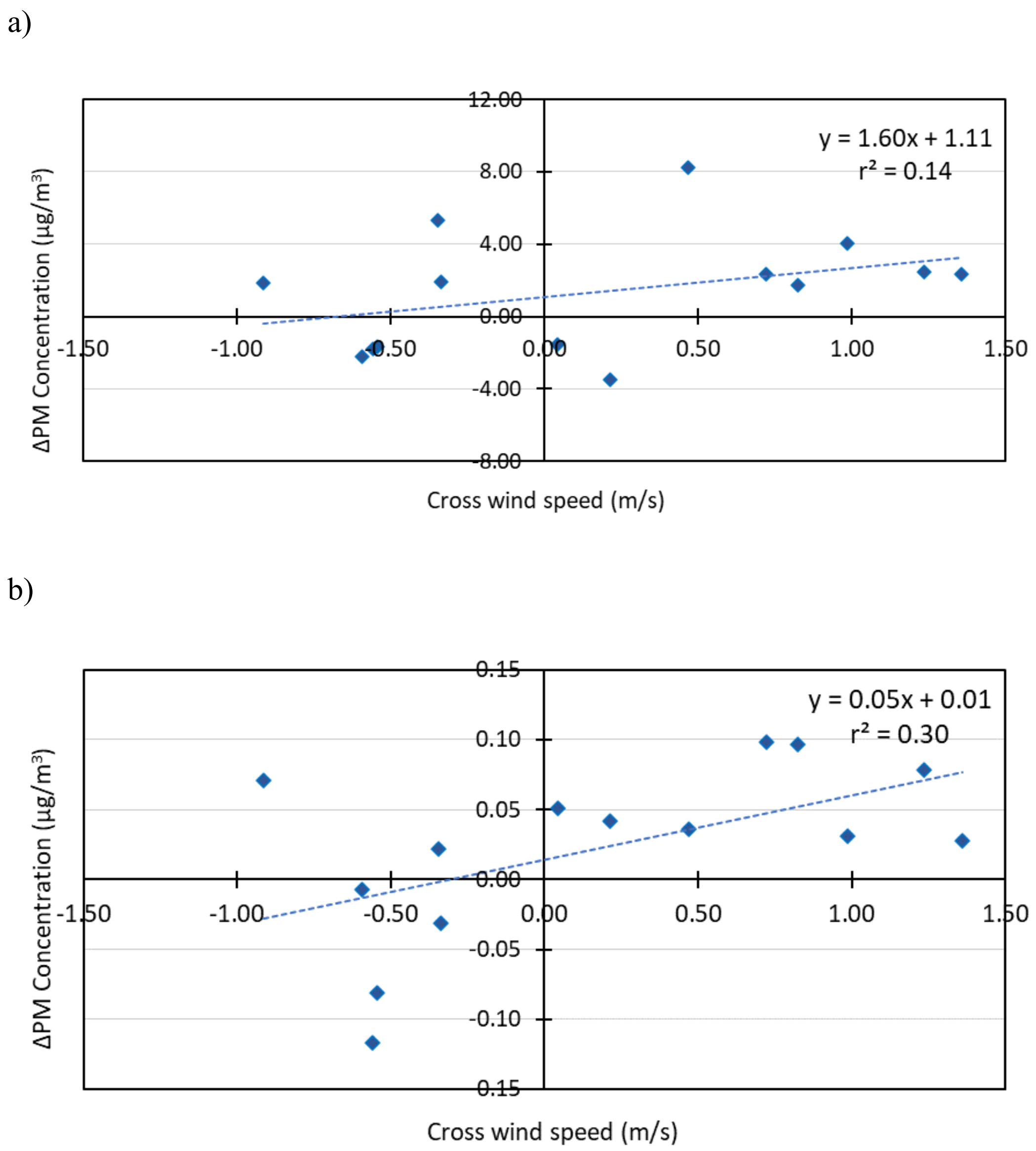

Figure 2-10: Crosswind speed versus a) total ΔPM2.5 and b) ΔPM2.5 Ba concentration at the I-5 highway location.

Figure 2-11 shows hourly PM2.5 elemental concentrations of brake wear markers Ti, Cu, and Fe along with the tire wear marker Zn at the I-5 downwind site measured by a Horiba PX-375 unit. The element Ba was not quantified by the PX-375 units. Ti and Cu concentrations consistently remain below 0.12 µg/m^3 while Fe varied from 0.10 to 0.90

μg/m^3. Fe had reoccurring peaks above 0.80 μg/m^3 near morning rush hour of 0700–0800 LST of the sampling dates from 1/28 to 1/31. Secondary Fe peaks with concentrations ranging from 0.48 to 0.59 μg/m^3 occurred between the afternoon rush hours of 1400–1600 LST as well as between the 2200–2400 LST hours. Lower Fe peaks on 2/1 (Sat) and 2/2 (Sun) is possibly due to lower traffic during the weekend. These findings agree with those by Wang et al. (2021) in their analysis of temporal variations of metal concentrations between weekday and Sunday measurements at an urban roadway and at a highway in Canada over a three year period (2015–2018). Fe is shown to have weekday/Sunday emission factor ratios of approximately greater than two while Zn had ratios near four at both locations. In this result, Zn peaks coincided with Fe peaks on 1/31, but other high peaks of Zn lagged behind the Fe peaks on 1/29 and 1/30. Zn peak showed a high concentration near 1.4 μg/m^3 on the 0800 to 0900 LST of 1/30.

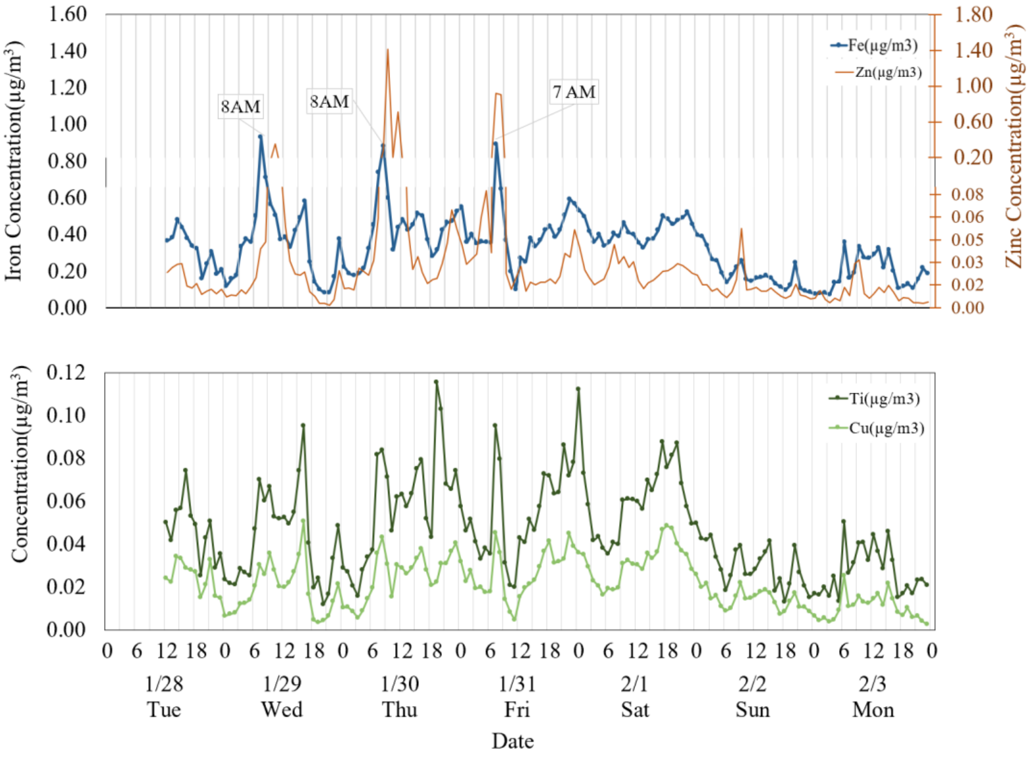

Figure 2-11: Hourly PM2.5 elemental concentration for brake (Fe, Ti, Cu) and tire (Zn) markers.

2.3.2 Particle size distributions

Hourly averaged particle distributions were collected for limited sampling dates and times depending on the availability and status of the HRELPI+. Number size distributions are shown in Figure 2-12 for 1/28 during the 1200–1400 LST. A trimodal distribution with a main submicron mode centered near 0.014 μm, a significant coarse mode centered near 6.5 μm, and a smaller but non-negligible mode centered near 2.1 μm was observed. The submicron mode can be related in the order of the exhaust particles, urban background particles, and brake and tire wear particles. It is speculated that the mode at 2.1 μm is brake wear particles generated from mechanical friction as the mode diameter is very close to what were reported in the brake dynamometer studies (Stanard et al., 2021). The third mode with 6.5 μm mode diameter is assumed to relate with the resuspended road dust particles. Hourly averaged mass distribution was converted from the number distribution at the I-5 downwind site during 1/ 28. As shown in Figure 2-13, the mass mode diameters were around 0.25 and 7 μm. Particle number and mass distributions measured from the downwind site of I-710 during 1200–1600 LST on 2/6 are shown in Figure 2-14 and Figure 2-15. Similar to the size distributions at the I-5 site, the particle number distributions were trimodal, with peak concentrations near $6.0 \cdot 10^4$ particle/cm^3, $7.8 \cdot 10^{-2}$ particle/cm^3, and 1.31 particle/cm^3 at the 0.15, 2.0 and 7 μm mode diameters, respectively. The particle mass distributions had bimodal characteristics with a maximum near ~7 μm.

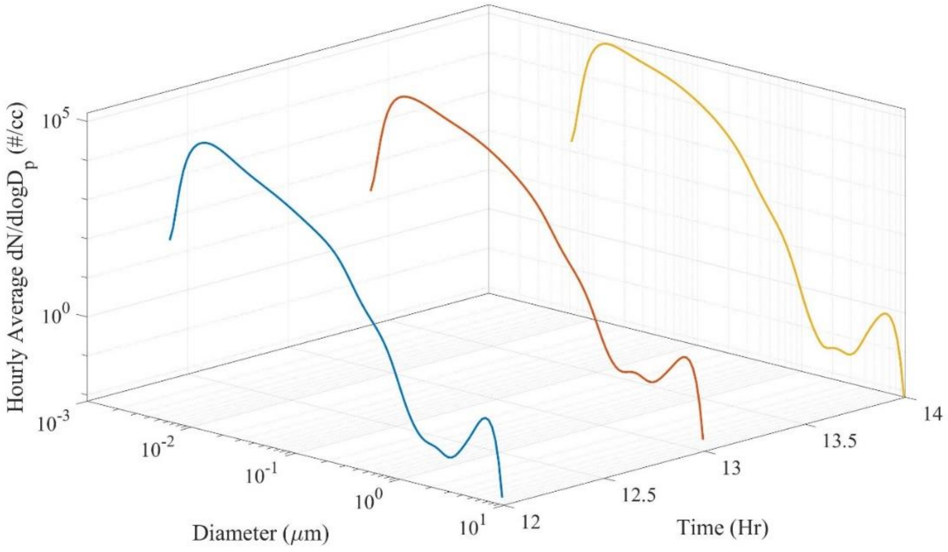

Figure 2-12: Hourly averaged particle number distribution at the I-5 downwind site on January 28, 2020.

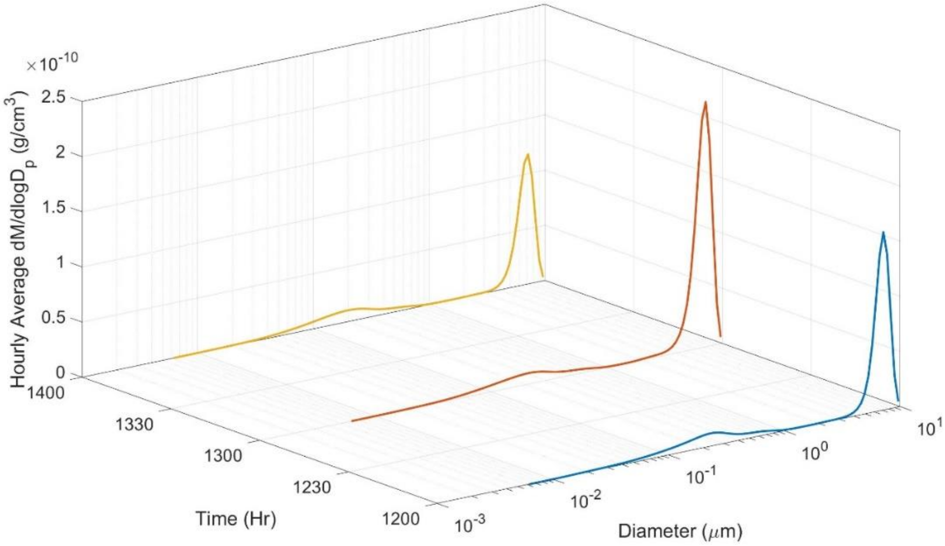

Figure 2-13: Particle mass distribution measured by ELPI at the I-5 highway on January 28, 2020.

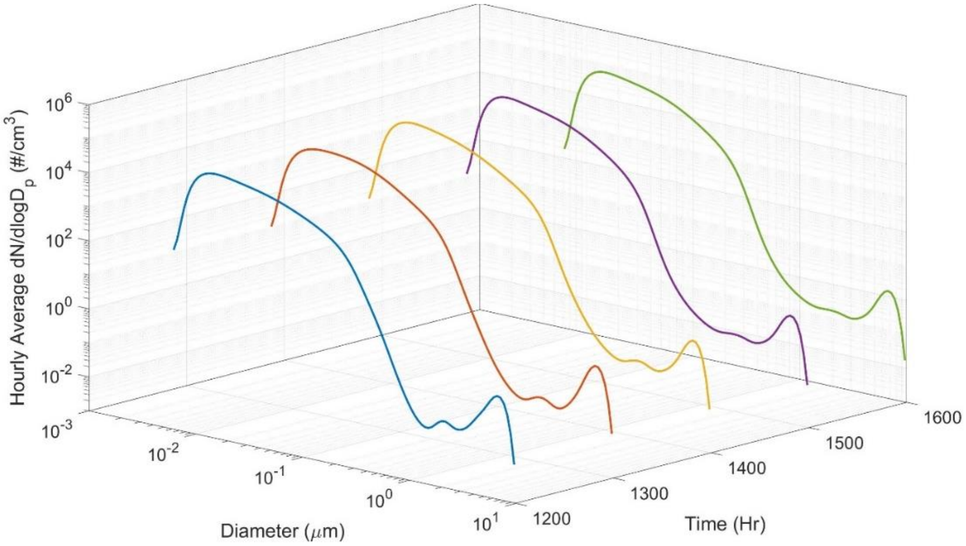

Figure 2-14: Particle number distribution measured by ELPI at the I-710 highway on February 6, 2020.

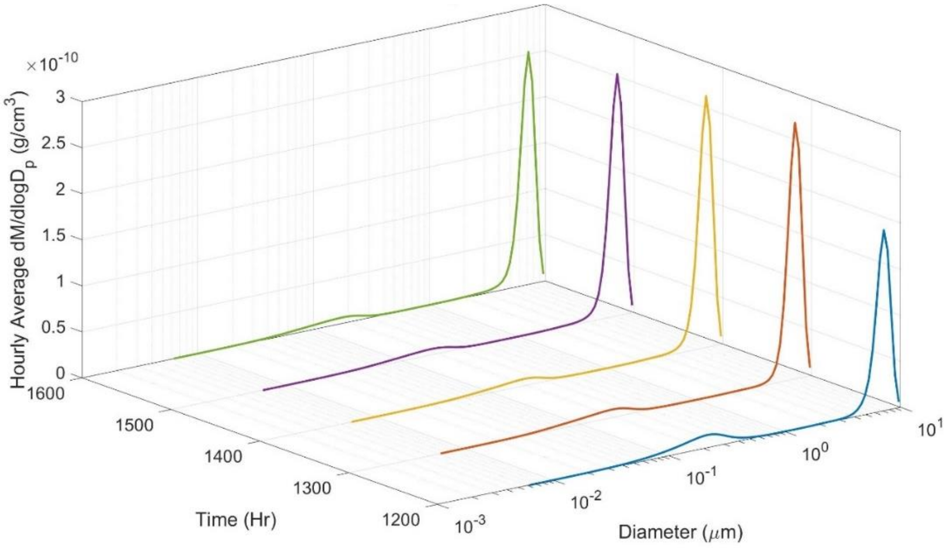

Figure 2-15: Particle mass distribution measured by ELPI at the I-710 highway on February 6, 2020.

Figure 2-16 shows size resolved time series plots of HRELPI+ data. Size bins centered at 0.014, 0.104, 2.18 and 6.64 μm were chosen to represent nucleation, accumulation, brake, and tire/dust modes, respectively. Cross wind speed is also plotted at the bottom of the figure. The nucleation and accumulation modes in the sub-micrometer range show different temporal patterns as their formation processes are different (homogeneous nucleation of semi volatile species during atmospheric dilution vs. soot formation from engines). There was one outstanding incidence when three modes (accumulation, brake, and tire/dust) spiked together around 13:32. Wind data does not report any abrupt gust and therefore we speculate this high emitting event has occurred on the highway at that moment. Excluding this one exceptional incidence, brake and tire mode particles show no significant correlation with nucleation and accumulation modes. Figure 2-17 further investigated correlations among different modes in detail. Figure 2-17a shows that accumulation and brake modes are independent as expected. Interestingly, Figure 2-17b shows that brake and tire/dust modes are highly correlated. We speculate tire/dust and brake particles may have correlation for a few of reasons: (1) both brake and tire particles are generated during braking events due to abrasion; (2) they have partially overlapped size ranges; and (3) resuspended particles may transport together. Further investigation will warrant deeper understanding on the transport of non-tailpipe particle emissions.

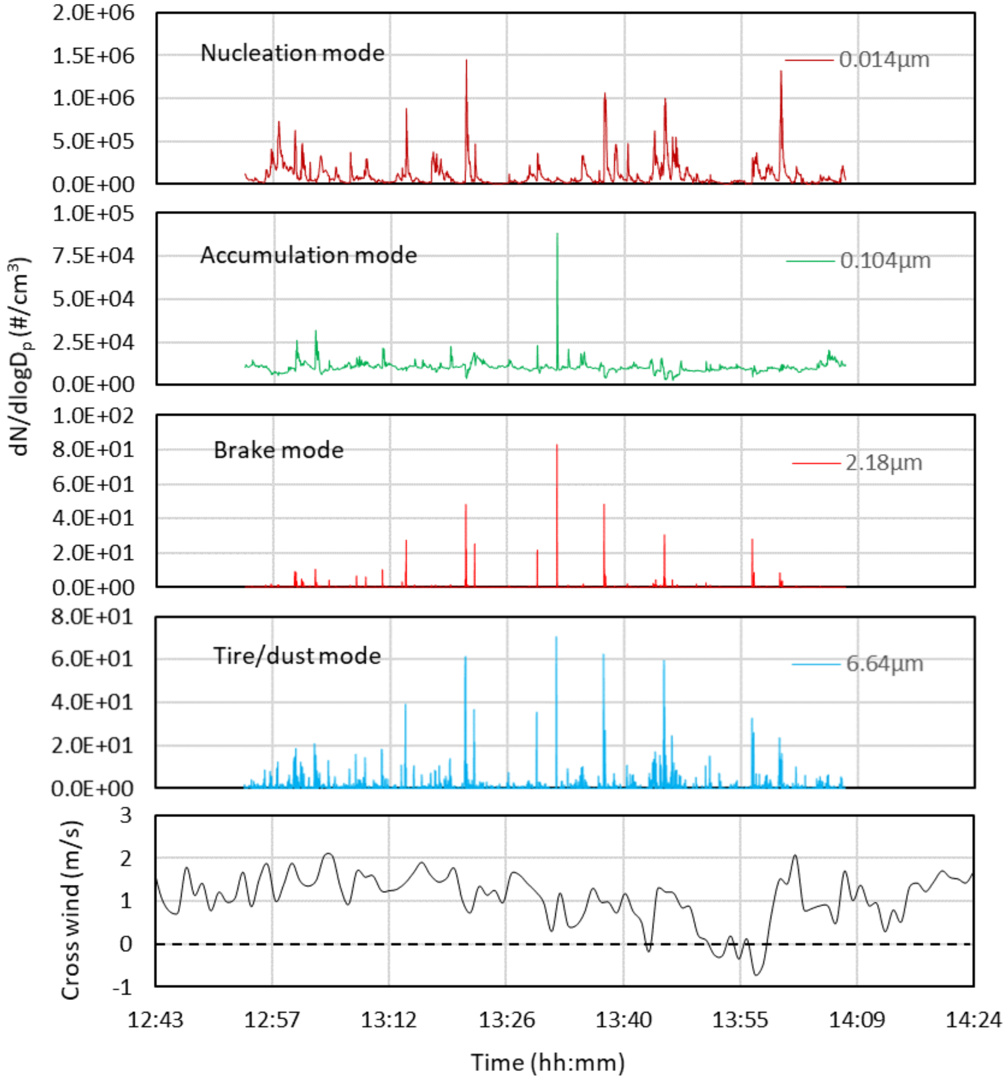

Figure 2-16: Size classified time series plots for HRELPI+ measured particle number size distribution at the I-5 downwind site on January 28, 2020. The legend denotes the size bin at HRELPI+. Cross wind data are included.

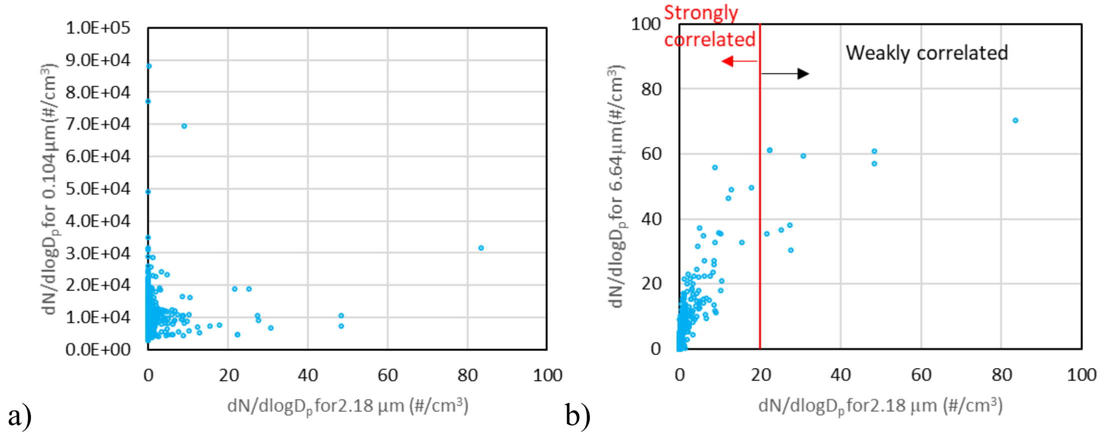

a) b)

Figure 2-17: (a) Correlation between accumulation mode and brake mode particles (b) correlation between brake mode and tire/dust mode particles (brake and tire mode are strongly correlated at low concentrations of brake mode particles).

2.3.3 Mass size distributions by elements

MOUDI samples were analyzed and mass size distributions by element were plotted in Figure 2-18. The size-segregated elemental concentrations are compared between the two near road sites and an urban background site in Irvine, CA. The peak concentrations of elements were in the order of Si, Al, Ca, Fe, K, Zn, Ti, Cu, Ba, Mn, Zr, Sr, Sb, and Mo and this order is similar to the order shown in Figure 2-7. The concentrations of most elements were the highest near I-5 and the lowest at the Irvine site, indicating strong influence of traffic related emissions near highways. The concentrations of nominal resuspended road dust markers Al and Si in the 1-10 µm size range at the I-5 downwind site were 2-3 times higher than those near I-710 and more than 4 times higher than those in Irvine. The concentrations of brake wear markers Cu, Zr, and Ba were 1.5–4 times higher at the I-5 site than those at I-710 and 2–10 times higher than those in Irvine across all size ranges. Ba is a marker of brake wear particles and mass concentration peaked 3.2–10 µm bin at both near-road locations. Considering the size shift between mass and number distribution, this is consistent with brake mode which peaked at 2.1 µm bin in number distribution. Ba was broadly present above 0.56 µm at the background location. Sb is another well-known marker for brake wear particles. It peaks at 3.2–10 µm bin in the near-road location as expected. It is unsure why Sb concentration in the background location was similar to that of near-road location. Zn is a well-known marker for tire wear particles. Zn can also be found in exhaust particles originating from lube oil (Jung et al., 2003). Zn peaks at 10–18 µm bin are likely from tire wear due to their sizes. Zn present below 0.56 µm is likely from engine exhaust. Zn peaks at 0.56–1 µm can be possibly from both brake and tire wear but further investigation is necessary. Zn concentrations near I-5 were 1.8 times higher than those near I-710 and 2 times higher than those in Irvine for the 1-10 µm size ranges. As a result, non-exhaust exposures are greater in the near road environment than in the urban background environment. Multiple tire elements (Ti, Mn, and Sr) showed peaks at 10–18 µm bin. O'Loughlin et al. (2023) analyzed 60 car tires and reported metals are present in the order of Zn, Al, Fe, Mg, Ti, Cu, Ba, Pb, Ni, Sn, Sr, and Mn.

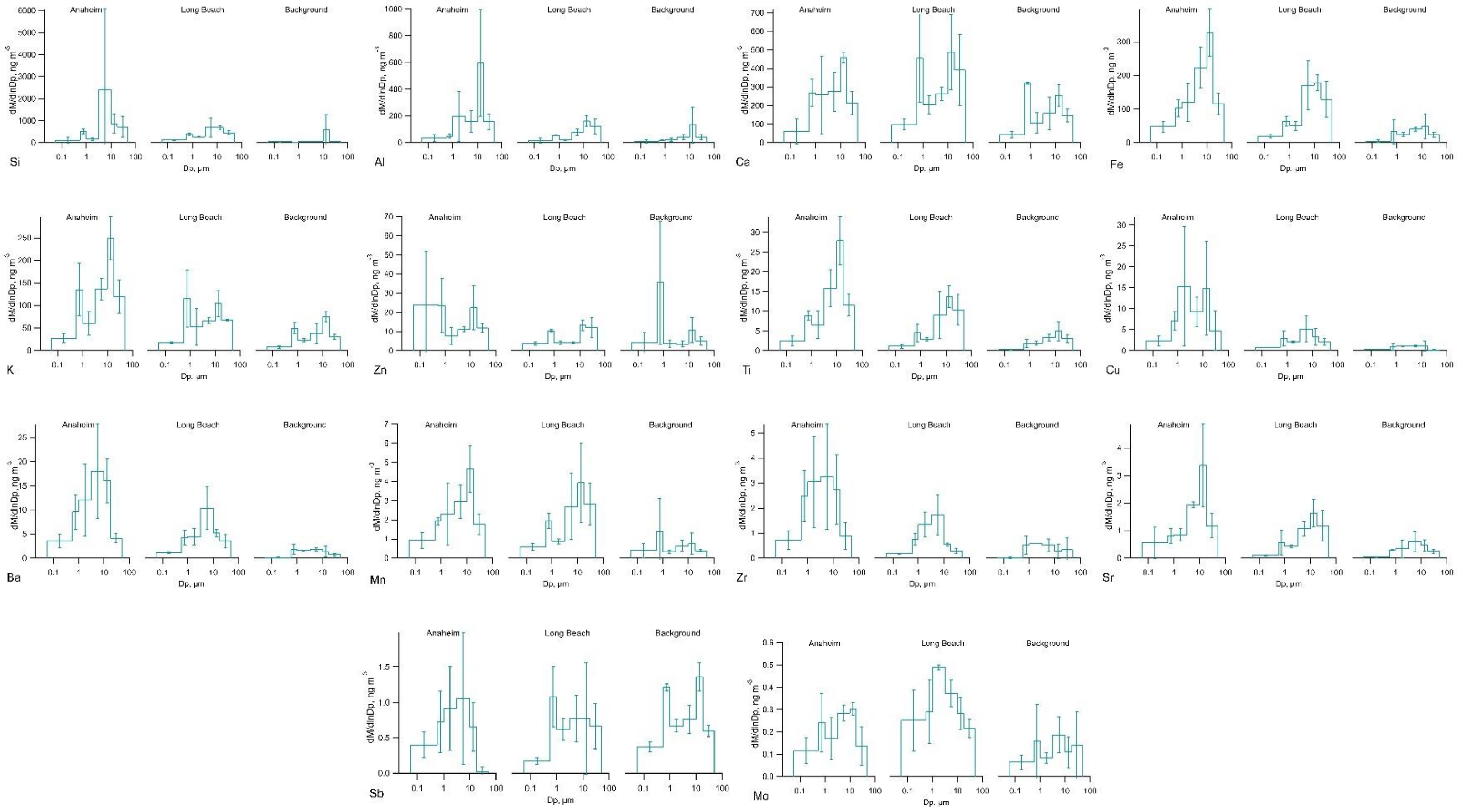

Figure 2-18: Mass size distribution by element at two near-road locations (downwind sites in Anaheim and Long Beach) and one background location (Campus of University of California, Irvine).

2.4 Conclusion

Non-tailpipe emissions are becoming more important with increasing implementation of zero emission vehicles and reducing tailpipe emissions in California and around the world. This study analyzed metal composition and size distributions of PM2.5 and PM10 at near-roadway environments where non-tailpipe emissions are significant. Background subtraction was estimated by placing instruments at a nominal upwind site while simultaneously measuring across the highway at a nominal downwind site. Two major highways in California were selected to represent different fleet compositions. Si and Fe were the two most abundant elements measured at both locations. Si is likely from road dust as it had strong correlations with crustal elements Ca, Al, and K. Fe had strong correlations with other brake wear markers, indicating their common origin of brake wear. While correlation analysis provides qualitative indication of sources of elements in PM2.5 and PM10, more quantitative source apportionment using chemical mass balance receptor modeling is reported in a separate publication Chen et al. (2023). Moderate correlations existed between brake markers and the tire wear marker Zn; however, Ba had the weakest correlation with the tire wear marker. The source of Ba is likely explained by the composition of brake materials and is cited to be a good indicator of brake wear by previous studies. Among the trimodal particle number distributions, the submicron mode assumed to be tailpipe exhaust and heat-generated wear particles, the mode centered at 2.1 µm is assumed to be brake wear, and the coarse mode centered at 6.5 µm is assumed to be from tire/road dust. The mode centered around 7 µm of mass distributions is likely a mixture of brake and tire wear and road dust. Further evaluation of size classified time plots of particle distributions showed no significant correlation between the nucleation and accumulation modes with brake (2.18µm) and tire (6.64µm) modes. The brake mode and tire mode were highly correlated to each other indicating that particles may be generated through abrasion, overlapping in size ranges, and may be transported together after generation. Mass size distribution by element from MOUDI samples showed tire markers in the size range above 10 µm and brake markers in the size range of 1–10 µm. Additional investigation is needed to analyze the effect of vehicle parameters, such as weight and regenerative braking, and their effect on non-tailpipe emissions.

Fe and Si correlations weaken when background influence was removed, indicating that they may not come from a common traffic-related source. Background removal also caused increases in correlations between Fe and other common brake wear markers Ti, Cu, Ba, Mn, Zr, and Zn ($0.67 < r^2 < 0.90$). The fact that brake wear markers showed similar variability for ΔPM10 Ti vs. Cu, Fe vs. Ti, and Fe vs. Cu at $r^2 = 0.90$ with moderate associations with Ba and Zr further confirm their common brake wear sources.

Observing higher resolution data, the PX-375 units measured hourly PM2.5 elemental concentrations over 24 h each day. Although Ba was not measured by these units, other non-tailpipe markers such as Fe for brake wear and Zn for tire wear showed cyclic peaks over three consecutive days during 0800–1000 LST. Higher concentrations were observed during weekdays compared to the weekend measurements.

2.5 References

Abu-Allaban, Mahmoud, John A. Gillies, Alan W. Gertler, Russ Clayton, and David Proffitt. 2003. "Tailpipe, Resuspended Road Dust, and Brake-Wear Emission Factors from on-Road Vehicles." *Atmospheric Environment* 37 (January):5283–93. https://doi.org/10.1016/j.atmosenv.2003.05.005.

Adachi, Kouji, and Yoshiaki Tainosho. 2004. "Characterization of Heavy Metal Particles Embedded in Tire Dust." *Environment International* 30 (8): 1009–17. https://doi.org/10.1016/j.envint.2004.04.004.

Apeagyei, Eric, Michael Bank, and John Spengler. 2011. "Distribution of Heavy Metals in Road Dust Along an Urban-Rural Gradient in Massachusetts." *Atmospheric Environment - ATMOS ENVIRON* 45 (April):2310–23. https://doi.org/10.1016/j.atmosenv.2010.11.015.

Blau, P. J. 2001. "Compositions, Functions, and Testing of Friction Brake Materials and Their Additives." ORNL/TM-2001/64. Oak Ridge National Lab. (ORNL), Oak Ridge, TN (United States). https://doi.org/10.2172/788356.

Cadle, S.H., and R.L. Williams. 1978. "Gas and Particle Emissions from Automobile Tires in Laboratory and Field Studies." *Journal of the Air Pollution Control Association* 28 (5): 502–7. https://doi.org/10.1080/00022470.1978.10470623.

Caltrans, California Department of Transportation. 2021. "PeMS Data Source | Caltrans." 2021. https://dot.ca.gov/programs/traffic-operations/mpr/pems-source.

Chan, D, and G W Stachowiak. 2004. "Review of Automotive Brake Friction Materials." *Proceedings of the Institution of Mechanical Engineers, Part D: Journal of Automobile Engineering* 218 (9): 953–66. https://doi.org/10.1243/0954407041856773.

Chen, L. -W. Antony, Xiaoliang Wang, Brenda Lopez, Guoyuan Wu, Steven Sai Hang Ho, Judith C. Chow, John G. Watson, Qi Yao, Seungju Yoon, and Heejung Jung. 2023. "Contributions of Non-Tailpipe Emissions to near-Road PM2.5 and PM10: A Chemical Mass Balance Study." *Environmental Pollution* 335 (October):122283. https://doi.org/10.1016/j.envpol.2023.122283.

Cohen, Aaron J., Michael Brauer, Richard Burnett, H. Ross Anderson, Joseph Frostad, Kara Estep, Kalpana Balakrishnan, et al. 2017. "Estimates and 25-Year Trends of the Global Burden of Disease Attributable to Ambient Air Pollution: An Analysis of Data from the Global Burden of Diseases Study 2015." *The Lancet* 389 (10082): 1907–18. https://doi.org/10.1016/S0140-6736(17)30505-6.

Dannis, M. L. 1974. "Rubber Dust from the Normal Wear of Tires." *Rubber Chemistry and Technology* 47 (4): 1011–37. https://doi.org/10.5254/1.3540458.

Erika, Matsumoto. 2018. "Feature Article: Continuous Particulate Monitor with X-Ray Fluorescence PX-375 - HORIBA." *Readout Horiba Technical Reports*, no. No.50 (September). https://www.horiba.com/kr/publications/readout/article/feature-article-continuous-particulate-monitor-with-x-ray-fluorescence-px-375-59191/.

Fang, Ting, Brian C. H. Hwang, Sukriti Kapur, Katherine S. Hopstock, Jinlai Wei, Vy Nguyen, Sergey A. Nizkorodov, and Manabu Shiraiwa. 2023. "Wildfire Particulate Matter as a Source of Environmentally Persistent Free Radicals and Reactive Oxygen Species." *Environmental Science: Atmospheres* 3 (3): 581–94. https://doi.org/10.1039/D2EA00170E.

Garg, Bhagwan D., Steven H. Cadle, Patricia A. Mulawa, Peter J. Groblicki, Chris Laroo, and Graham A. Parr. 2000. "Brake Wear Particulate Matter Emissions." *Environmental Science & Technology* 34 (21): 4463–69. https://doi.org/10.1021/es001108h.

Gietl, Johanna K., Roy Lawrence, Alistair J. Thorpe, and Roy M. Harrison. 2010. "Identification of Brake Wear Particles and Derivation of a Quantitative Tracer for Brake Dust at a Major Road." *Atmospheric Environment* 44 (2): 141–46. https://doi.org/10.1016/j.atmosenv.2009.10.016.

Grigoratos, Theodoros, and Giorgio Martini. 2014. "Non-Exhaust Traffic Related Emissions – Brake and Tyre Wear PM." JRC Publications Repository. June 17, 2014. https://doi.org/10.2790/22000.

———. 2015. "Brake Wear Particle Emissions: A Review." *Environmental Science and Pollution Research* 22 (4): 2491–2504. https://doi.org/10.1007/s11356-014-3696-8.

Gustafsson, Mats, Göran Blomqvist, Anders Gudmundsson, Andreas Dahl, Erik Swietlicki, Mats Bohgard, John Lindbom, and Anders Ljungman. 2008. "Properties and Toxicological Effects of Particles from the Interaction between Tyres, Road Pavement and Winter Traction Material." *The Science of the Total Environment* 393 (May):226–40. https://doi.org/10.1016/j.scitotenv.2007.12.030.

Habre, Rima, Mariam Girguis, Robert Urman, Scott Fruin, Fred Lurmann, Martin Shafer, Patrick Gorski, et al. 2021. "Contribution of Tailpipe and Non-Tailpipe Traffic Sources to Quasi-Ultrafine, Fine and Coarse Particulate Matter in Southern California." *Journal of the Air & Waste Management Association* 71 (2): 209–30. https://doi.org/10.1080/10962247.2020.1826366.

Hu, Haibin, Qinghua Chen, Qingrong Qian, Xingwen Zhou, Yilan Chen, and Yangsheng Cai. 2022. "Field Investigation for Ambient Wind Speed and Direction Effects Exposure of Cyclists to PM2.5 and PM10 in Urban Street Environments." *Building and*

Environment 223 (September):109483. https://doi.org/10.1016/j.buildenv.2022.109483.

Hulskotte, J. H. J., G. D. Roskam, and H. A. C. Denier van der Gon. 2014. "Elemental Composition of Current Automotive Braking Materials and Derived Air Emission Factors." *Atmospheric Environment* 99 (December):436–45. https://doi.org/10.1016/j.atmosenv.2014.10.007.

Hwang, Brian, Ting Fang, Randy Pham, Jinlai Wei, Steven Gronstal, Brenda Lopez, Chas Frederickson, et al. 2021. "Environmentally Persistent Free Radicals, Reactive Oxygen Species Generation, and Oxidative Potential of Highway PM2.5." *ACS Earth and Space Chemistry* 5 (8): 1865–75. https://doi.org/10.1021/acsearthspacechem.1c00135.

Iijima, Akihiro, Keiichi Sato, Kiyoko Yano, Masahiko Kato, Kunihisa Kozawa, and Naoki Furuta. 2008. "Emission Factor for Antimony in Brake Abrasion Dusts as One of the Major Atmospheric Antimony Sources." *Environmental Science & Technology* 42 (8): 2937–42. https://doi.org/10.1021/es702137g.

Iijima, Akihiro, Keiichi Sato, Kiyoko Yano, Hiroshi Tago, Masahiko Kato, Hirokazu Kimura, and Naoki Furuta. 2007. "Particle Size and Composition Distribution Analysis of Automotive Brake Abrasion Dusts for the Evaluation of Antimony Sources of Airborne Particulate Matter." *Atmospheric Environment* 41 (23): 4908–19. https://doi.org/10.1016/j.atmosenv.2007.02.005.

Jia, Zhanfeng, Chao Chen, B. Coifman, and P. Varaiya. 2001. "The PeMS Algorithms for Accurate, Real-Time Estimates of g-Factors and Speeds from Single-Loop Detectors." In *ITSC 2001. 2001 IEEE Intelligent Transportation Systems. Proceedings (Cat. No.01TH8585)*, 536–41. https://doi.org/10.1109/ITSC.2001.948715.

Johansson, Christer, Michael Norman, and Lars Burman. 2009. "Road Traffic Emission Factors for Heavy Metals." *Atmospheric Environment*, Urban Air Quality, 43 (31): 4681–88. https://doi.org/10.1016/j.atmosenv.2008.10.024.

Jung, Heejung, David B. Kittelson, and Michael R. Zachariah. 2003. "The Influence of Engine Lubricating Oil on Diesel Nanoparticle Emissions and Kinetics of Oxidation." SAE Technical Paper 2003-01–3179. Warrendale, PA: SAE International. https://doi.org/10.4271/2003-01-3179.

Keskinen, J., K. Pietarinen, and M. Lehtimäki. 1992. "Electrical Low Pressure Impactor." *Journal of Aerosol Science* 23 (4): 353–60. https://doi.org/10.1016/0021-8502(92)90004-F.

Koupal, John, Allison DenBleyker, Sandeep Kishan, Ravi Vedula, and Carlos Agudelo. 2021. "Brake Wear Particulate Matter Emissions Modeling." Final Report CA21-3232. Eastern Research Group, LINK Engineering.

Kreider, Marisa L., Julie M. Panko, Britt L. McAtee, Leonard I. Sweet, and Brent L. Finley. 2010. “Physical and Chemical Characterization of Tire-Related Particles: Comparison of Particles Generated Using Different Methodologies.” *The Science of the Total Environment* 408 (3): 652–59. https://doi.org/10.1016/j.scitotenv.2009.10.016.

Kulkarni, Pranav, Shankararaman Chellam, James B. Flanagan, and R. K. M. Jayanty. 2007. “Microwave Digestion-ICP-MS for Elemental Analysis in Ambient Airborne Fine Particulate Matter: Rare Earth Elements and Validation Using a Filter Borne Fine Particle Certified Reference Material.” *Analytica Chimica Acta* 599 (2): 170–76. https://doi.org/10.1016/j.aca.2007.08.014.

Mosleh, Mohsen, Peter J Blau, and Delia Dumitrescu. 2004. “Characteristics and Morphology of Wear Particles from Laboratory Testing of Disk Brake Materials.” *Wear* 256 (11): 1128–34. https://doi.org/10.1016/j.wear.2003.07.007.

O’Loughlin, David, Molly Haugen, Jason Day, Andrew Brown, Emma Braysher, Nick Molden, Anne Willis, Marion MacFarlane, and Adam Boies. 2023. “Analysis of Tyre Tread for Metal Tracers with Applications in Environmental Monitoring.” ChemRxiv. https://doi.org/10.26434/chemrxiv-2023-rrc6v.

Panko, Julie, Marisa Kreider, and Kenneth Unice. 2018. “Chapter 7 - Review of Tire Wear Emissions: A Review of Tire Emission Measurement Studies: Identification of Gaps and Future Needs.” In *Non-Exhaust Emissions*, edited by Fulvio Amato, 147–60. Academic Press. https://doi.org/10.1016/B978-0-12-811770-5.00007-8.

Pant, Pallavi, and Roy Harrison. 2013. “Estimation of the Contribution of Road Traffic Emissions to Particulate Matter Concentrations from Field Measurements: A Review.” *Atmospheric Environment* 77 (October):78–97. https://doi.org/10.1016/j.atmosenv.2013.04.028.

Saari, Sampo, Anssi Arffman, Juha Harra, Topi Rönkkö, and Jorma Keskinen. 2018. “Performance Evaluation of the HR-ELPI + Inversion.” *Aerosol Science and Technology* 52 (9): 1037–47. https://doi.org/10.1080/02786826.2018.1500679.

Sanderson, Paul, Juana Maria Delgado-Saborit, and Roy M. Harrison. 2014. “A Review of Chemical and Physical Characterisation of Atmospheric Metallic Nanoparticles.” *Atmospheric Environment* 94 (September):353–65. https://doi.org/10.1016/j.atmosenv.2014.05.023.

Stanard, Alan, Tim DeFries, Cindy Palacios, and Sandeep Kishan. 2021. “Brake and Tire Wear Emissions Project 17RD016 Prepared for the California Air Resources Board and the California Environmental Protection Agency.”

Thorpe, Alistair, and Roy M. Harrison. 2008. “Sources and Properties of Non-Exhaust Particulate Matter from Road Traffic: A Review.” *Science of The Total Environment* 400 (1): 270–82. https://doi.org/10.1016/j.scitotenv.2008.06.007.

Timmers, Victor R. J. H., and Peter A. J. Achten. 2016. “Non-Exhaust PM Emissions from Electric Vehicles.” *Atmospheric Environment* 134 (June):10–17. https://doi.org/10.1016/j.atmosenv.2016.03.017.

Tong, Ruipeng, Jiefeng Liu, Wei Wang, and Yingqian Fang. 2020. “Health Effects of PM2.5 Emissions from on-Road Vehicles during Weekdays and Weekends in Beijing, China.” *Atmospheric Environment* 223 (February):117258. https://doi.org/10.1016/j.atmosenv.2019.117258.

Wahlström, Jens, Lars Olander, and Ulf Olofsson. 2010. “Size, Shape, and Elemental Composition of Airborne Wear Particles from Disc Brake Materials.” *Tribology Letters* 38 (1): 15–24. https://doi.org/10.1007/s11249-009-9564-x.

Wallington, Timothy J., James E. Anderson, Rachael H. Dolan, and Sandra L. Winkler. 2022. “Vehicle Emissions and Urban Air Quality: 60 Years of Progress.” *Atmosphere* 13 (5): 650. https://doi.org/10.3390/atmos13050650.

Wang, Jonathan M., Cheol-Heon Jeong, Nathan Hilker, Robert M. Healy, Uwayemi Sofowote, Jerzy Debosz, Yushan Su, Anthony Munoz, and Greg J. Evans. 2021. “Quantifying Metal Emissions from Vehicular Traffic Using Real World Emission Factors.” *Environmental Pollution* 268 (January):115805. https://doi.org/10.1016/j.envpol.2020.115805.

Wang, Xiaoliang, Steven Gronstal, Brenda Lopez, Heejung Jung, L. -W. Antony Chen, Guoyuan Wu, Steven Sai Hang Ho, et al. 2023. “Evidence of Non-Tailpipe Emission Contributions to PM2.5 and PM10 near Southern California Highways.” *Environmental Pollution* 317 (January):120691. https://doi.org/10.1016/j.envpol.2022.120691.

Yao, Qi. 2021. “Non-Exhaust Emissions Research at the California Air Resources Board.” https://wiki.unece.org/download/attachments/117508405/CARB%20presentation%20PMP%20workshop.pdf?api=v2.

2.1 Appendix

Table 2-9: Statistical summary and minimum detection limit of elements quantified by XRF on gravimetric filter samples at the I-5 downwind location in PM2.5 and PM10.

	I-5 $PM_{2.5}$				I-5 PM_{10}				
	Mean	σ	Min	Max	Mean	SD	Min	Max	MDL
Fe	0.6791	0.2321	0.1923	1.0912	1.8515	0.6754	0.6491	3.2929	0.024
Si	0.5601	0.2968	0.0992	1.1708	2.2352	1.0472	0.5268	4.1411	0.012
Ca	0.2884	0.1337	0.0869	0.5513	1.0434	0.4775	0.3140	2.0856	0.014
S	0.2660	0.1357	0.1096	0.6223	0.5339	0.2840	0.1877	0.8036	0.003
Al	0.1844	0.1088	0.0203	0.4042	0.7670	0.3734	0.1905	1.4051	0.057
K	0.1133	0.0403	0.0650	0.1893	0.3681	0.1378	0.1868	0.5880	0.003
Zn	0.1034	0.1433	0.0160	0.4651	0.1599	0.2000	0.0326	0.7015	0.004
Cl	0.0943	0.0820	0.0178	0.3506	0.6537	0.6809	0.0463	2.9077	0.003
Ti	0.0445	0.0151	0.0127	0.0676	0.1458	0.0506	0.0533	0.2426	0.004
Cu	0.0353	0.0101	0.0162	0.0517	0.0839	0.0267	0.0433	0.1270	0.003
V	0.0001	0.0003	0.0000	0.0011	0.0002	0.0006	0.0000	0.0024	0.000
Ni	0.0032	0.0025	0.0003	0.0108	0.0020	0.0014	0.0001	0.0062	0.001
Ba	0.0682	0.0359	0.0000	0.1430	0.1784	0.0654	0.0777	0.2939	0.046
Sb	0.0052	0.0059	0.0000	0.0241	0.0147	0.0116	0.0001	0.0439	0.015
Rb	0.0009	0.0011	0.0000	0.0035	0.0020	0.0014	0.0000	0.0048	0.005
Sr	0.0033	0.0023	0.0000	0.0083	0.0117	0.0066	0.0026	0.0273	0.004
Cr	0.0035	0.0032	0.0000	0.0127	0.0027	0.0018	0.0000	0.0077	0.002
Mn	0.0127	0.0051	0.0059	0.0222	0.0306	0.0114	0.0088	0.0556	0.008
As	0.0011	0.0019	0.0000	0.0064	0.0010	0.0019	0.0000	0.0045	0.003
Pb	0.0010	0.0021	0.0000	0.0068	0.0021	0.0022	0.0000	0.0077	0.010
Co	0.0030	0.0018	0.0000	0.0075	0.0084	0.0041	0.0006	0.0158	0.003
P	0.0000	0.0000	0.0000	0.0000	0.0005	0.0014	0.0000	0.0057	0.004
Sc	0.0010	0.0042	0.0000	0.0185	0.0023	0.0068	0.0000	0.0274	0.060
Ga	0.0014	0.0030	0.0000	0.0100	0.0003	0.0011	0.0000	0.0050	0.003
Se	0.0003	0.0005	0.0000	0.0018	0.0003	0.0008	0.0000	0.0028	0.005
Br	0.0034	0.0022	0.0001	0.0082	0.0055	0.0033	0.0002	0.0128	0.006
Y	0.0006	0.0008	0.0000	0.0025	0.0006	0.0008	0.0000	0.0025	0.005
Zr	0.0190	0.0099	0.0000	0.0353	0.0553	0.0210	0.0260	0.0842	0.008
Nb	0.0033	0.0033	0.0000	0.0121	0.0016	0.0019	0.0000	0.0063	0.006
Mo	0.0016	0.0022	0.0000	0.0070	0.0012	0.0021	0.0000	0.0060	0.005
Pd	0.0015	0.0029	0.0000	0.0115	0.0008	0.0019	0.0000	0.0077	0.021
Ag	0.0003	0.0009	0.0000	0.0036	0.0016	0.0055	0.0000	0.0241	0.024
Cd	0.0048	0.0088	0.0000	0.0321	0.0069	0.0089	0.0000	0.0363	0.016

In	0.0038	0.0048	0.0000	0.0162	0.0033	0.0046	0.0000	0.0162	0.017
Sn	0.0031	0.0041	0.0000	0.0128	0.0095	0.0104	0.0000	0.0364	0.013
Cs	0.0131	0.0116	0.0000	0.0333	0.0072	0.0074	0.0000	0.0257	0.059
La	0.0172	0.0160	0.0000	0.0474	0.0120	0.0121	0.0000	0.0341	0.108
Ce	0.0191	0.0203	0.0000	0.0690	0.0182	0.0230	0.0000	0.0687	0.100
Sm	0.0405	0.0364	0.0000	0.1031	0.0104	0.0151	0.0000	0.0448	0.148
Eu	0.0334	0.0316	0.0000	0.0913	0.0179	0.0261	0.0000	0.0739	0.174
Tb	0.0140	0.0372	0.0000	0.1500	0.0000	0.0000	0.0000	0.0000	0.195
Hf	0.0000	0.0000	0.0000	0.0000	0.0000	0.0000	0.0000	0.0000	0.136
Ta	0.0000	0.0000	0.0000	0.0000	0.0000	0.0000	0.0000	0.0000	0.136
W	0.0074	0.0149	0.0000	0.0474	0.0221	0.0467	0.0000	0.1548	0.019
Ir	0.0000	0.0000	0.0000	0.0000	0.0000	0.0000	0.0000	0.0000	0.023
Au	0.0044	0.0039	0.0000	0.0115	0.0048	0.0037	0.0000	0.0115	0.010
Hg	0.0008	0.0017	0.0000	0.0067	0.0017	0.0026	0.0000	0.0095	0.012
Tl	0.0016	0.0019	0.0000	0.0069	0.0014	0.0020	0.0000	0.0071	0.007
U	0.0030	0.0038	0.0000	0.0146	0.0088	0.0049	0.0000	0.0167	0.015

Table 2-10: Statistical summary and minimum detection limit of elements quantified by XRF on gravimetric filter samples at the I-710 downwind location in PM2.5 and PM10.

	I-710 $PM_{2.5}$				I-710 PM_{10}				
	Mean	SD	Min	Max	Mean	SD	Min	Max	MDL
Fe	0.5119	0.2201	0.2432	0.9792	1.5073	0.6731	0.7861	3.0281	0.024
Si	0.4996	0.2169	0.1180	0.9182	1.9171	0.8534	0.8673	3.6352	0.012
Ca	0.2085	0.0978	0.0392	0.3759	0.7793	0.3419	0.3852	1.4820	0.014
S	0.2534	0.2058	0.1186	0.9692	0.4117	0.2342	0.2158	1.1866	0.003
Al	0.1747	0.1043	0.0156	0.4247	0.6951	0.3440	0.2832	1.4911	0.057
K	0.0956	0.0442	0.0393	0.1893	0.3036	0.1197	0.1530	0.5247	0.003
Zn	0.0341	0.0138	0.0193	0.0671	0.0654	0.0311	0.0301	0.1301	0.004
Cl	0.3961	1.2506	0.0071	4.9022	0.7117	1.4677	0.0688	5.9721	0.003
Ti	0.0513	0.0592	0.0084	0.2545	0.1372	0.1326	0.0391	0.5754	0.004
Cu	0.0190	0.0091	0.0092	0.0392	0.0465	0.0256	0.0188	0.1023	0.003
V	0.0016	0.0051	0.0000	0.0199	0.0027	0.0058	0.0000	0.0225	0.000
Sc	0.0058	0.0091	0.0000	0.0306	0.0034	0.0054	0.0000	0.0162	0.060
Cr	0.0016	0.0015	0.0000	0.0048	0.0055	0.0054	0.0000	0.0175	0.002
Mn	0.0127	0.0057	0.0047	0.0218	0.0293	0.0121	0.0122	0.0565	0.008
P	0.0003	0.0010	0.0000	0.0037	0.0002	0.0007	0.0000	0.0026	0.004
Co	0.0011	0.0015	0.0000	0.0044	0.0071	0.0041	0.0014	0.0167	0.003
Ni	0.0025	0.0016	0.0004	0.0062	0.0042	0.0028	0.0001	0.0103	0.001
Ga	0.0013	0.0027	0.0000	0.0080	0.0007	0.0024	0.0000	0.0094	0.003
As	0.0003	0.0007	0.0000	0.0028	0.0015	0.0030	0.0000	0.0103	0.003
Se	0.0007	0.0011	0.0000	0.0039	0.0006	0.0010	0.0000	0.0030	0.005
Br	0.0047	0.0040	0.0008	0.0134	0.0065	0.0047	0.0000	0.0169	0.006
Rb	0.0002	0.0003	0.0000	0.0008	0.0013	0.0014	0.0000	0.0041	0.005
Sr	0.0017	0.0017	0.0000	0.0063	0.0088	0.0051	0.0022	0.0225	0.004
Y	0.0008	0.0013	0.0000	0.0045	0.0008	0.0009	0.0000	0.0028	0.005
Zr	0.0066	0.0058	0.0000	0.0223	0.0261	0.0182	0.0065	0.0631	0.008
Nb	0.0026	0.0025	0.0000	0.0077	0.0022	0.0023	0.0000	0.0069	0.006
Mo	0.0025	0.0036	0.0000	0.0119	0.0032	0.0042	0.0000	0.0111	0.005
Pd	0.0005	0.0012	0.0000	0.0043	0.0018	0.0034	0.0000	0.0111	0.021
Ag	0.0004	0.0013	0.0000	0.0049	0.0023	0.0036	0.0000	0.0110	0.024
Cd	0.0069	0.0077	0.0000	0.0202	0.0048	0.0070	0.0000	0.0207	0.016
In	0.0015	0.0027	0.0000	0.0082	0.0051	0.0051	0.0000	0.0129	0.017
Sn	0.0036	0.0065	0.0000	0.0220	0.0083	0.0091	0.0000	0.0276	0.013
Sb	0.0072	0.0094	0.0000	0.0291	0.0102	0.0086	0.0000	0.0273	0.015
Cs	0.0130	0.0140	0.0000	0.0485	0.0201	0.0149	0.0000	0.0433	0.059
Ba	0.0406	0.0346	0.0000	0.1217	0.1161	0.0582	0.0405	0.2353	0.046

La	0.0119	0.0133	0.0000	0.0397	0.0191	0.0196	0.0000	0.0744	0.108
Ce	0.0183	0.0190	0.0000	0.0530	0.0214	0.0213	0.0000	0.0684	0.100
Sm	0.0177	0.0326	0.0000	0.0966	0.0154	0.0337	0.0000	0.1286	0.148
Eu	0.0419	0.0463	0.0000	0.1430	0.0370	0.0396	0.0000	0.1114	0.174
Tb	0.0067	0.0172	0.0000	0.0601	0.0075	0.0185	0.0000	0.0598	0.195
Hf	0.0000	0.0000	0.0000	0.0000	0.0000	0.0000	0.0000	0.0000	0.136
Ta	0.0000	0.0000	0.0000	0.0000	0.0000	0.0000	0.0000	0.0000	0.136
W	0.0011	0.0021	0.0000	0.0068	0.0055	0.0085	0.0000	0.0327	0.019
Ir	0.0000	0.0000	0.0000	0.0000	0.0000	0.0000	0.0000	0.0000	0.023
Au	0.0024	0.0034	0.0000	0.0092	0.0022	0.0035	0.0000	0.0097	0.010
Hg	0.0011	0.0020	0.0000	0.0058	0.0002	0.0006	0.0000	0.0018	0.012
Tl	0.0013	0.0021	0.0000	0.0063	0.0012	0.0015	0.0000	0.0043	0.007
Pb	0.0015	0.0022	0.0000	0.0068	0.0011	0.0015	0.0000	0.0044	0.010
U	0.0017	0.0016	0.0000	0.0047	0.0070	0.0049	0.0000	0.0156	0.015

3 Chapter 3: Non-tailpipe contribution to $PM_{2.5}$ and PM_{10} at near road highways

3.1 Introduction

In 2010, the United States EPA set up national near road networks to monitor traffic-related exposures and characterize pollutant behavior, interaction, and dispersion (Gantt, Owen, and Watkins 2021). Many sites can measure NO_2, CO_2, O_3, $PM_{2.5}$, BC, and meteorological data. However, PM_{10} is not typically available which are related to non-tailpipe emissions from brake, tire, and road dust (Amato et al. 2014; Denier van der Gon et al. 2013; Wang et al. 2023). The Los Angeles area typically experiences high population density and heavy traffic, resulting in elevated levels of PM pollution (Jerrett et al. 2005). As a result, studies have established provided insight into PM characterization. The study by Chow et al. (1994), a Southern California Air Quality Study (SCAPS), focused on evaluating the cause of increased concentrations of ozone and airborne PM. Their findings report ratios of 0.5-0.6 between $PM_{2.5}$ and PM_{10} with secondary inorganic ions and primary tailpipe emissions contributing more to $PM_{2.5}$ while dust emissions contribute more to PM_{10} (Watson et al. 1994; Wang et al. 2023). Another study by Cheung et al. (2011), sampled ten sites in the Los Angeles Basin (urban, semi-rural, desert, etc) to study special and seasonal characteristics of coarse PM. Their study found a large contribution of crustal material at 40-60% of coarse PM, while secondary inorganic ions were 23%, organic matter 20%, and sea salt 9% (Cheung et al. 2011; Wang et al. 2023).

3.2 . Experimental

3.2.1 Chemical analysis

The sampling methods and set up are discussed in Chapter 2. This section relies on the use of DRI medium-volume samplers to collect upwind and downwind $PM_{2.5}$ and PM_{10} filter samples at the I-5 and I-710. PM samples were collected on pre-weighed and equilibrated Teflon-membrane filters before gravimetric analysis according to standard methods (Watson et al. 2017; U.S. EPA 2017; 1997; Wang et al. 2023). The filters were quantified for elemental markers using a Panalytical XRF (Model Epsilon 5, Almelo, The Netherlands) (Wang et al. 2023). A total of 51 elements were quantified and included key non-tailpipe markers like Al, Si, Ca found in road dust, Fe, Sb, Ba found in brakes, and Zn found in tire wear (Thorpe and Harrison 2008; Grigoratos and Martini 2015; Kukutschová and Filip 2018).

3.2.2 Meteorological data

Wind direction and wind speed data was obtained from the AQMD Meteorology Data Query Tool for near road sites in Anaheim and Long Beach (AQMD 2020). Wind data was produced in vector component form by using the meteorological wind direction convention shown in Figure 3-1, where ϕ_{Met} is the meteorological degree describing the direction from which the wind is blowing (Grange 2014). Met wind direction increases from true north designated at zero degrees toward, easternly winds at 90 degrees, true south at 180 degrees, and westerly winds at 270 degrees (Grange 2014). Using Eq. (2) and (3), wind components are computed given the meteorological wind angle and speed scalar.

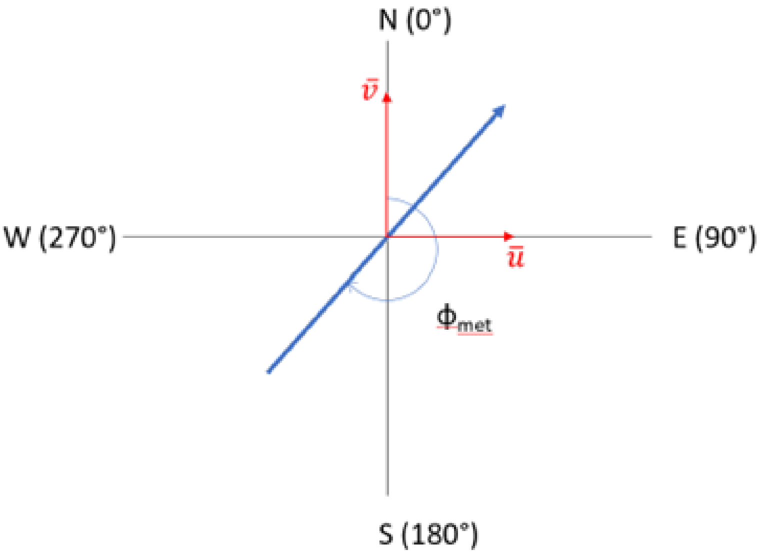

Figure 3-1: meteorological wind direction convention and vector components.

$$u = -|\vec{u}|\sin\left[\frac{\pi}{180}\cdot \emptyset_{met}\right] \qquad (2)$$

$$v = -|\vec{v}|\cos\left[\frac{\pi}{180}\cdot \emptyset_{met}\right] \qquad (3)$$

Two sonic anemometers (Campbell Scientific, CSAT3) were set up at both near road sites with the positive x direction aligned approximately parallel to the road and the positive y component aligned approximately perpendicular to the road. The compass (Sportneer-0717) measurements showed the positive x component facing 130 degrees from North at the Anaheim location and 24 degrees from north at the Long Beach location. The x axis was aligned in parallel to the flow of traffic on both the I-5 and I-710. This information was used to orient the AQMD meteorological axes to the sonic axes. Therefore, a rotation of axes was performed, see Eq (4) and (5) (Abramson 2015).

$$u' = u \cdot cos\theta - v \cdot sin\theta \qquad (4)$$

$$v' = u \cdot sin\theta - v \cdot cos\theta \qquad (5)$$

Crosswind refers to wind flow from the upwind site to the downwind site. Therefore, the angle used in the rotation of axis was defined as the angle counterclockwise from the positive u vector at 90 degrees (East). At the I-5 site, this angle was 50° while Long Beach the angle was 24°. Unit vectors at each location were used to facilitate calculations and are shown in Eq (6) and (7) (Abramson 2015). Once rotation is established, u' was the focus of this analysis as it is the vector perpendicular to the road. A dot product was applied between the unit vector created and the component form of AQMD's meterological data. This creates a scalar magnitude showing crosswind from upwind to downwind as positive and the oposite as negative. Hourly averaged and four hour averages of cross wind magnitudes were calculated.

$$u'_{AH} = \cos(50°)\,\hat{\imath} + \sin(50°)\,\hat{\jmath} \tag{6}$$

$$u'_{LB} = \cos(24°)\,\hat{\imath} - \sin(24°)\,\hat{\jmath} \tag{7}$$

3.3 Results and Discussions

3.3.1 PM mass concentrations

The $PM_{2.5}$ and PM_{10} concentrations at the I-5 and I-710 sites from gravimetric samples are shown in Figure 3-2 and Figure 3-3, respectively. The concentrations are reported based on their nominal upwind and downwind sites over each sampling period. In general, PM_{10} was approximately 2-3 times higher than $PM_{2.5}$ with average concentrations of 30 and 10-15 μg/m^3, respectively, see Table 3-1. The abundance of coarse particles leads to larger $PM_{10}/PM_{2.5}$ than those reported by non-near road studies (1.5-2) (Chow et al. 1994; Habre et al. 2021; Oroumiyeh et al. 2022). The average concentrations at the downwind sites from both locations were only higher by approximately 1-4 µg/m^3 in both PM size fractions. Highest PM concentrations had repetitive patterns around the same sampling time of 0600-1000 LST. Although samples did not cover a 24 hour period, the average concentrations did not exceed maximum concentrations of 35 µg/m^3 for PM$_{2.5}$ and 150 µg/m^3 for PM$_{10}$. based on the 24 hour average National Ambient Air Quality Standards (NAAQs) (US EPA 2020).

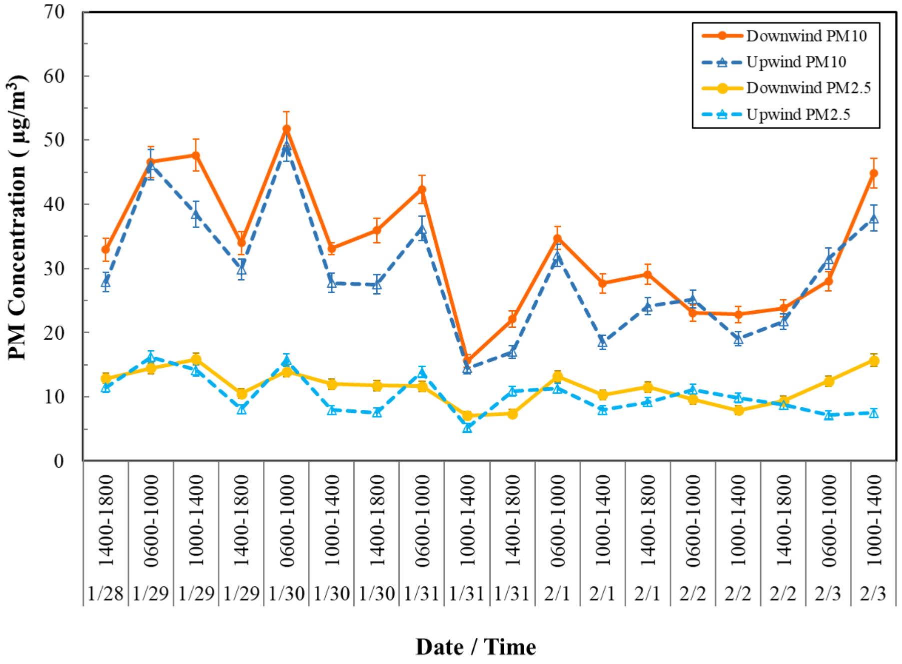

Figure 3-2: Time series of PM2.5 and PM10 mass concentrations at the I-5 upwind and downwind sites.

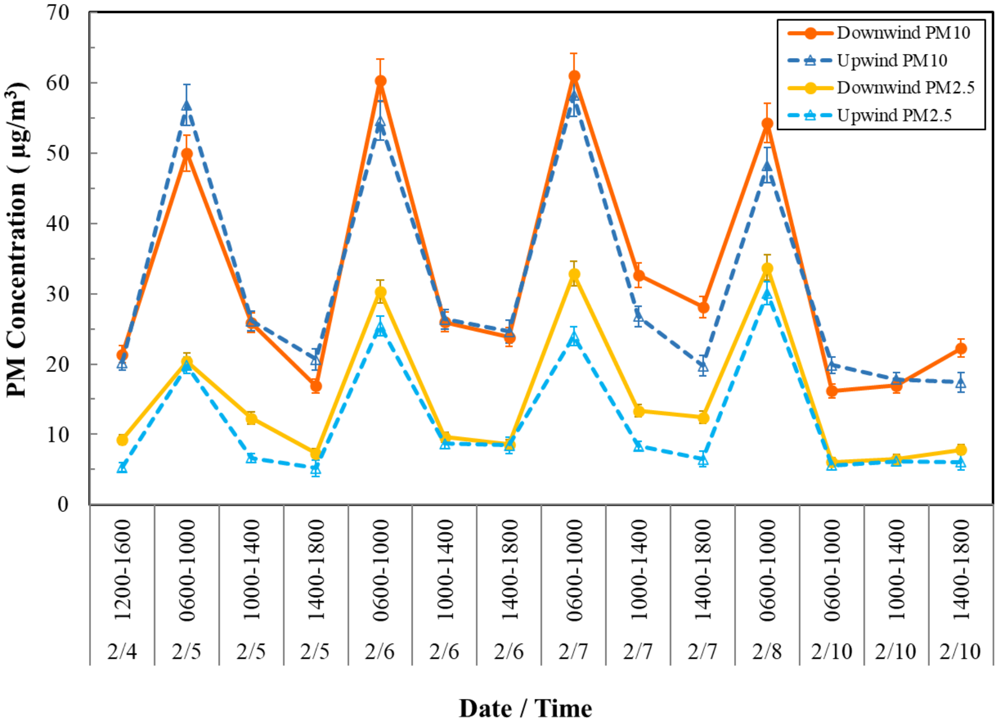

Figure 3-3: Time series of PM2.5 and PM10 mass concentrations at the I-710 upwind and downwind sites.

Table 3-1: Average upwind and downwind PM Concentrations in µg/m^3 at the I-5 and I-710

Site	Upwind $PM_{2.5}$	Upwind PM_{10}	Downwind $PM_{2.5}$	Downwind PM_{10}
I-5	9.56	28.47	10.88	32.49
I-710	11.00	30.37	14.36	31.87

Highest PM concentrations at both locations typically occurred during the early morning rush hours (0600-1000 LST).

The wind speed and wind direction at both sampling sites during the field dates are shown in Figure 3-4. Both sampling sites had consistent diurnal patterns with low speed during the 1st to 8th hour of the day. Wind speeds remained below 1.5 m/s in the early hours of the day and increased in the afternoon. The downwind and upwind sites can change depending on the wind direction. Approximately, the first filter sampling period (0600-1000) the AQMD sites (nominally downwind sites) were upwind of the highways, although the windspeeds were low, while the AQMD sites were downwind the highway during the second (1000-1400) and third (1400-1800) filter sampling periods. This means that the wind direction changes from offshore to onshore in the middle of the afternoon (1400-1600 LST). However, the daily wind direction and speed need be examined to determine the upwind and downwind designation. The traffic data shown in Figure 3-6 provides a 4 hour average of vehicle counts and speeds at both the I-5 and I-710. This was created to observe traffic patterns within the gravimetric sampling periods. The truck counts were amplified by a factor of 10 to better observe changes throughout the sampling periods. The previously reported, hourly traffic data in Figure 2-1 through Figure 2-4, showed cyclic patterns of vehicle flow during the weekdays. Both locations showed bimodal peaks during the early morning and afternoon rush hours. The variations of average traffic flow and speed in the four data were lower than those from hourly data. However, the peaks and valleys of PM concentration did not coincide with those of averaged flow and speed. This suggests that fluctuations in PM concentrations alone cannot be explained by using speed and flow. In low wind conditions, traffic induced flow could create similar PM concentrations on each side of the road, therefore making it difficult to eliminate background influence.

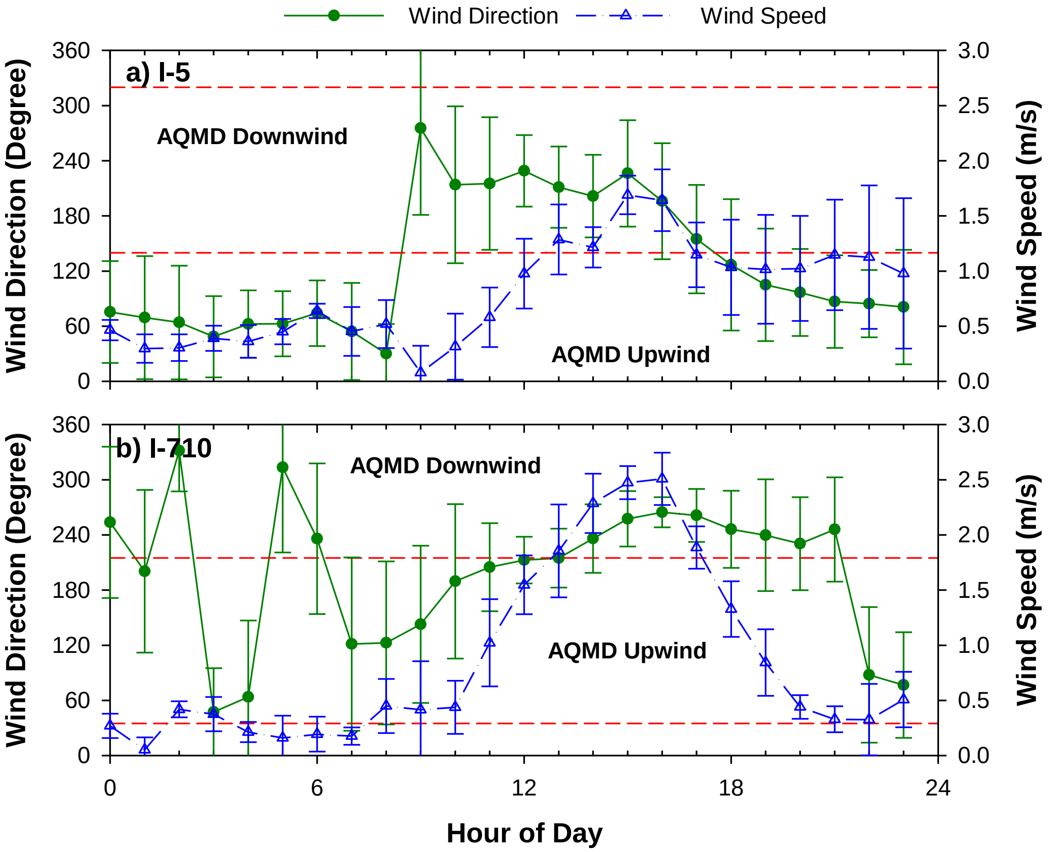

Figure 3-4: Diurnal variation of wind direction and speed with standard deviations at the a) I-5 and b) I-710. Red horizontal lines indicate the angle at which the wind direction changes. Figure by Wang et al. (2023).

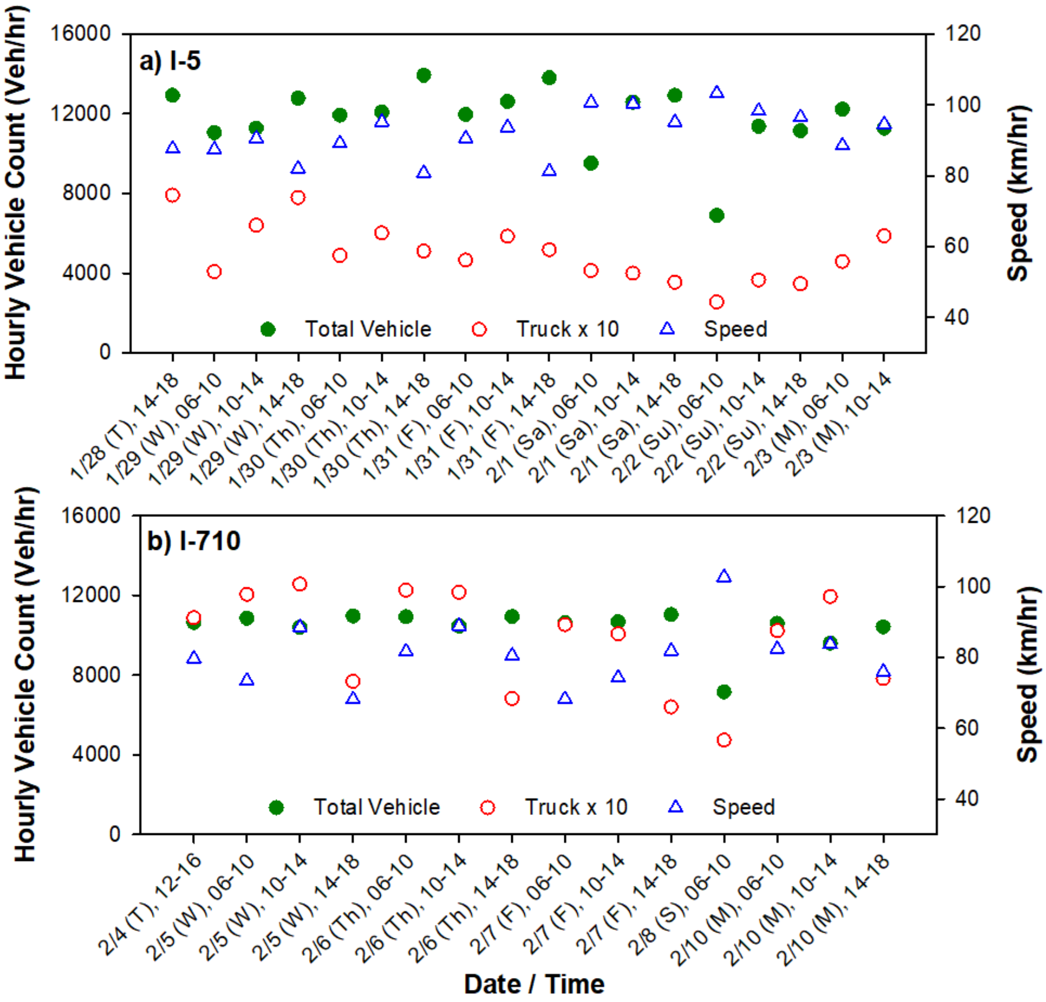

Figure 3-5: Four hour average vehicle counts and speeds at the a) I-5 and b) I-710 highways for filter sampling periods. Truck counts are amplified by a factor of 10. Figure by Wange et al. (2023).

3.3.2 Laboratory versus real world XRF analysis

Figure 3-6 compares the concentrations of the four elements measured by PX-375 with those by the laboratory XRF on Teflon membrane filters collected by medvol samplers. The two measurements showed a strong correlation for Zn (r^2=1), moderate correlation for Fe (r^2 =0.60) and Cu (r^2= 0.68), and weaker correlation for Ti (r^2 = 0.44). The regression slope was 1.01 for Zn, but was only 0.50–0.65 for Fe, Cu, and Ti. Weaker correlations are partially due to low concentration measurement near or below detection limit. The different slopes are likely caused by different calibration factors applied to the two XRFs. The laboratory XRF analyses routinely run quality check standards and have passed proficiency tests by the U.S. EPA. Therefore, the laboratory data is deemed more accurate. The metal concentrations in Figure 2-11 have not been corrected using data in Figure 3-6 but they are sufficient to illustrate the temporal pattern of concentration changes.

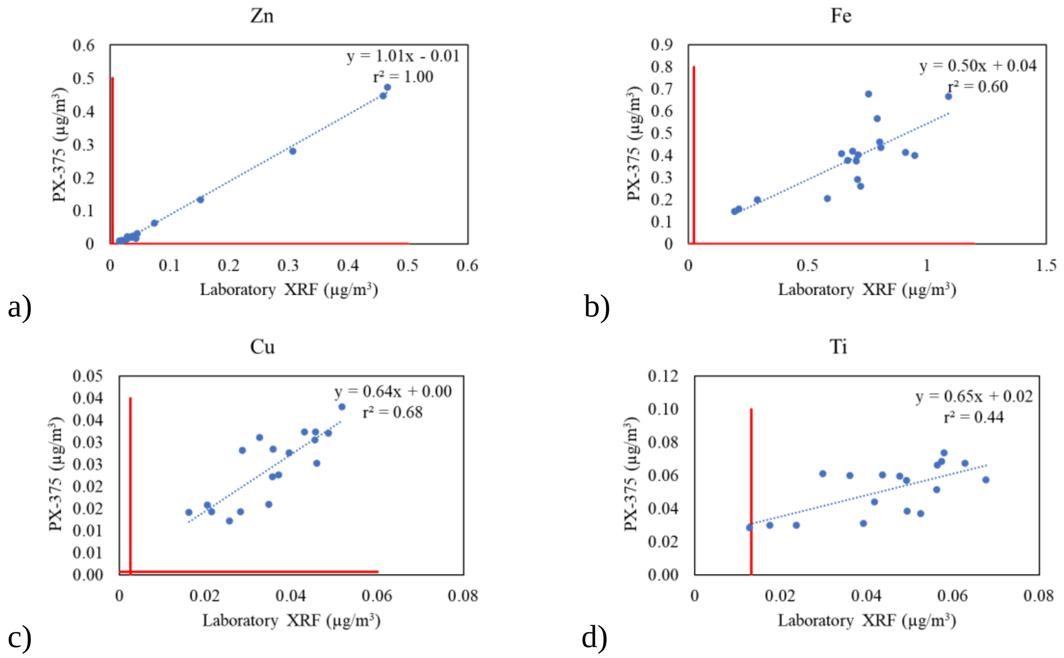

a) b) c) d)

Figure 3-6: Comparison of elemental concentrations and limit of detection boundaries between the PX-375 and laboratory XRF for: a) Zinc, b) Iron, c) Copper, and d) Titanium.

3.4 Conclusion

The temporal trends of PM2.5 and PM10 at both upwind and downwind sites of the I-5 and I-710 show concentrations levels at 10-15 µg/m^3 and 30 µg/m^{3,} respectively. The PM10 concentration was approximately double to triple the concentration of PM2.5 at both locations. The PM concentration difference within the upwind and downwind sites were minimal and remained below 1-4 μg/m^3. The low difference is explained to result from measurement sites being close to one another spaced 10 m (I-5) from the road. Meteorological data from SCAQMD sites and sonic anemometers were obtained to observe the true upwind and downwind patterns. The PM concentrations measured showed they were affected more by wind direction and vehicle induced flow, than to the vehicle flow and speeds. The nominal downwind sites in this study showed to be true downwind locations outside the early morning hours (0600-1000 LST) even with low wind speeds. The wind direction tends to switch mostly in the middle of the day between 1000-1400 LST. As a result, the afternoon sampling periods of 1000-1400 and 1400-1800 LST represented true upwind and downwind conditions. The gravimetric filter samples were analyzed using XRF analysis to quantify elemental concentrations. Comparison between the element concentrations measured by the Horiba PX-375 and in lab XRF analysis showed strong correlations for Zn (r^2=1), moderate correlation for Fe (r^2 =0.60) and Cu (r^2= 0.68), and weaker correlation for Ti (r^2 = 0.44). This suggests correlations between elements and collected data were consistent with laboratory results.

3.5 References

Abramson, Jay. 2015. "10.4: Rotation of Axes." In *Mathematics LibreTexts*. OpenStax. https://math.libretexts.org/Bookshelves/Precalculus/Precalculus_1e_(OpenStax)/10%3A_Analytic_Geometry/10.04%3A_Rotation_of_Axes.

Amato, Fulvio, Flemming R. Cassee, Hugo A. C. Denier van der Gon, Robert Gehrig, Mats Gustafsson, Wolfgang Hafner, Roy M. Harrison, et al. 2014. "Urban Air Quality: The Challenge of Traffic Non-Exhaust Emissions." *Journal of Hazardous Materials* 275 (June):31–36. https://doi.org/10.1016/j.jhazmat.2014.04.053.

AQMD. 2020. “Meteorology Data Query Tool (PST).” 2020. https://www.arb.ca.gov/aqmis2/metselect.php.

Cheung, Kalam, Nancy Daher, Winnie Kam, Martin M. Shafer, Zhi Ning, James J. Schauer, and Constantinos Sioutas. 2011. “Spatial and Temporal Variation of Chemical Composition and Mass Closure of Ambient Coarse Particulate Matter (PM10–2.5) in the Los Angeles Area.” *Atmospheric Environment* 45 (16): 2651–62. https://doi.org/10.1016/j.atmosenv.2011.02.066.

Chow, Judith C., Eric M. Fujita, John G. Watson, Zhiqiang Lu, Douglas R. Lawson, and Lowell L. Ashbaugh. 1994. “Evaluation of Filter-Based Aerosol Measurements during the 1987 Southern California Air Quality Study.” *Environmental Monitoring and Assessment* 30 (1): 49–80. https://doi.org/10.1007/BF00546199.

Denier van der Gon, Hugo A.C., Miriam E. Gerlofs-Nijland, Robert Gehrig, Mats Gustafsson, Nicole Janssen, Roy M. Harrison, Jan Hulskotte, et al. 2013. “The Policy Relevance of Wear Emissions from Road Transport, Now and in the Future—An International Workshop Report and Consensus Statement.” *Journal of the Air & Waste Management Association* 63 (2): 136–49. https://doi.org/10.1080/10962247.2012.741055.

Gantt, Brett, R. Chris Owen, and Nealson Watkins. 2021. “Characterizing Nitrogen Oxides and Fine Particulate Matter near Major Highways in the United States Using the National Near-Road Monitoring Network.” *Environmental Science & Technology* 55 (5): 2831–38. https://doi.org/10.1021/acs.est.0c05851.

Grange, Stuart K. 2014. “Averaging Wind Speeds and Directions.” *No. October*, 12.

Grigoratos, Theodoros, and Giorgio Martini. 2015. “Brake Wear Particle Emissions: A Review.” *Environmental Science and Pollution Research* 22 (4): 2491–2504. https://doi.org/10.1007/s11356-014-3696-8.

Habre, Rima, Mariam Girguis, Robert Urman, Scott Fruin, Fred Lurmann, Martin Shafer, Patrick Gorski, et al. 2021. “Contribution of Tailpipe and Non-Tailpipe Traffic Sources to Quasi-Ultrafine, Fine and Coarse Particulate Matter in Southern California.” *Journal of the Air & Waste Management Association* 71 (2): 209–30. https://doi.org/10.1080/10962247.2020.1826366.

Jerrett, Michael, Richard T. Burnett, Renjun Ma, C. Arden III Pope, Daniel Krewski, K. Bruce Newbold, George Thurston, et al. 2005. “Spatial Analysis of Air Pollution and Mortality in Los Angeles.” *Epidemiology* 16 (6): 727. https://doi.org/10.1097/01.ede.0000181630.15826.7d.

Kukutschová, Jana, and Peter Filip. 2018. “Chapter 6 - Review of Brake Wear Emissions: A Review of Brake Emission Measurement Studies: Identification of Gaps and Future

Needs." In *Non-Exhaust Emissions*, edited by Fulvio Amato, 123–46. Academic Press. https://doi.org/10.1016/B978-0-12-811770-5.00006-6.

Oroumiyeh, Farzan, Michael Jerrett, Irish Del Rosario, Jonah Lipsitt, Jonathan Liu, Suzanne E. Paulson, Beate Ritz, et al. 2022. "Elemental Composition of Fine and Coarse Particles across the Greater Los Angeles Area: Spatial Variation and Contributing Sources." *Environmental Pollution* 292 (January):118356. https://doi.org/10.1016/j.envpol.2021.118356.

Thorpe, Alistair, and Roy M. Harrison. 2008. "Sources and Properties of Non-Exhaust Particulate Matter from Road Traffic: A Review." *Science of The Total Environment* 400 (1): 270–82. https://doi.org/10.1016/j.scitotenv.2008.06.007.

U.S. EPA. 1997. "Appendix L to Part 50 - Reference Method for the Determination of Fine Particulate Matter as PM2.5 in the Atmosphere."

US EPA, OAR. 2020. "National Ambient Air Quality Standards (NAAQS) for PM." Other Policies and Guidance. April 13, 2020. https://www.epa.gov/pm-pollution/national-ambient-air-quality-standards-naaqs-pm.

U.S. EPA, QA. 2017. "Handbook for Air Pollution Measurement Systems. Volume II. Ambient Air Quality Monitoring Program." U.S. Environmental Protection Agency, Office of Air Quality Planning and Standards, Air Quality Assesment Division: Research, Triangle Park, NC.

Wang, Xiaoliang, Steven Gronstal, Brenda Lopez, Heejung Jung, L. -W. Antony Chen, Guoyuan Wu, Steven Sai Hang Ho, et al. 2023. "Evidence of Non-Tailpipe Emission Contributions to PM2.5 and PM10 near Southern California Highways." *Environmental Pollution* 317 (January):120691. https://doi.org/10.1016/j.envpol.2022.120691.

Watson, John G., Judith C. Chow, Zhiqiang Lu, Eric M. Fujita, Douglas H. Lowenthal, Douglas R. Lawson, and Lowell L. Ashbaugh. 1994. "Chemical Mass Balance Source Apportionment of PM10 during the Southern California Air Quality Study." *Aerosol Science and Technology* 21 (1): 1–36. https://doi.org/10.1080/02786829408959693.

Watson, John G., Richard J. Tropp, Steven D. Kohl, Xiaoliang Wang, and Judith C. Chow. 2017. "Filter Processing and Gravimetric Analysis for Suspended Particulate Matter Samples." *Aerosol Science and Engineering* 1 (2): 93–105. https://doi.org/10.1007/s41810-017-0010-4.

4 Chapter 4: Source apportionment of non-tailpipe emissions to near-road PM2. 5 and PM10

4.1 Introduction

Health effects studies in the past have linked vehicular emission exposure to an increased risk of developing a chronic respiratory or cardiovascular disease, premature mortality, and hospitalization (Brandt et al. 2014; Brugge, Durant, and Rioux 2007; Ghosh et al. 2016). Regulatory efforts have successfully decreased the contribution from tailpipe emissions, however, as technological advances lead to zero tailpipe emissions with the increase in electric vehicle fleets, the non-tailpipe contribution will remain unchanged as a positive relationship exists between vehicle weight and non-exhaust emissions (Wahlström et al. 2020; Timmers and Achten 2016). Electric vehicles are heavier than internal combustion powered vehicles by 25%, thus the importance of non-tailpipe emissions to ambient PM will increase (Timmers and Achten 2016; Vasiljevic et al. 2022; Amato et al. 2014; Denier van der Gon et al. 2013). The CARB EMFAC2021 model provides a measure of estimated PM2.5 emission from on-road vehicles at statewide or regional levels (CARB 2021). Their estimation of brake and tire wear PM2.5 shows that these non-tailpipe sources have exceeded their tailpipe counterpart since 2020 and will continue to grow at a steady rate. Therefore, it is a motivation to further investigate as non-tailpipe becomes an important contributor to total PM2.5 emissions.

Among the key tracers for brake wear includes, iron (Fe), copper (Cu), lead (Pb) manganese (Mn), titanium (Ti), antimony (Sb), and barium (Ba) (Thorpe and Harrison 2008; Wahlström, Olander, and Olofsson 2010; Bukowiecki et al. 2009; Hulskotte, Roskam, and Denier van der Gon 2014; Iijima et al. 2007; Grigoratos and Martini 2015; Pant and Harrison 2013). Tire tread contains zinc oxide (ZnO) particles, therefore zinc (Zn) particle concentrations, although also seen in brake dust, are found to be approximately 15 times higher in tires than in brakes, while ZnO specifically is seen in tire tread (Apeagyei et al., 2011; Wik and Dave 2009; Klöckner et al. 2019). Zinc in tires can originate from zinc oxide and organozinc compounds that are used in the vulcanization process (Pant and Harrison, 2013). Tread particles can also mix with the existing particles present in road dust (Panko et al., 2018). Tire dust is expected to have higher levels of mineral materials silicon (Si), aluminum (Al), and calcium (Ca), and heavy metal elements than to tire tread alone (Adachi and Tainosho 2004; Harrison et al. 2012; Lough et al. 2005).

It is challenging to extract precise estimations of each non-tailpipe source contribution to ambient PM since it is dependent on various parameters including sampling location (Grigoratos and Martini 2015). This is mainly because they have an overlapping commonality in tracer elements, specifically Zn. Key tracers used by various researchers in the last 20 years include Zn among the list of prominent brake tracers (Schauer et al. 2006; Hjortenkrans, Bergbäck, and Häggerud 2007; Bukowiecki et al. 2009; Amato et al. 2014). The mixing of non-tailpipe emissions with tailpipe emissions can lead to bias in source apportionment due to temporal correlations. Despite the uncertainty, non-tailpipe particles were found to be equally abundant as exhaust particles, especially in urban PM10 and PM10-2.5 (Harrison et al. 2021; Chen et al. 2010).

The Los Angeles metropolitan area in southern California experiences high population density and heavy traffic, resulting in elevated air pollution levels (Jerrett et al. 2005). Research by Hasheminassab et al. (2014a,b) showed that vehicular emissions, secondary nitrate, secondary sulfate, soil, aged sea salt, fresh sea salt, and biomass burning contribute to long-term PM2.5 concentrations, with vehicular emissions making up approximately 20% from 2002 to 2013. Habre et al. (2021) identified similar sources in Los Angeles between a one-year period (2008–2009). They attribute brake and tire to contribute 11% of total PM2.5 while 21% to exhaust particles. In the $PM_{10-2.5}$ size fraction, the brake and tire contribution increased to 18%. The study by Jalali Farahani et al. (2022) near Los Angeles highways found comparable contributions of non-tailpipe and exhaust particles to PM10, at 16% and 26%, respectively.

In this study, the real-world non-tailpipe emissions and contributions of near road PM2.5 and PM10 samples are estimated using an effective variance-chemical mass balance (EV-CMB) model by Chen et al. 2023. PM samples at the downwind wind and upwind, described in Chapter 2, were collected for elemental and organic composition analysis.

4.2 Experimental

4.2.1 Collection of PM samples

The I-5 freeway in Anaheim and the I-710 highway in Long Beach are paved with concrete and asphalt, respectively. The med-vol time integrated PM samples previously discussed in Chapter 2 were used for this the purpose of this study. Chemical analysis was performed on a total of 64 PM$_{2.5}$ and 64 PM$_{10}$ samples that include 32 pairs at each downwind and upwind measurement sites.

Each sample set was characterized for PM2.5 or PM10 mass, 51 elements, water soluble cations and anions such as sodium (Na^+), potassium (K^+), sulfate ($SO4_2^-$) and nitrate (NO_3^-), as well as organic carbon (OC), elemental carbon (EC), and thermal carbon fractions (OC1-OC4, OP, EC1-EC3) (Chen et al. 2023). For combustion markers, non-polar organic speciation included PAHs, alkanes, alkenes, hopanes, steranes, and phthalates (Ambade et al., 2023; Fadel et al., 2021; Kumar et al., 2020; Chen et al. 2023). Tire markers such as benzothiazole and its derivatives, as well as thermal decomposition fragments of rubber (styrene, butadiene, etc.), were also analyzed (Chen et al. 2023). Wang et al. (2023) documents the analytical methods and quality assurance and control in greater detail.

4.2.2 Chemical mass balance model

The EV-CMB model used in this study comes from Watson el al. (1984) and is shown by Eq. (8) below. This equation helps quantify source-specific contributions to both PM$_{2.5}$ and PM$_{10}$ where C_{jt} is the measured concentration of species i in PM samples at time t. Using a given source profile j, then F_{ij} is the fraction of species i in that source profile, while S_{jt} is the contribution of source j at time t. The value S_{jt} is referred to as source contribution estimates (SCEs). Further discussion of SCEs and sensitivity tests performed on selected samples to evaluate the combinations of source profiles and species that can affect SCEs can be found in Chen et al. (2023).

$$C_{it} = \sum_{J=1}^{J} F_{ij} S_{jt} \qquad \text{Eq (8)}$$

4.2.3 Source profiles

The source profile categories considered for the EV-CMB model include geological (road dust), mobile (brake wear, tire wear, diesel exhaust, gasoline exhaust), and secondary (secondary sulfate, secondary nitrate). In the geological category, four dust samples were collected at the near road monitoring sites to develop local $PM_{2.5}$ and PM_{10} dust profiles. The dust profiles can be characterized as local resuspended dust as they are expected to contain a combination of road dust and windblown dust, including local soil and geological material.

Brake dust samples were collected using prior laboratory data analyzed for chemical composition by the California Regional Particulate Air Quality Study (CRPAQs) Fitz et al. (2004). From this study, the brake trace markers, Fe, Ba, Mn, and Cu were found to be 20-66%, 3-13%, 0.2-0.6%, and 0.04-0.08%, respectively in brake $PM_{2.5}$. These fractions were 11-47%, 1-11%, 0.1-0.07%, and 0.04-4.9% respectively in another inertial dynamometer study by Agudelo et al. (2020). The second study showed two brake profiles based on their copper content than what is reported by CRPAQs. The two brake profiles are quantified based on their higher Cu content at 4.9% and 1.7%. Therefore, two source profiles were used in the classification of brake wear. Therefore, element markers used for brake dust included Fe, Ba, Mn, Cu, and Sb.

Tire wear profiles were also obtained from dynamometer tests of Michelin and Cooper tires (Wang et al. 2023). The tire profiles are dominated by organic carbon (OC) and elemental carbon (EC) and contained 0.1-0.2% Fe, 0.5-1% Zn, 0.04-0.2% Al, 0.07-0.1%

Ca, 2% Ca, and .003-.004% Cu. The Michelin tire dust contained 0.06% Si while the Cooper tire dust was 6%. Zn was a consistent marker for tire wear.

Deisel and gasoline exhaust profiles were acquired from the National Renewable Energy Laboratory Gas/Diesel Split study (Fujita et al. 2007a, 2007b). In this study, vehicles used ranged from light duty to heavy duty with 57 LDV gasoline-powered, 2 LDV diesel-powered, 30 MDV, and HDV diesel-powered vehicles. $PM_{2.5}$ emissions were measured at a grocery distribution center in Riverside, CA during summer and winter of 2021. The data set includes profiles from vehicles considered low emitters, high emitters, and black carbon (BC) emitters for gasoline powered engines in cold and war start conditions. This study has previously been used in source apportionment of $PM_{2.5}$ for California and Nevada fleets (Chen et al., 2012; Chow et al., 2007).

In the EV-CMB model, the secondary nitrate and sulfate were represented from pure ammonium nitrate (NH_4NO_3) and ammonia sulfate ($[NH_4]_2SO_4$) profiles (Chen et al. 2023). The SOA contribution from wildfire smoke, biomass burning, and sea salt were excluded.

4.3 Results and Discussions

4.3.1 Source Contribution Estimates

Using the EV-CMB model with sensitivity tests (Chen et al. 2023), the SCEs with uncertainties were calculated for $PM_{2.5}$ and PM_{10} at both downwind and upwind sites for both I-5 and I-710 locations. Exclusion of wildfire smoke, biomass burning, and sea salt lead to total percentage mass at less than 100%. A combination of two brake profiles were used to include brakes with low copper content and brakes with high copper content. The source combinations for the I-710 were similar to those used for I-5, besides the downwind dust profiles used pertain to I-710 road dust collected. The average and standard error of the sour5ce contributions from all sources are shown in Table 4-1 for the I-5 location and Table 4-2 for the I-710 location. Road dust was found to be the most abundant fraction and contributes significantly more to the coarse size particles when compared to fine particle contributions. The brake and tire wear were higher in coarse particles however the difference in both particle size fractions were not significant due to large standard errors in reported SCEs. The varying traffic mix in HDVs between the I-5 and I-710 can serve as an explanation of the variation between contribution from brakes with low copper and brakes with high copper content. It is also important to note, the overall difference between non-tailpipe sources at the downwind versus upwind are small with the downwind sites having generally higher average SCEs. The tailpipe contribution had similar SCEs for both particle size fractions and minimal differences between the upwind and downwind at both locations. Within the tailpipe $PM_{2.5}$ contribution, diesel sources were higher at the I-710 than the I-5 while gasoline contributions had the opposite trend. This is speculated to be a result of the higher fraction of HVD at the I-710. With this in mind, the total brake and tire contribution did not increase from higher HDV proportions to both PM fractions. However, the flow of traffic was lower at the I-710 location, suggesting an explanation to this observation (Wang et al. 2023). Lastly, the secondary ammonium nitrate was higher at the I-710 and is consistent to higher NOx emissions produced by a higher proportion of HDVs. Secondary ammonium sulfate showed a uniform average source contribution at the I-710. The high concentration of both sources in the coarse particle range are explained to displacement of chloride in coarse sea salt by NO_3^- and SO_4^{2-} and the reactions of NO_3^- and SO_4^{2} with mineral dust (Wang et al. 2023; Chen et al. 2023).

Table 4-1: Average and standard error of source contribution estimates in µg/m^3 for $PM_{2.5}$ and PM_{10} at the I-5 downwind and upwind locations.

	I-5	I-5	I-5	I-5
	Downwind	Downwind	Upwind	Upwind
	$PM_{2.5}$	PM_{10}	$PM_{2.5}$	PM_{10}
# of Data	18	18	18	18
Total Mass	10.9	32.5	9.6	28.5
Road Dust	3.60±0.57	17.1±1.44	2.50±0.47	14.4±1.30
Brake Low Cu	1.44±0.96	2.10±1.26	1.21±0.90	1.76±1.29
Brake High Cu	0.54±0.36	1.18±0.61	0.34±0.31	0.68±0.55
Tire Wear	1.28±0.73	2.01±1.10	1.21±0.70	1.60±0.99
Gasoline	0.77±0.47	0.65±0.41	0.61±0.36	0.62±0.36
Diesel	1.34±0.68	1.48±0.85	1.40±0.64	1.13±0.78
S. Nitrate	0.99±0.11	2.34±0.16	0.92±0.11	2.18±0.17
S. Sulfate	0.69±0.19	1.28±0.27	0.65±0.18	1.28±0.26
Others	0.23±1.88	4.37±3.11	0.72±1.74	4.83±2.88

Table 4-2: Average and standard error of source contribution estimates in µg/m^3 for $PM_{2.5}$ and PM_{10} at the I-710 downwind and upwind locations.

	I-710	I-710	I-710	I-710
	Downwind	Downwind	Upwind	Upwind
	$PM_{2.5}$	PM_{10}	$PM_{2.5}$	PM_{10}
# of Data	14	14	14	14
Total Mass	14.4	31.9	11.0	30.4
Road Dust	3.39±0.29	10.3±1.36	2.50±0.29	10.5±1.39
Brake I	0.40±0.22	1.23±1.17	0.34±0.19	0.93±1.10
Brake II	0.74±0.34	1.81±1.39	0.55±0.33	1.97±1.63
Tire Wear	1.05±0.42	1.84±1.56	0.96±0.42	1.25±1.53
Gasoline	0.26±0.13	0.73±0.72	0.31±0.15	0.47±0.46
Diesel	1.84±0.45	1.92±1.32	1.75±0.45	1.80±1.26
S. Nitrate	2.56±0.21	4.81±0.46	2.51±0.22	3.13±0.37
S. Sulfate	0.78±0.12	1.16±0.38	0.74±0.13	1.13±0.37
Others	3.33±1.43	8.08±3.74	1.34±1.52	9.23±3.76

4.3.2 Non-tailpipe source fractions

The fractions of non-tailpipe and tailpipe contributions to $PM_{2.5}$ and PM_{10} at the I-5 upwind and downwind sites are shown in Figure 4-1: Fractions of non-tailpipe and tailpipe contributions in µg/m^3 to $PM_{2.5}$ and PM_{10} at the I-5 upwind (a,b) and downwind (c,d) sites.. The fractions at the I-710 upwind and downwind sites are shown in Figure 4-2. At both locations, the road dust fractions were dominant at 24-53% over other source contributions except for the I-710 $PM_{2.5}$ upwind site. In general, the road dust contribution was higher at the I-5 than at the I-710 locations. The I-5 $PM_{2.5}$ brake and tire fractions accounted for approximately 30% and exceeded the tailpipe counterpart coming from diesel and gasoline sources at 20%. The I-5 PM_{10} brake and tire fractions were approximately 15% and are more than double the tailpipe fractions of diesel and gasoline sources at 6%. The unaccounted PM mass remained below 2-7% for $PM_{2.5}$ and were larger at 14-17% for PM_{10}. The I-710 $PM_{2.5}$ brake and tire wear fractions (15-17%) were comparable to the fraction coming from tailpipe sources (15-19%). In the coarse size range, PM_{10}, the I-710 brake and tire fractions (14-16%) were about twice that of tailpipe sources (8%). These findings are in agreement with the CARB EMFAC prediction as this study campaign occurred during the early winter months of 2020. The similar source breakdowns between upwind and upwind sites highlights the importance of non-tailpipe source contributions, which suggests a similar impact of on-road traffic emissions from both sides of the road (Chen et al. 2023).

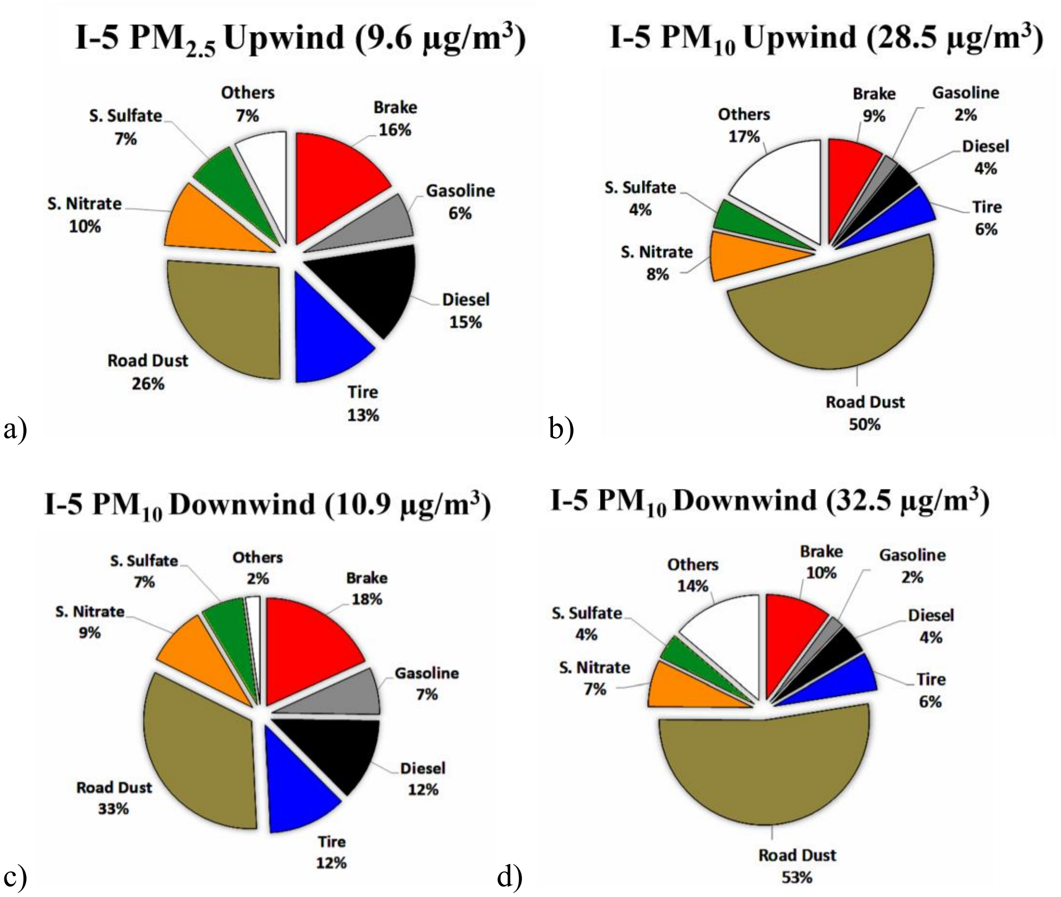

Figure 4-1: Fractions of non-tailpipe and tailpipe contributions in µg/m^3 to PM$_{2.5}$ and PM$_{10}$ at the I-5 upwind (a,b) and downwind (c,d) sites.

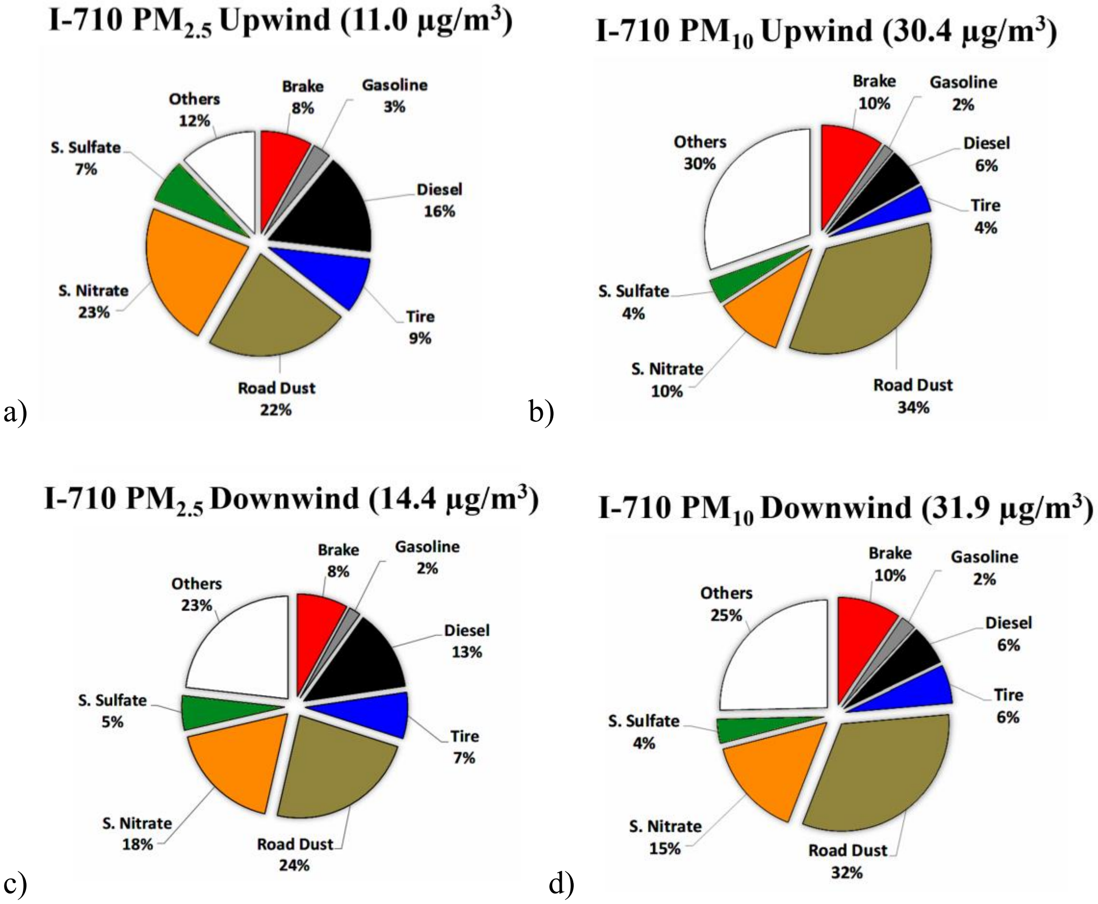

Figure 4-2: Fractions of non-tailpipe and tailpipe contributions in µg/m^3 to $PM_{2.5}$ and PM_{10} at the I-710 upwind (a,b) and downwind (c,d) sites.

Further examination was done to crosscheck the source apportionment results and the use of PM mass difference between downwind and upwind in element correlations. This was performed by comparison of the source apportioned brake PM to that of laboratory results which is shown in Figure 4-3. The laboratory data was obtained from a brake dynamometer project conducted by Eastern Research Group (ERG) and Link Engineering Company (LINK) through the CARB project 17RD016 (Stanard et al. 2021). Their results showed that the $PM_{2.5}$ fraction of PM_{10} for brake wear tends to range between ratios of 0.25 and 0.6 and can be explained by the following equation $PM_{2.5} = 0.039PM_{10} + 0.2023$.

with $r^2 = 0.95$. This equation is plotted as a red line in Figure 4-3a,b. Assuming the effect of background PM concentration can be removed through subtracting the upwind PM concentrations, $\Delta PM_{2.5brake}$ and $\Delta PM_{10brake}$ source apportioned data is plotted. The source apportioned brake $PM_{2.5}$ is displayed in Figure 4-3a with a trendline slope of 0.37 and $r^2=0.53$. The ΔPM has both negative and positive values depending on the wind direction influencing higher concentrations either at the upwind or downwind sites. Data is scattered due to uncertainties related analysis. This ratio is in agreement with the laboratory range and provides a measurement within the expected values. In Figure 4-3b, the I-710 $\Delta PM_{2.5brake}$ and $\Delta PM_{10brake}$ source apportioned data is plotted. This result gives a slope of 0.14 and $r^2 = 0.22$, however, there are two data points that skew this value located in the second and third quadrants. These are attributed to uncertainty related analysis, and if corrected, it is expected that the ratio between the PM fractions will match within the laboratory range.

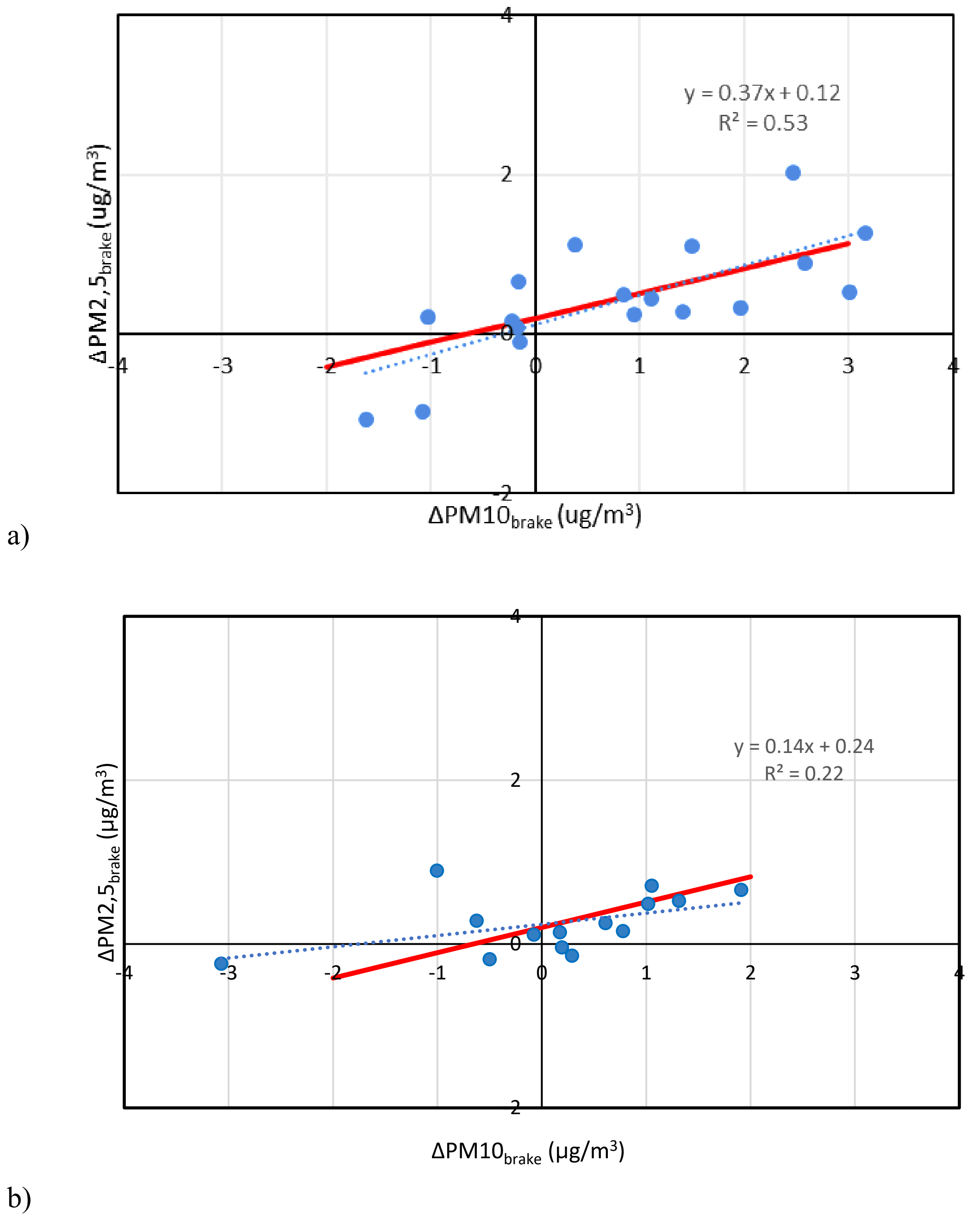

Figure 4-3: Relationship between $\Delta PM_{2.5brake}$ and $\Delta PM_{10brake}$ (a) Anaheim site (I-5) and (b) Long Beach site (I-710)

4.4 Conclusion

Studies have outlined the health risks associated with exposure pre vehicle emissions. The California Air Resources Board EMFAC 2021 model predicted that the non-tailpipe sources of $PM_{2.5}$ from on road vehicles will exceed tailpipe emissions by 2020 and will continue to be a dominant source. The is difficulty in accurately estimating the contribution of non-tailpipe sources to ambien PM due to various factors, including the sampling location and presence of overlapping trace elements in the non-tailpipe sources. This chapter discusses the use of an effective variance-chemical mass balance (EC-CMB) model from source profiles to obtain source contribution estimates at the I-5 and I-710 highways in Southern California. $PM_{2.5}$ and PM_{10} samples were collected at near-road sites downwind and upwind at both sampling sites. The source profile categories considered for the EV-CMB model included geological (road dust), mobile (brake wear, tire wear, diesel exhaust, gasoline exhaust), and secondary (secondary sulfate, secondary nitrate). Brake dust source profiles were obtained from laboratory studies (CRPAQs data and Agudelo et al (2020)) and were categorized based on their low copper and high copper content to achieve the optimal model fitting performance. Tire wear profiles were obtained from dynamometer tests of Michelin and Cooper tires. Diesel and gasoline exhaust profiles were obtained using a gas/diesel split study by Fujita el al 2007a, 2007b. secondary nitrate and sulfate were represented from pure ammonium nitrate (NH4NO3) and ammonia sulfate ([NH4]2SO4) profiles. Source contribution estimates explained an average of 95% and 82% of $PM_{2.5}$ and 85% and 72% of PM_{10} at the I-5 and I-710 locations, respectively. Source contributions show the non-tailpipe sources exceed the tailpipe counterparts at the I-5 and are comparable at the I-710. Non-tailpipe contributes 29-30% of $PM_{2.5}$ mass while tailpipe is at 19-21% at the I-5. A non-tailpipe contribution of 15-17% of $PM_{2.5}$ mass and 15-19% tailpipe contribution are seen at the I-710 site. In general, the PM_{10} fraction at both sites accounted for 2-3 times the tailpipe contribution. A higher diesel source contribution and brake (high copper content) was observed at the I-710 indicating an influence of HDVs since the opposite trend was observed at the I-5 (higher gasoline source and low copper brakes). A comparison between the source apportioned upwind and downwind difference ($\Delta PM_{2.5brake}$ and $\Delta PM_{10brake}$) showed ratios of 0.37 and 0.14 which are comparable to those reported by prior laboratory results.

4.5 References

Adachi, Kouji, and Yoshiaki Tainosho. 2004. “Characterization of Heavy Metal Particles Embedded in Tire Dust.” *Environment International* 30 (8): 1009–17. https://doi.org/10.1016/j.envint.2004.04.004.

Agudelo, Carlos, Ravi Teja Vedula, Sonya Collier, and Alan Stanard. 2020. “Brake Particulate Matter Emissions Measurements for Six Light-Duty Vehicles Using Inertia Dynamometer Testing.” *SAE International Journal of Advances and Current Practices in Mobility* 3 (2): 994–1019. https://doi.org/10.4271/2020-01-1637.

Amato, Fulvio, Flemming R. Cassee, Hugo A. C. Denier van der Gon, Robert Gehrig, Mats Gustafsson, Wolfgang Hafner, Roy M. Harrison, et al. 2014. “Urban Air Quality: The Challenge of Traffic Non-Exhaust Emissions.” *Journal of Hazardous Materials* 275 (June):31–36. https://doi.org/10.1016/j.jhazmat.2014.04.053.

Ambade, Balram, Shrikanta Shankar Sethi, and Madhusudana Rao Chintalacheruvu. 2023. “Distribution, Risk Assessment, and Source Apportionment of Polycyclic Aromatic Hydrocarbons (PAHs) Using Positive Matrix Factorization (PMF) in Urban Soils of East India.” *Environmental Geochemistry and Health* 45 (2): 491–505. https://doi.org/10.1007/s10653-022-01223-x.

Apeagyei, Eric, Michael Bank, and John Spengler. 2011. “Distribution of Heavy Metals in Road Dust Along an Urban-Rural Gradient in Massachusetts.” *Atmospheric*

Environment - ATMOS ENVIRON 45 (April):2310–23. https://doi.org/10.1016/j.atmosenv.2010.11.015.

Brandt, Sylvia, Laura Perez, Nino Künzli, Fred Lurmann, John Wilson, Manuel Pastor, and Rob McConnell. 2014. "Cost of Near-Roadway and Regional Air Pollution–Attributable Childhood Asthma in Los Angeles County." *Journal of Allergy and Clinical Immunology* 134 (5): 1028–35. https://doi.org/10.1016/j.jaci.2014.09.029.

Brugge, Doug, John L. Durant, and Christine Rioux. 2007. "Near-Highway Pollutants in Motor Vehicle Exhaust: A Review of Epidemiologic Evidence of Cardiac and Pulmonary Health Risks." *Environmental Health* 6 (1): 23. https://doi.org/10.1186/1476-069X-6-23.

Bukowiecki, Nicolas, Peter Lienemann, Matthias Hill, Renato Figi, Agnes Richard, Markus Furger, Karen Rickers, et al. 2009. "Real-World Emission Factors for Antimony and Other Brake Wear Related Trace Elements: Size-Segregated Values for Light and Heavy Duty Vehicles." *Environmental Science & Technology* 43 (21): 8072–78. https://doi.org/10.1021/es9006096.

CARB, California Air Resources Board. 2021. "EMFAC2021 Volume III Technical Document." https://ww2.arb.ca.gov/sites/default/files/2021-03/emfac2021_volume_3_technical_document.pdf.

Chen, L. -W. Antony, Xiaoliang Wang, Brenda Lopez, Guoyuan Wu, Steven Sai Hang Ho, Judith C. Chow, John G. Watson, Qi Yao, Seungju Yoon, and Heejung Jung. 2023. "Contributions of Non-Tailpipe Emissions to near-Road PM2.5 and PM10: A Chemical Mass Balance Study." *Environmental Pollution* 335 (October):122283. https://doi.org/10.1016/j.envpol.2023.122283.

Chen, L.-W. A., J. G. Watson, J. C. Chow, M. C. Green, D. Inouye, and K. Dick. 2012. "Wintertime Particulate Pollution Episodes in an Urban Valley of the Western US: A Case Study." *Atmospheric Chemistry and Physics* 12 (21): 10051–64. https://doi.org/10.5194/acp-12-10051-2012.

Chen, L.-W. Antony, Douglas H. Lowenthal, John G. Watson, Darko Koracin, Naresh Kumar, Eladio M. Knipping, Neil Wheeler, Kenneth Craig, and Stephen Reid. 2010. "Toward Effective Source Apportionment Using Positive Matrix Factorization: Experiments with Simulated PM2.5 Data." *Journal of the Air & Waste Management Association* 60 (1): 43–54. https://doi.org/10.3155/1047-3289.60.1.43.

Chow, J. C., J. G. Watson, D. H. Lowenthal, L. W. A. Chen, B. Zielinska, L. R. Mazzoleni, and K. L. Magliano. 2007. "Evaluation of Organic Markers for Chemical Mass Balance Source Apportionment at the Fresno Supersite." *Atmospheric Chemistry and Physics* 7 (7): 1741–54. https://doi.org/10.5194/acp-7-1741-2007.

Denier van der Gon, Hugo A.C., Miriam E. Gerlofs-Nijland, Robert Gehrig, Mats Gustafsson, Nicole Janssen, Roy M. Harrison, Jan Hulskotte, et al. 2013. "The Policy Relevance of Wear Emissions from Road Transport, Now and in the Future—An International Workshop Report and Consensus Statement." *Journal of the Air & Waste Management Association* 63 (2): 136–49. https://doi.org/10.1080/10962247.2012.741055.

Fadel, Marc, Frédéric Ledoux, Mariana Farhat, Adib Kfoury, Dominique Courcot, and Charbel Afif. 2021. "PM2.5 Characterization of Primary and Secondary Organic Aerosols in Two Urban-Industrial Areas in the East Mediterranean." *Journal of Environmental Sciences* 101 (March):98–116. https://doi.org/10.1016/j.jes.2020.07.030.

Fitz, D. R., J. C. Chow, and B. Zielinska. 2004. "Development of a Gas and Particulate Matter Organic Speciation Profile Database, Prepared for Draft Final Report June 2003." *Prepared Fro San Joaquin Valleywide Air Pollution Study Agency*.

Fujita, Eric M., David E. Campbell, William P. Arnott, Judith C. Chow, and Barbara Zielinska. 2007. "Evaluations of the Chemical Mass Balance Method for Determining Contributions of Gasoline and Diesel Exhaust to Ambient Carbonaceous Aerosols." *Journal of the Air & Waste Management Association*, a, 57 (6): 721–40. https://doi.org/10.3155/1047-3289.57.6.721.

Fujita, Eric M., Barbara Zielinska, David E. Campbell, W. Patrick Arnott, John C. Sagebiel, Lynn Mazzoleni, Judith C. Chow, et al. 2007. "Variations in Speciated Emissions from Spark-Ignition and Compression-Ignition Motor Vehicles in California's South Coast Air Basin." *Journal of the Air & Waste Management Association*, b, 57 (6): 705–20. https://doi.org/10.3155/1047-3289.57.6.705.

Ghosh, Rakesh, Frederick Lurmann, Laura Perez, Bryan Penfold, Sylvia Brandt, John Wilson, Meredith Milet, Nino Künzli, and Rob McConnell. 2016. "Near-Roadway Air Pollution and Coronary Heart Disease: Burden of Disease and Potential Impact of a Greenhouse Gas Reduction Strategy in Southern California." *Environmental Health Perspectives* 124 (2): 193–200. https://doi.org/10.1289/ehp.1408865.

Grigoratos, Theodoros, and Giorgio Martini. 2015. "Brake Wear Particle Emissions: A Review." *Environmental Science and Pollution Research* 22 (4): 2491–2504. https://doi.org/10.1007/s11356-014-3696-8.

Habre, Rima, Mariam Girguis, Robert Urman, Scott Fruin, Fred Lurmann, Martin Shafer, Patrick Gorski, et al. 2021. "Contribution of Tailpipe and Non-Tailpipe Traffic Sources to Quasi-Ultrafine, Fine and Coarse Particulate Matter in Southern California." *Journal of the Air & Waste Management Association* 71 (2): 209–30. https://doi.org/10.1080/10962247.2020.1826366.

Harrison, Roy M., James Allan, David Carruthers, Mathew R. Heal, Alastair C. Lewis, Ben Marner, Tim Murrells, and Andrew Williams. 2021. "Non-Exhaust Vehicle Emissions of Particulate Matter and VOC from Road Traffic: A Review." *Atmospheric Environment* 262 (October):118592. https://doi.org/10.1016/j.atmosenv.2021.118592.

Harrison, Roy M., Alan M. Jones, Johanna Gietl, Jianxin Yin, and David C. Green. 2012. "Estimation of the Contributions of Brake Dust, Tire Wear, and Resuspension to Nonexhaust Traffic Particles Derived from Atmospheric Measurements." *Environmental Science & Technology* 46 (12): 6523–29. https://doi.org/10.1021/es300894r.

Hasheminassab, Sina, Nancy Daher, Bart D. Ostro, and Constantinos Sioutas. 2014. "Long-Term Source Apportionment of Ambient Fine Particulate Matter (PM2.5) in the Los Angeles Basin: A Focus on Emissions Reduction from Vehicular Sources." *Environmental Pollution* 193 (October):54–64. https://doi.org/10.1016/j.envpol.2014.06.012.

Hasheminassab, Sina, Nancy Daher, Martin M. Shafer, James J. Schauer, Ralph J. Delfino, and Constantinos Sioutas. 2014. "Chemical Characterization and Source Apportionment of Indoor and Outdoor Fine Particulate Matter (PM2.5) in Retirement Communities of the Los Angeles Basin." *Science of The Total Environment* 490 (August):528–37. https://doi.org/10.1016/j.scitotenv.2014.05.044.

Hjortenkrans, David S. T., Bo G. Bergbäck, and Agneta V. Häggerud. 2007. "Metal Emissions from Brake Linings and Tires: Case Studies of Stockholm, Sweden 1995/1998 and 2005." *Environmental Science & Technology* 41 (15): 5224–30. https://doi.org/10.1021/es070198o.

Hulskotte, J. H. J., G. D. Roskam, and H. A. C. Denier van der Gon. 2014. "Elemental Composition of Current Automotive Braking Materials and Derived Air Emission Factors." *Atmospheric Environment* 99 (December):436–45. https://doi.org/10.1016/j.atmosenv.2014.10.007.

Iijima, Akihiro, Keiichi Sato, Kiyoko Yano, Hiroshi Tago, Masahiko Kato, Hirokazu Kimura, and Naoki Furuta. 2007. "Particle Size and Composition Distribution Analysis of Automotive Brake Abrasion Dusts for the Evaluation of Antimony Sources of Airborne Particulate Matter." *Atmospheric Environment* 41 (23): 4908–19. https://doi.org/10.1016/j.atmosenv.2007.02.005.

Jalali Farahani, Vahid, Abdulmalik Altuwayjiri, Sina Taghvaee, and Constantinos Sioutas. 2022. "Tailpipe and Nontailpipe Emission Factors and Source Contributions of PM10 on Major Freeways in the Los Angeles Basin." *Environmental Science & Technology* 56 (11): 7029–39. https://doi.org/10.1021/acs.est.1c06954.

Jerrett, Michael, Richard T. Burnett, Renjun Ma, C. Arden III Pope, Daniel Krewski, K. Bruce Newbold, George Thurston, et al. 2005. "Spatial Analysis of Air Pollution and Mortality in Los Angeles." *Epidemiology* 16 (6): 727. https://doi.org/10.1097/01.ede.0000181630.15826.7d.

Klöckner, Philipp, Thorsten Reemtsma, Paul Eisentraut, Ulrike Braun, Aki Sebastian Ruhl, and Stephan Wagner. 2019. "Tire and Road Wear Particles in Road Environment – Quantification and Assessment of Particle Dynamics by Zn Determination after Density Separation." *Chemosphere* 222 (May):714–21. https://doi.org/10.1016/j.chemosphere.2019.01.176.

Kumar, Amit, Balram Ambade, Tapan Kumar Sankar, Shrikanta Shankar Sethi, and Sudarshan Kurwadkar. 2020. "Source Identification and Health Risk Assessment of Atmospheric PM2.5-Bound Polycyclic Aromatic Hydrocarbons in Jamshedpur, India." *Sustainable Cities and Society* 52 (January):101801. https://doi.org/10.1016/j.scs.2019.101801.

Lough, Glynis C., James J. Schauer, June-Soo Park, Martin M. Shafer, Jeffrey T. DeMinter, and Jason P. Weinstein. 2005. "Emissions of Metals Associated with Motor Vehicle Roadways." *Environmental Science & Technology* 39 (3): 826–36. https://doi.org/10.1021/es048715f.

Panko, Julie, Marisa Kreider, and Kenneth Unice. 2018. "Chapter 7 - Review of Tire Wear Emissions: A Review of Tire Emission Measurement Studies: Identification of Gaps and Future Needs." In *Non-Exhaust Emissions*, edited by Fulvio Amato, 147–60. Academic Press. https://doi.org/10.1016/B978-0-12-811770-5.00007-8.

Pant, Pallavi, and Roy Harrison. 2013. "Estimation of the Contribution of Road Traffic Emissions to Particulate Matter Concentrations from Field Measurements: A Review." *Atmospheric Environment* 77 (October):78–97. https://doi.org/10.1016/j.atmosenv.2013.04.028.

Schauer, James J., Glynis C. Lough, Martin M. Shafer, William F. Christensen, Michael F. Arndt, Jeffrey T. DeMinter, and June-Soo Park. 2006. "Characterization of Metals Emitted from Motor Vehicles." *Research Report (Health Effects Institute)*, no. 133 (March), 1–76; discussion 77-88.

Stanard, Alan, Tim DeFries, Cindy Palacios, and Sandeep Kishan. 2021. "Brake and Tire Wear Emissions Project 17RD016 Prepared for the California Air Resources Board and the California Environmental Protection Agency."

Thorpe, Alistair, and Roy M. Harrison. 2008. "Sources and Properties of Non-Exhaust Particulate Matter from Road Traffic: A Review." *Science of The Total Environment* 400 (1): 270–82. https://doi.org/10.1016/j.scitotenv.2008.06.007.

Timmers, Victor R. J. H., and Peter A. J. Achten. 2016. "Non-Exhaust PM Emissions from Electric Vehicles." *Atmospheric Environment* 134 (June):10–17. https://doi.org/10.1016/j.atmosenv.2016.03.017.

Vasiljevic, Sasa, Jasna Glišović, Blaza Stojanovic, Nadica Stojanovic, and Ivan Grujic. 2022. "The Analysis of the Influential Parameters That Cause Particles Formation during the Braking Process: A Review." *Proceedings of the Institution of Mechanical Engineers, Part J: Journal of Engineering Tribology* 236 (1): 31–48. https://doi.org/10.1177/13506501211004798.

Wahlström, Jens, Mara Leonardi, Minghui Tu, Yezhe Lyu, Guido Perricone, Stefano Gialanella, and Ulf Olofsson. 2020. "A Study of the Effect of Brake Pad Scorching on Tribology and Airborne Particle Emissions." *Atmosphere* 11 (5): 488. https://doi.org/10.3390/atmos11050488.

Wahlström, Jens, Lars Olander, and Ulf Olofsson. 2010. "Size, Shape, and Elemental Composition of Airborne Wear Particles from Disc Brake Materials." *Tribology Letters* 38 (1): 15–24. https://doi.org/10.1007/s11249-009-9564-x.

Wang, Xiaoliang, Steven Gronstal, Brenda Lopez, Heejung Jung, L. -W. Antony Chen, Guoyuan Wu, Steven Sai Hang Ho, et al. 2023. "Evidence of Non-Tailpipe Emission Contributions to PM2.5 and PM10 near Southern California Highways." *Environmental Pollution* 317 (January):120691. https://doi.org/10.1016/j.envpol.2022.120691.

Watson, John G., John A. Cooper, and James J. Huntzicker. 1984. "The Effective Variance Weighting for Least Squares Calculations Applied to the Mass Balance Receptor Model." *Atmospheric Environment (1967)* 18 (7): 1347–55. https://doi.org/10.1016/0004-6981(84)90043-X.

Wik, Anna, and Göran Dave. 2009. "Occurrence and Effects of Tire Wear Particles in the Environment – A Critical Review and an Initial Risk Assessment." *Environmental Pollution* 157 (1): 1–11. https://doi.org/10.1016/j.envpol.2008.09.028.

5 Chapter 5: Development of brake activity measurement method for heavy-duty vehicles

5.1 Introduction

Brake wear particles are produced as a result of the abrasion between the brake pad surface lining and the rotor or drum, which are dominant in the coarse to fine particle size ranges (Bukowiecki et al. 2009; Chan and Stachowiak 2004; Garg et al. 2000; Grigoratos and Martini 2015; Sanders et al. 2003; Thorpe and Harrison 2008). Modern brake pads vary in composition of fibers, matrix binders, friction modifiers, abrasives and fillers (Chan and Stachowiak 2004; Grigoratos and Martini 2015). This leads to a variability of elemental concentrations composed of iron (Fe), potassium (K), copper (Cu), manganese (Mn), antimony (Sb), aluminum (Al), barium (Ba) and zinc (Zn) that are amongst some of the most common elements reported to be present in brake wear PM2.5 and PM10 (Garg et al. 2000; Grigoratos and Martini 2015; Iijima et al. 2007; Thorpe and Harrison 2008; Wahid 2018; Wahlström, Olander, and Olofsson 2010).

Previous studies have used laboratory and track tests to simulate real-world driving conditions and have suggested that brake wear PM emission rates are dependent on brake pad lining materials, braking conditions such as deceleration rates and pattern, brake pad temperature, and vehicle size or weight (Agudelo et al. 2020; Hagino, Oyama, and Sasaki 2016; Iijima et al. 2007; Sanders et al. 2003; Wahlström, Olander, and Olofsson 2010). California's Air Resource Board (CARB) funded several studies in efforts to understand

and quantify brake wear PM emissions for both the laboratory (Agudelo et al. 2020) and real world near road environments (CARB project 18RD017). Koupal et al. (2021) used track test brake temperature measurements on a range of heavy duty vehicles to simulate real-world thermal regimes for dynamometer emissions testing. The track tests followed trends where brake temperatures are seen to be a function of braking power, braking density, and loading. Although their study focused on developing EMFAC rates using a heavy-duty test matrix, their real time data during event-based braking indicates that particle number and mass are influenced by braking energy, braking vehicle speed, and brake temperature. Additionally, temperature trends during their track testing showed the class 8 vehicle had median brake temperatures of about 65°C and maximum temperature above 121°C when fully loaded compared to median temperature of around 52°C and maximum temperature about 71°C in unloaded condition. Previous studies suggest that brake PM emissions are dependent on brake pad temperature, vehicle speed, and braking patterns (Agudelo et al. 2020; Garg et al. 2000; Grigoratos and Martini 2015). However, the frequency and extent of braking activity varies dynamically in the real world suggesting it is necessary to investigate brake activity for diverse vehicle classes and sizes under in-use conditions. The same vehicle can have different braking activity based on its vocation (such as goods movement, refuse, people transit, and other) as well as route differences.

The goal of the current study is to establish a test method and analysis of brake activity measurement for heavy-duty vehicles. A market representative class 8 truck was tested in the laboratory on chassis dynamometer as well as on the road under real-world conditions. The heavy- duty truck was evaluated during in-use chassis dynamometer and on-road testing. Brake activity was quantified with an instrumented brake pad system that measures brake temperature, brake fluid pressure, vehicle speed, vehicle position, elevation, and ambient conditions. The results from this study will be of value to calculate accurate emission inventory for brake wear PM.

5.2 Experimental

5.2.1 Chassis dynamometer tests

Two chassis dynamometer cycles were selected for testing different braking activity patterns represented by heavy duty transportation buses and urban delivery trucks. These chassis cycles were selected as they provide a basis for understanding commonly used emissions testing cycles and their representativeness for brake pressure, temperature, braking activity, frequency, and intensity compared to the real-world conditions. The first cycle selected was the Central Business District (CBD) and the second cycle is the Urban Dynamometer Driving Schedule (UDDS). The CBD and UDDS cycles were selected to represent real in-use driving activity. The CBD was selected since this represents the typical operation of heavy-duty buses on-road and is commonly used for emissions testing. The UDDS was selected because it is representative of typical operation of a HD delivery trucks and is the representative cycle used for certification-like emissions testing on chassis dynamometers.

The CBD cycle follows a sawtooth driving pattern with 14 repetitions of idle, acceleration, cruise, and deceleration modes with a time duration of approximately 560 seconds. Speeds range from 0 to 20 miles per hour with cyclic acceleration and deceleration. The CBD cycle was performed first with a single cycle to warm-up the truck and brakes followed by three consecutive CBD cycles used for testing. This approach is similar to how emissions testing is performed by other research (Miller et al. 2013). A single UDDS cycle is approximately 1060 seconds where the vehicle speed can range from 0 to 60 miles per hour with varying acceleration, deceleration, and idle modes. Three consecutive UDDS cycles were performed without warm-up as it was performed within 15 minutes of the triplicate CBD cycles. The chassis was configured for a total test weight of 65,000 lb. (=29484 kg) which represents the tractor plus trailer weight. This weight is representative of typical goods movement operation in the South Coast Air Basin (Miller et al. 2013) and also matches the on-road weight of the tractor trailer combination.

5.2.2 On-road tests

On-road tests were performed to compare real world operation with the laboratory chassis testing. The same chassis test vehicle was driven along two different California routes where the HDV was configured with a total weight of 65,000 lb. (=29484 kg) to maintain consistency between on-road and laboratory testing. One route was designed to be representative of the CBD and UDDS type of stop and go activity and is denoted as the Local route. The Local route is represented by local Riverside city streets which primarily follows straight paths with frequent stops due to stop signs and traffic lights, average elevations near ~263 m, and average slope of ±1.6% (Figure 5-1). The pavement was asphalt.

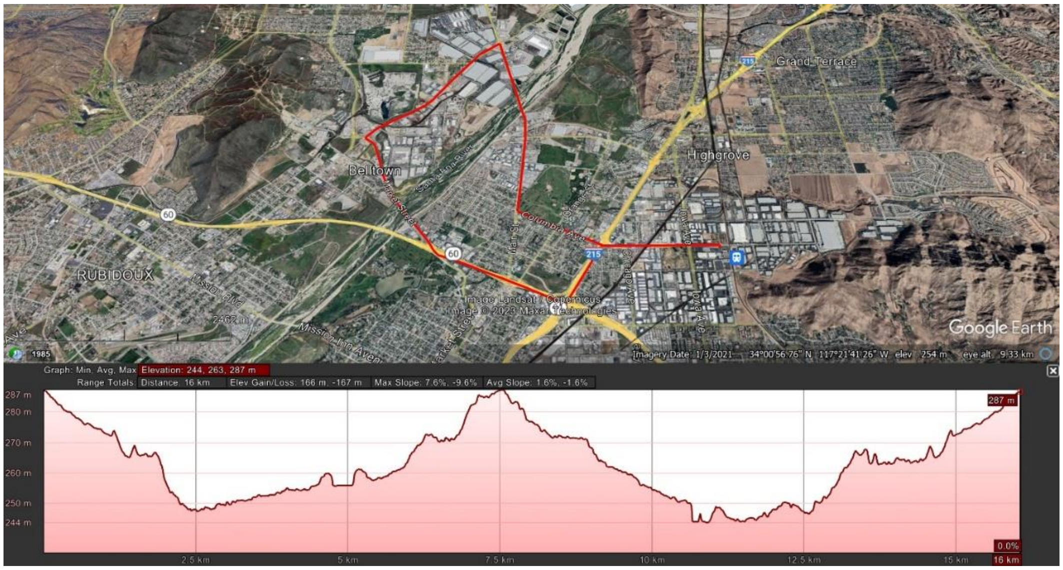

Figure 5-1: Map of the local Riverside City route driven by the test vehicle. The route's start and end points are located at 1084 Columbia Ave, Riverside, CA 92507 (Jung et al., 2022).

The second route was designed to represent higher speed cruise conditions where higher braking energy is expected. This route is denoted as the Cruise route. The Cruise route is representative of long-distance driving on the I-215 freeway connecting the City of Riverside and Victorville, CA. The route elevation ranges from ~288m in Riverside City which gradually increases over a ~60 km distance to a maximum of 1,280 m, then decreases to 896m at the City of Victorville (Figure 5-2). This Cruise route was selected to investigate braking activity during higher vehicle speeds and varying acceleration and deceleration conditions. In addition, the Cruise route also was selected to investigate brake activity during downhill heating and uphill cooling conditions. The route contains a 14 km uphill section of the Cajon Pass with an average slope of 3.5% that becomes a downhill section in the return trip. The pavement was made of concrete.

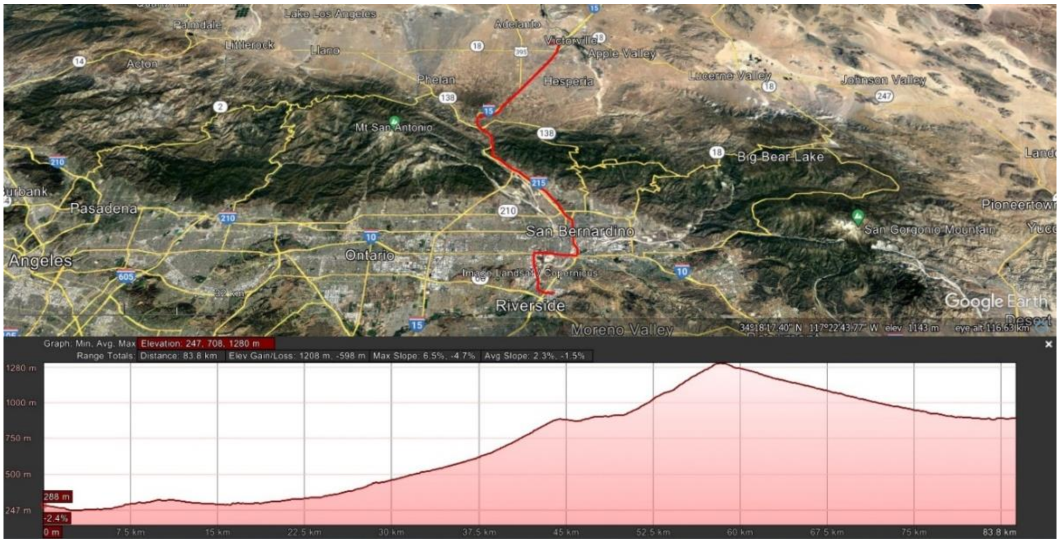

Figure 5-2: Map of the long-distance Riverside City to Victorville route driven with the test vehicle. The route's start and end points are located at 1084 Columbia Ave, Riverside, CA 92507 with an intermediate stop at 14818 Mojave Dr Victorville, California (Jung et al., 2022).

5.2.3 Test vehicle and brake system

A Freightliner Cascadia model year 2015 tandem axle day cab equipped with a 12.8 L Detroit Diesel DD13 engine and drum brakes was selected for this study. The Cascadia model truck represents a market share of 37.7% as of 2021 (National Automobile Dealers Association 2022), and is, thus, representative of a commonly utilized test vehicle for this study. This class of vehicles are commonly used as goods movement trucks, transit buses, and refuse haulers (Hill 2021). The curbside vehicle weight was reported as 15,892 lb. (=7,208 kg) and was tested at a total vehicle weight of 65,000 lb. (=29484 kg). The test vehicle uses an air brake drum system as opposed to the less common disk brake type of system for heavy-duty vehicles. Each of the vehicle's left and right rear drum brake was equipped with a pair of Meritor Genuine Q Plus brake shoes (Model KSMA20014711QP).

A new pair of brake replacement components weighs about 20 kg with a brake diameter of 42 cm and shoe width of 22 cm. Although the brake lining material is not detailed by the manufacturer, it is classified as MA2001.

5.2.4 Data collection

Brake pressure, brake temperature, vehicle speed and GPS were measured in real-time, and meteorological data was obtained from nearby weather stations. The test vehicle brake pressure from the fluid line of the right rear canister was measured using an Omega PX319-200G5V pressure transducer. This method allowed for the closest measurement of the braking pressure at the drum assembly. The installation was completed by a third-party certified heavy-duty truck brake and repair facility. Given that the test vehicle brake system pressure was set at 135 psi, the pressure transducer selected had a maximum range of 150 psi. The left rear brake pressure was not measured but estimated to be equivalent to the measured right rear brake.

Brake pad (or liner) temperature was measured with a custom-made type K thermocouple with a 1/8 inch (=3 mm) diameter cap encasing. Figure 5-3 shows a schematic of the brake drum assembly showing the leading edge of the brake lining and thermocouple installation location relative to the entire brake shoe. The cap material is a copper tube with approximately one inch (=2.5 cm) length and was inserted through the backing plate into the brake pad material. The backing plate was drilled providing a 1/8 inch (=3 mm) hole through the friction material and milled the last 10 mm to provide a flat square surface at the bottom of the hole. The thermocouple was installed by coating the cap with a layer of conductive paste. The thermocouple was installed 2 mm below the pad surface to reduce the risk of brake damage, as well as considering brake pad wear during testing. This approach was recommended by other brake measurement studies (Agudelo et al. 2019; 2020). Both the left and right wheel-brake assemblies contained this thermocouple to provide a back-up sensor in case one was damaged or failed to record during testing.

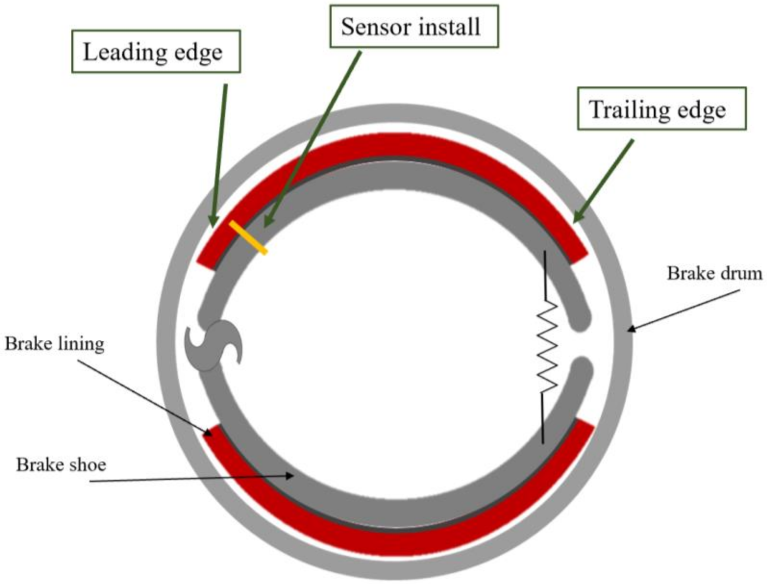

Figure 5-3: Schematic diagram of the Meritor Q Plus cam brake drum system with locations of the leading edge, temperature sensor installation, and trailing edge.

Both the thermocouple and pressure sensor had lead wires secured outside the wheel-brake assembly to allow for connection to a custom-made data logger. The datalogger contained inputs for the K-type thermocouple and pressure sensor, power supply, and a start & stop button. Data was recorded onto a micro-USB chip inside the data logger with a time resolution of 1 Hz. The logger recorded ambient temperature (°C), brake pad temperature (°C), and brake pressure (psi). The data logger was used during both chassis and on-road testing. It was powered using a Honda 220-watt generator and secured in the space between the truck and the cargo during the on-road testing. Prior to all testing, the logger underwent a set of three one-minute-long warm up tests to record an averaged offset start time between the equipment and NIST official U.S. time. In addition, an OBD2 HEM logger was used in conjunction with the brake logger to obtain data from the test vehicle ECM (Engine Control Module). Vehicle GPS (Global Positioning System) data including latitude, longitude, vehicle speed, and altitude were recorded. The HEM logger was used for both chassis and on-road testing. Ambient data was obtained using three local weather stations managed by the California Irrigation Management Information System (CIMIS). The CIMIS data is audited and well managed and is considered of high quality. To match the locations of the chassis and on-road testing sites, station 44 in Riverside, Station 251 in Highland, and station 117 in Victorville were used. Station 44 was used as an ambient temperature and relative humidity reference for both chassis tests as well as the Local Riverside city route. Stations 251 and 117 were used as a reference for the Cruise route as Highland is located near the I-215 freeway and is part of the route while Victorville is the turnaround point of the route.

5.3 Results and Discussions

5.3.1 Chassis and On-road tests

Figure 5-4 shows the braking energy, vehicle speed, and brake temperature during the triplicate CBD test cycle. The driving pattern was maintained between speeds from 0 to 32 km/h. The temperature profile of the right rear brake showed an initial brake pad temperature of about 65 °C. This starting temperature was due to a single CBD warm up cycle performed prior to the triplicate test. Due to the constant short periods of friction between the brake pad and drum during braking events, the temperature gradually increased linearly with a slope of 2.32 °C/min and reached a final temperature of 130°C at the end of the test. The recorded brake fluid pressure signals, as shown in Figure 5-5, were observed to increased and decreased in a cyclic pattern which coincided with the decreases and increases in speed. Therefore, pressure was used as a good indicator of braking events. When the brakes were not engaged, the brake pressure was less than 5.5 kPa and at the start of a braking the pressure exceeded values above 5.5 kPa where pressure peaks occurred between 150 to 200 kPa with a maximum reaching 250 kPa. To observe deceleration trends, the 1 Hz acceleration data was averaged over a three second period (Figure 5-6). The acceleration and deceleration trends for the first CBD contained magnitudes that ranged from -0.79 m/s^2 to -0.57 m/s^2 and were highest in frequency within the range of -.70 m/s^2 to -0.66 m/s^2 as shown in the histogram in Figure 5-7. For this study, the kinetic energy lost was also computed using the vehicle weight, change in speed during each braking event, and multiplied by a unit of -1 to observe results to compare with speed profiles in Figure 5-4. Absolute values of kinetic energy lost showed a bimodal trend within a range of 2.3x10^5 J to 3.1x10^5 J with a larger frequency in the 2.4x10^5 J to 2.5x10^5 J range in Figure 5-8. To determine the relationship between braking temperature and energy lost, the rate of temperature increase was divided by the sum of kinetic energy lost within each individual CBD cycle. Assuming braking load is equally distributed among all wheels, the ratio was divided by the number of drum brake assemblies. Therefore, the brake pad temperature increased by 2.4x10^{-5} °C/J for the first CBD cycle, followed by 2.3x10^{-5} °C/J for the second and third cycles.

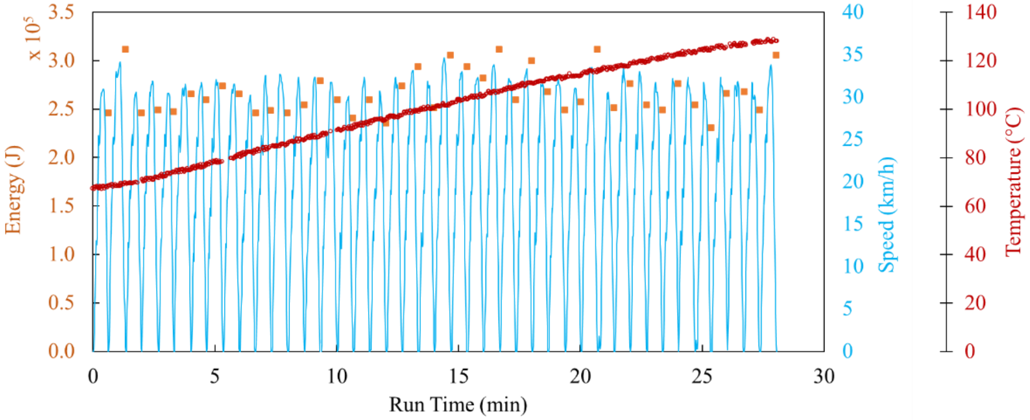

Figure 5-4: Magnitude of kinetic energy lost in Joules of braking events superimposed on the vehicle speed profile in km/h and brake temperature in °C during three consecutive CBD cycles.

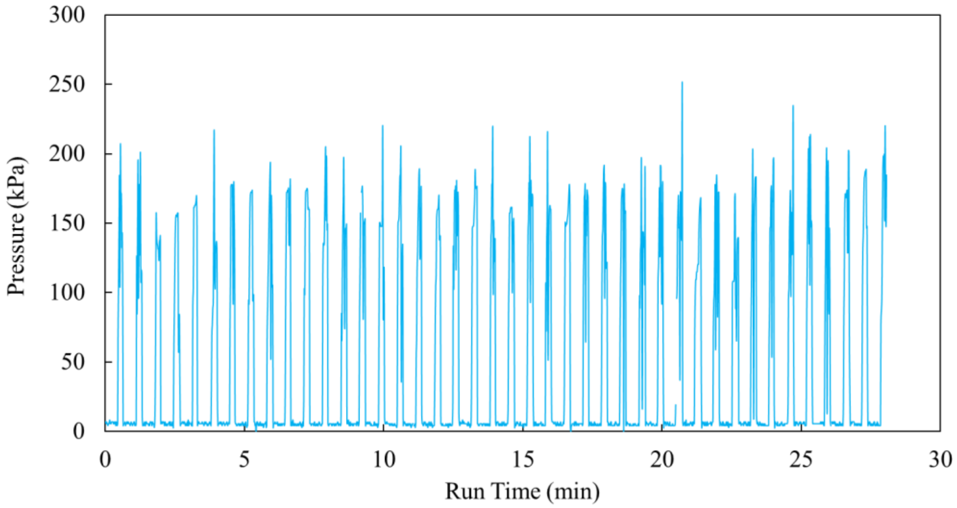

Figure 5-5: Braking pressure recorded from the pressure transducer installed on the right rear brake canister during three consecutive CBD cycles.

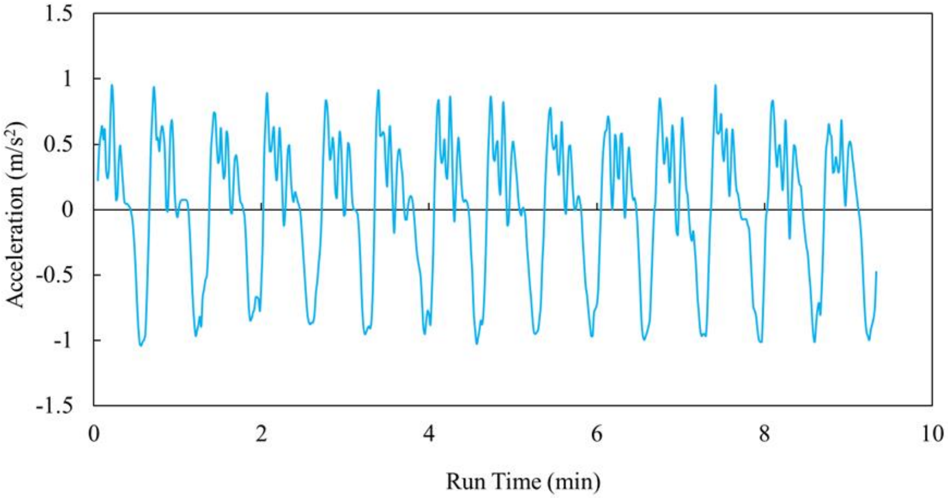

Figure 5-6: Three second moving-averaged acceleration rate over one CBD cycle.

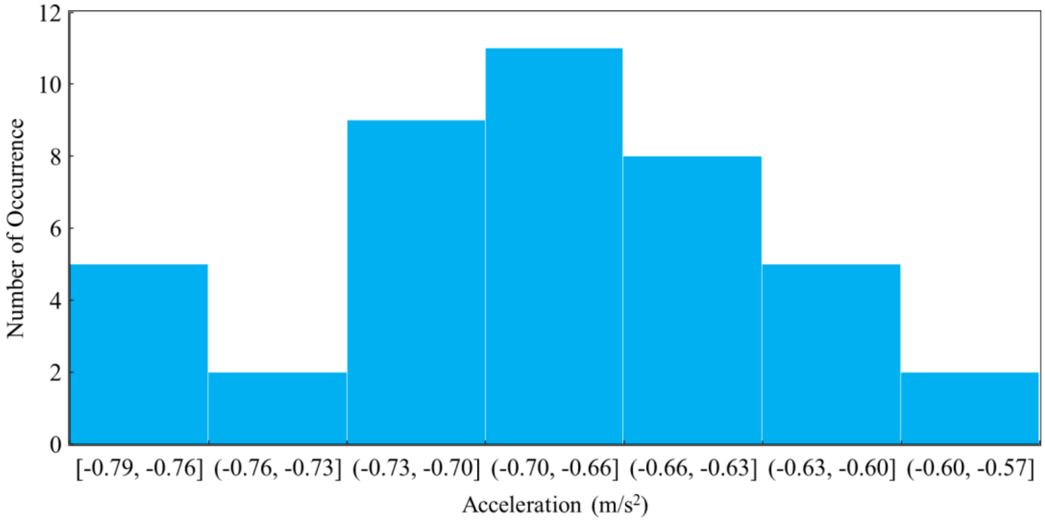

Figure 5-7: Histogram of the three second moving averaged acceleration rate in m/s^2 during the triplicate CBD test.

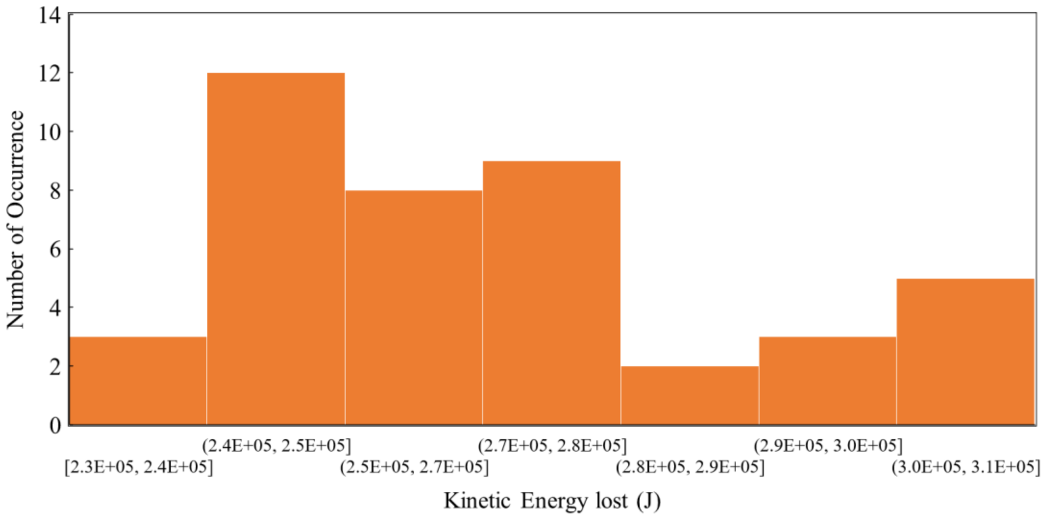

Figure 5-8: Histogram of the kinetic energy lost in Joules of braking events during the triplicate CBD test.

The braking energy, vehicle speed, and brake temperature for the triplicate UDDS test cycle are shown in Figure 5-9. The temperature uses data from the sensor installed on the rear left drum of the vehicle. However, the pressure remained on the right rear drum. A 20-minute rest period occurred between the triplicate CBD test and the triplicate UDDS test, therefore an initial temperature of 135°C was recorded. This indicates that the brakes may not cool down quickly between tests. The brake temperature profile cycled between short increases of about 2-3°C followed by longer intervals of temperature cool downs of about 5°C. This behavior results from the design of the UDDS test cycle where varying braking intensities occur after reaching vehicle speeds of about 30 km/h, 65 km/h, and 95 km/h. During braking events, the pressure increased up to 250 kPa with a single max around 300 kPa (Figure 5-10). The frequency distribution of the three second averaged deceleration during braking shows two main frequency modes in the -0.76 to -0.69 m/s^2 range and a second one in the -0.48 to -0.35 m/s^2 range (Figure 5-11). Two smaller distinct peaks occurred within the -0.55 to 0.48 m/s^2 range and -0.35 to -0.28 m/s^2 range. This occurrence is expected because of the varying speed profiles in a UDDS cycle. As a result, kinetic energy loss ranged from 3.2x10^3 J to 2.0x10^6 J in comparison to the speed profile. The energy range with the largest frequency occurred between 3.2x10^3 to 3.0x10^5 J (Figure 5-12).

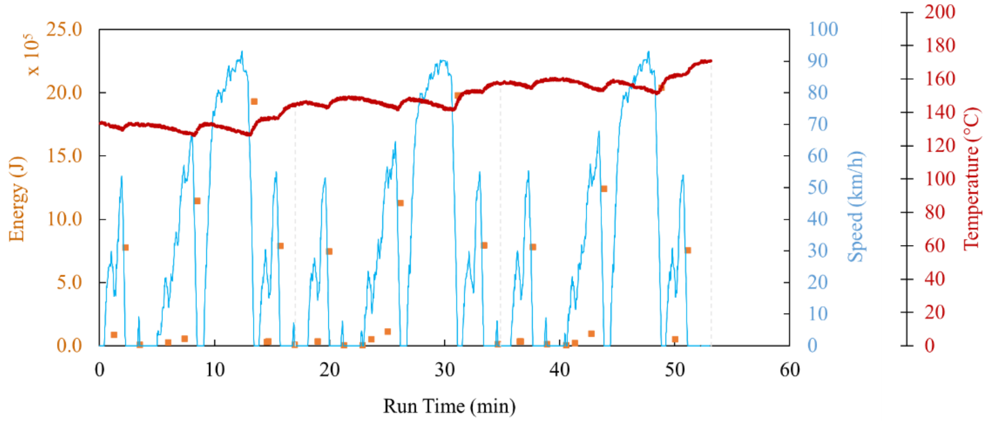

Figure 5-9: Magnitude of kinetic energy lost in Joules of braking events superimposed on the vehicle speed profile in km/h during three consecutive UDDS cycles.

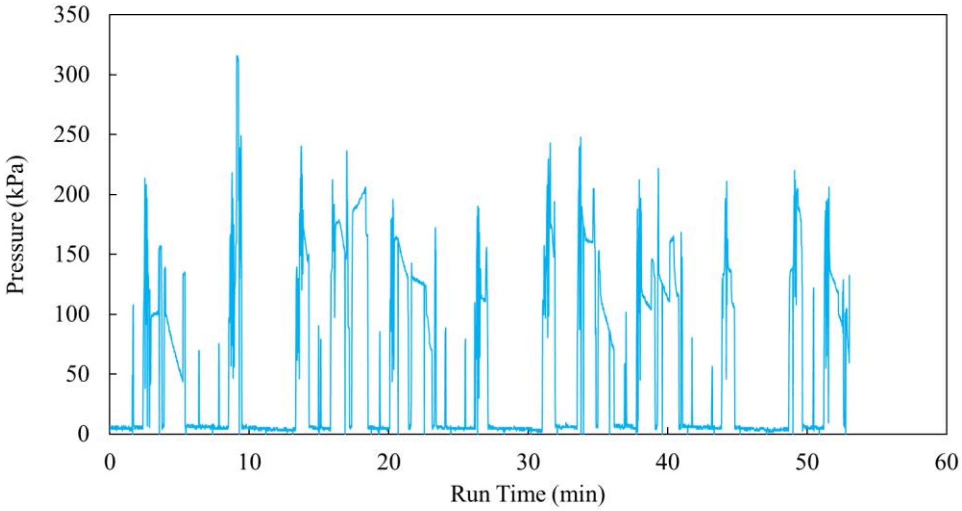

Figure 5-10: Braking pressure in kPa recorded from the pressure transducer installed on the left rear brake canister during three consecutive UDDS cycles.

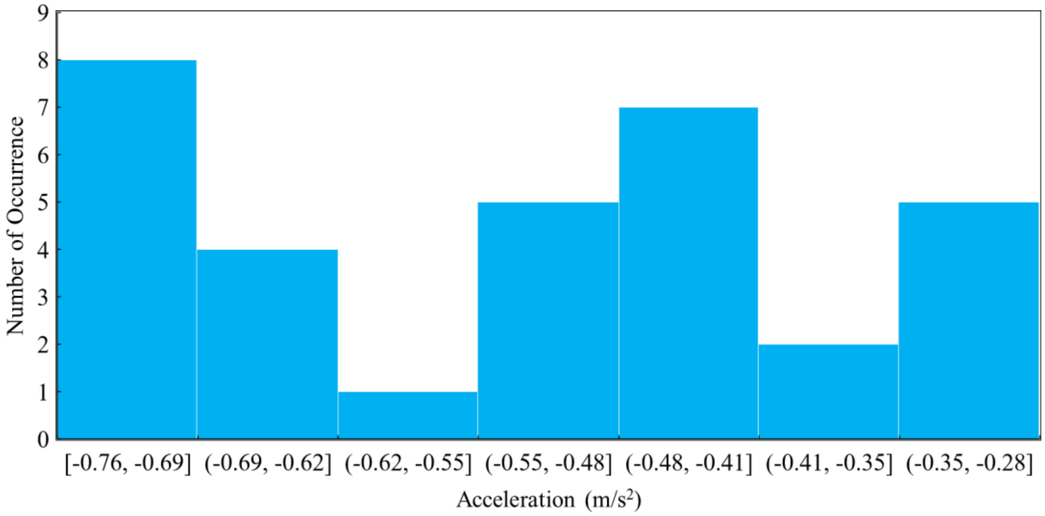

Figure 5-11: Histogram of three second averaged acceleration in m/s^2 during the triplicate UDDS test.

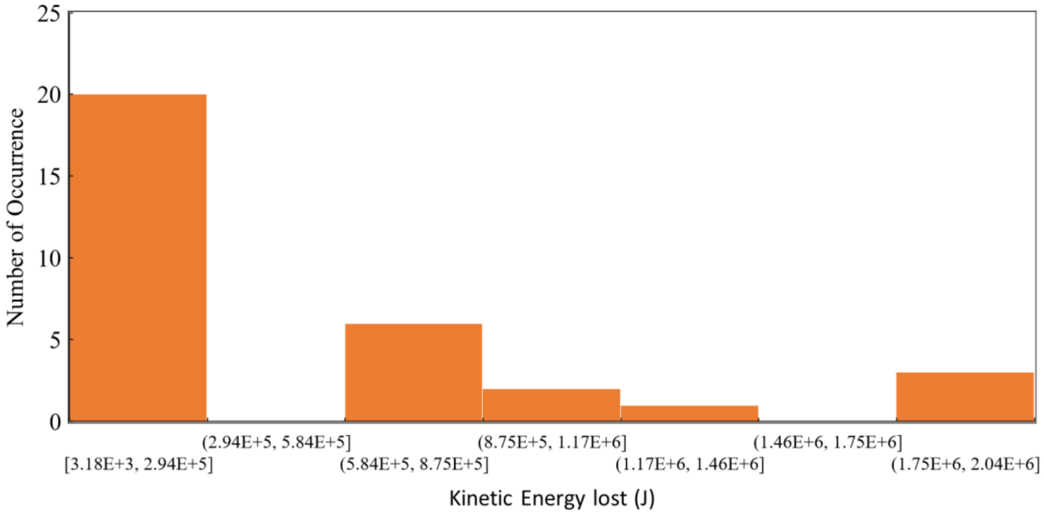

Figure 5-12: Histogram of the kinetic energy lost in Joules of braking events during the triplicate UDDS test.

Temperatures recorded and deceleration rates for both chassis tests are similar to those reported by Chasapidis et al. (2018). Their study also used chassis dynamometer tests on a light duty truck under urban driving conditions with initial speeds of 50 km/hr and 30 km/hr while varying deceleration rates at 0.5m/s^2 and 2.5m/s^2. The brake pad temperatures were measured using a thermocouple installed within the brake pad material at the center of all axes, and the temperature was seen to reach maximum values of 195°C to 220 °C for the 50 km/hr tests and 140 °C to 180 °C for the 30 km/hr tests. Their findings show that high brake pad temperatures above 140°C led to bimodal brake wear particle distributions with one peak in the ultrafine size range, while temperatures below 100°C show mean aerodynamic diameter of 1.5 µm. This relationship indicates the importance of developing a test method to quantify real-world braking temperatures.

During the Local on-road test route, vehicle speed for the GPS and backup ECU wheel-based speed were measured. The GPS data showed connection issues resulting in data loss during the majority of the test (Figure 5-13). Although the wheel-based vehicle speed measurements showed similar dropouts, it was used to provide speed profiles in areas where GPS was missing. There were no warmup tests performed prior to the Riverside City test, and the temperature measured on the left rear brake showed an initial temperature of 10°C which matched ambient conditions for that day.

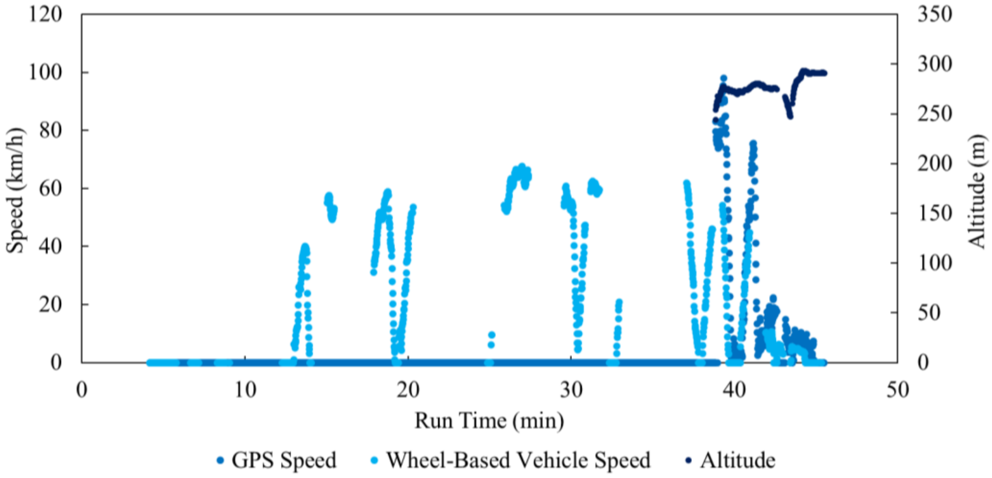

Figure 5-13: Vehicle speed recorded by the GPS and wheel-based vehicle speed and altitude recorded by the ECU during the local Riverside City on-road test.

The temperature profile in Figure 5-14 begins with a stable temperature at 10 °C for a period of 15 minutes during vehicle idle condition followed by a gradual increase to 75°C at 45 minutes. Similar to the triplicate CBD test, the temperature rise increased by 2.03°C / min. The Riverside route focused on low-speed urban driving with frequent braking due to stops at traffic signals. The temperature reached up to 70 °C at the end of the 45 minute local route test. Figure 5-15 shows no spikes in brake fluid pressure during the idle period of the test, followed by braking fluid pressures ranging from 75 to 150 kPa with maximums reaching 220 kPa. Pressure magnitude coincided with both chassis test results. The frequency of deceleration ranged from $-8.60\text{x}10^{-1}$ to $8.09\text{x}10^{-1}$ m/s^2, with a higher frequency between the $-4.43\text{x}10^{-1}$ to $-2.56\text{x}10^{-2}$ m/s^2 range (Figure 5-16). Kinetic energy lost during braking events, shown in Figure 5-14, was obtained following the same procedure used for the chassis tests using the wheel-based vehicle speed in conjunction with the GPS speed. The braking energy lost suggests a higher frequency in the $-7.33\text{x}10^{-5}$ to $1.43\text{x}10^{6}$ Joule bin compared to the chassis testing (Figure 5-17). Although kinetic energy calculations used a multiplying factor of -1, the Local route showed one frequency of energy loss in the negative range at $-2.89\text{x}10^{6}$ J as a result of downhill road conditions with low braking intensities between 55 kPa 60 kPa brake fluid pressure.

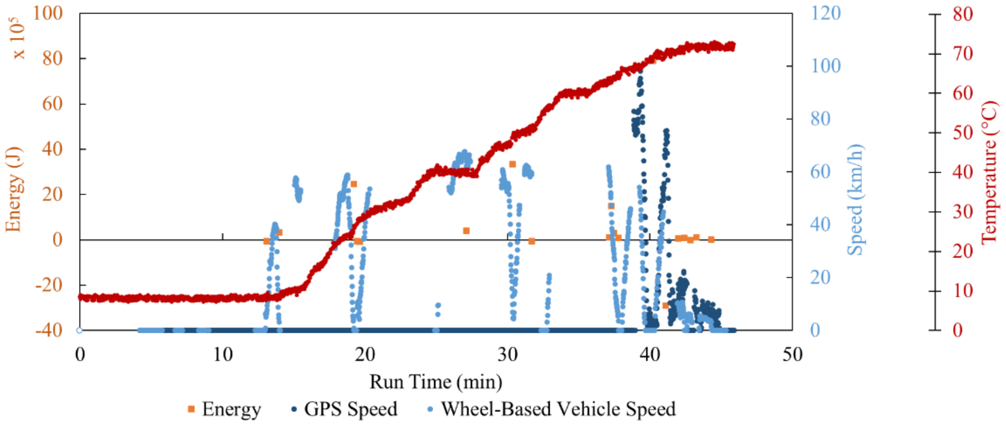

Figure 5-14: Magnitude of kinetic energy lost in Joules of braking events superimposed on the vehicle speed recorded by the GPS and wheel-based vehicle speed recorded by the ECU during the local Riverside City on-road test.

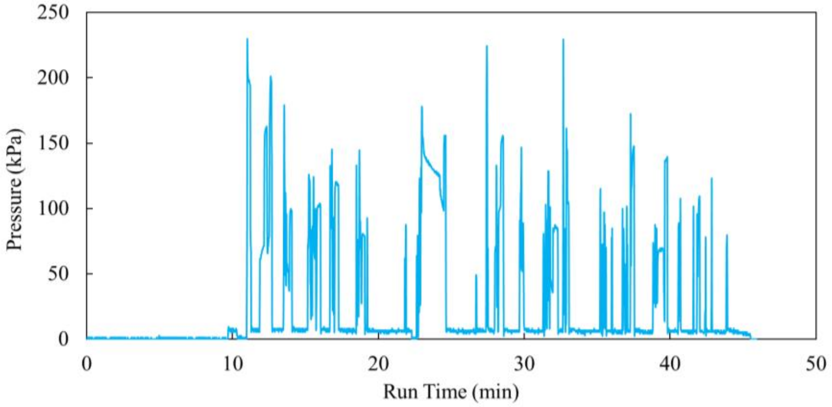

Figure 5-15: Braking pressure in kPa recorded from the pressure transducer installed on the left rear brake canister during the local Riverside City on-road test.

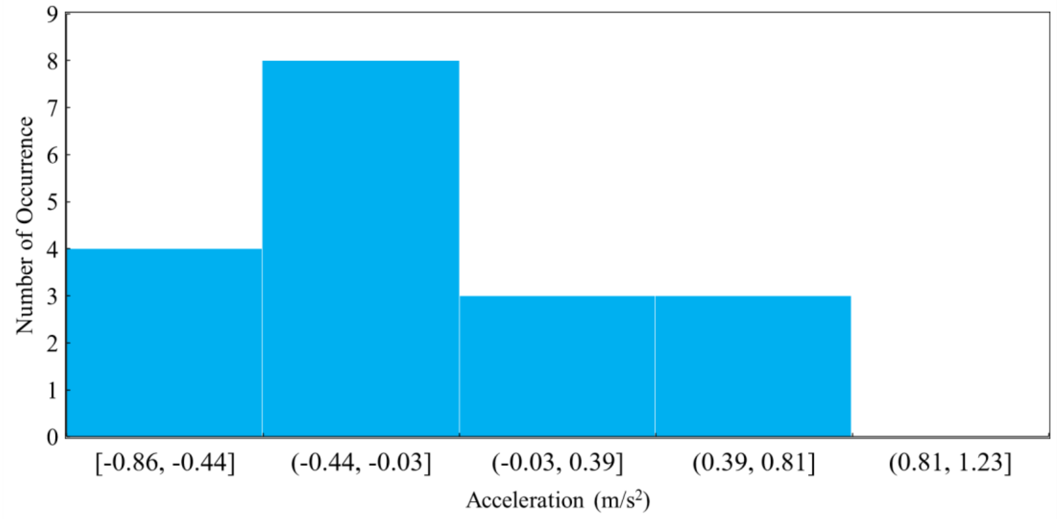

Figure 5-16: Histogram of three second averaged acceleration in m/s^2 during the local Riverside City on-road test.

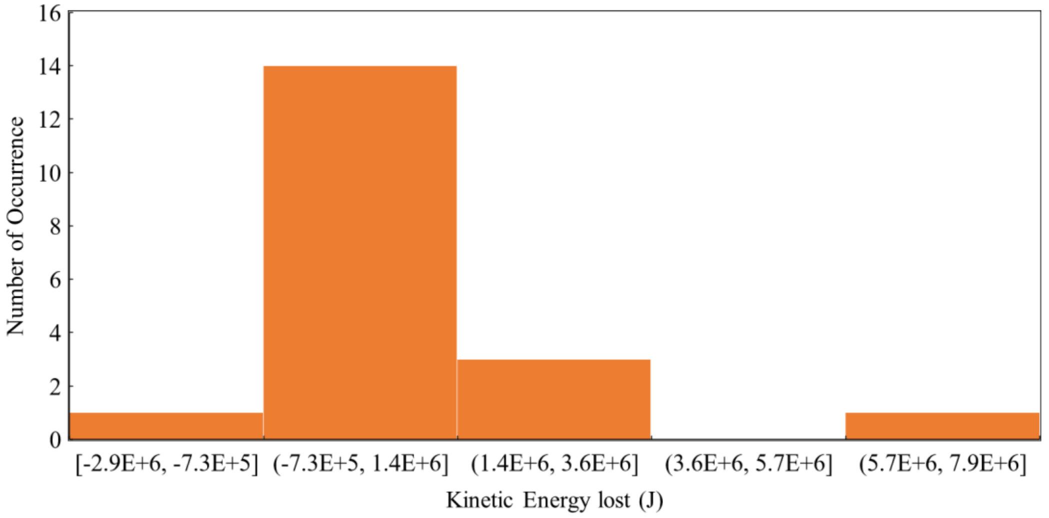

Figure 5-17: Histogram of the kinetic energy lost in Joules of braking events during the local Riverside City on-road test.

Figure 5-18 shows the braking energy, wheel-based vehicle speed, GPS vehicle speed and brake temperature measured during the long-distance Cruise route. Both vehicle speed and altitude were recorded during a run time of 2 hours and 20 minutes with missing data during the remainder of the test. The altitude was recorded to show the difference in elevation between Riverside city and Victorville (Figure 5-19). The brake temperature showed an increasing trend with a few periods of brake cooling. Maximum brake temperature occurred at 165 °C similar to the UDDS test. The brake fluid pressure was the highest during the long-distance Cruise route testing and was typically around 100 to 150 kPa with several spikes near 200 kPa. A maximum pressure occurred at 255 kPa as shown in Figure 5-20. The brake pressure averaged 135 kPa during the downhill grade in the middle of the route suggesting downhill brake fluid pressure is similar to other stop and go brake pressures for a truck loaded at 65,000 total lb.

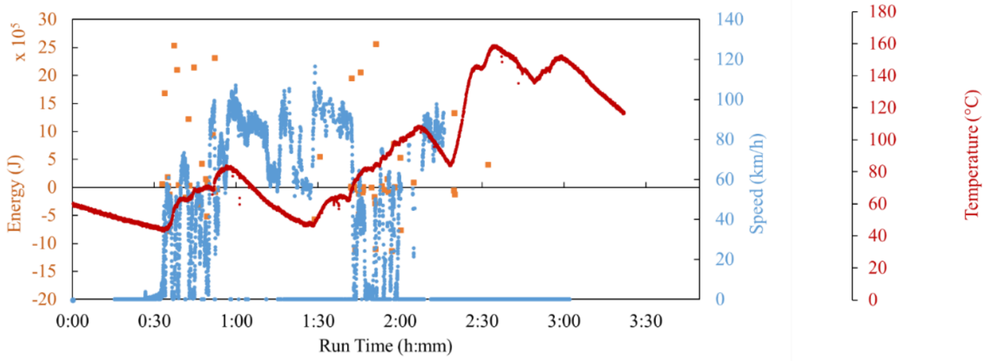

Figure 5-18: Magnitude of kinetic energy lost in Joules of braking events superimposed on the vehicle speed recorded by the during the long-distance Cruise route.

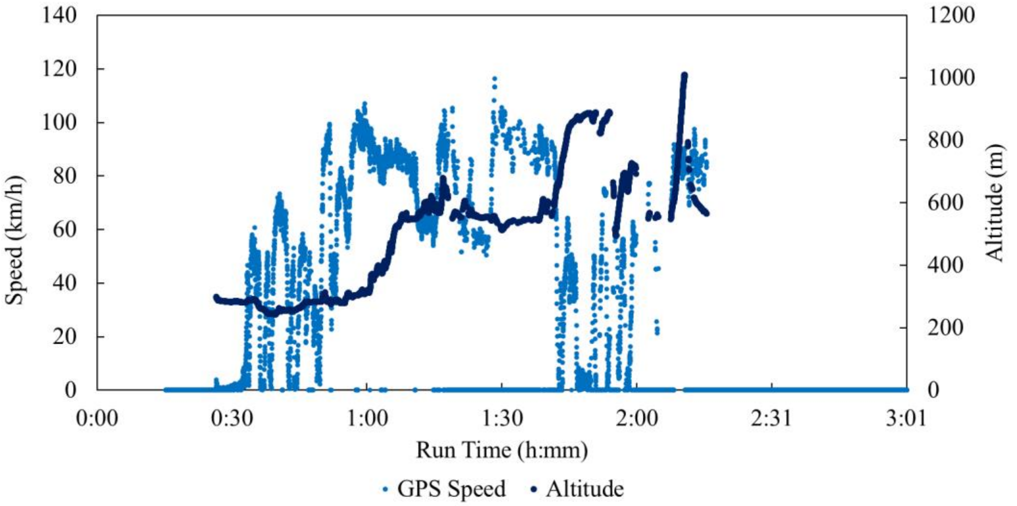

Figure 5-19: Vehicle speed recorded by the GPS and altitude recorded by the ECU during the long-distance Cruise route.

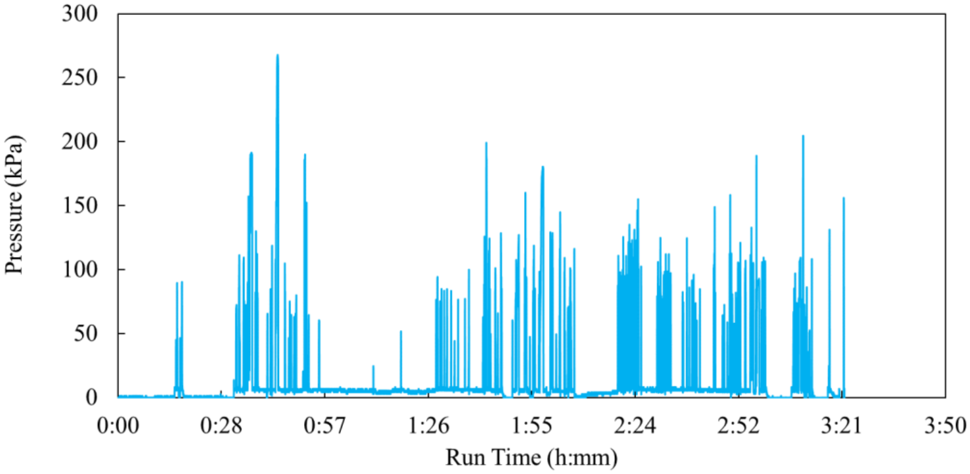

Figure 5-20: Braking pressure in kPa recorded from the pressure transducer installed on the left rear brake canister during the long-distance Cruise route.

The braking activity acceleration profile consisted of a large frequency in the -9.1×10^{-1} to 1.5 m/s^2 range (Figure 5-21). For the energy lost during braking, the positive values correspond to braking events with an initial speed larger than the final speed. The negative values are likely due to changes in road elevation where brakes are applied but the vehicle increases speed while traveling downhill. The histogram of kinetic energy ranged from -2.4 x10^7 J to 6.64x10^6 J (Figure 5-22). The most frequent values of kinetic energy lost are in the -1.92x10^6 to 2.36x10^6 J. The kinetic energy loss for the on-road tests are an order of magnitude larger than that of the dynamometer tests where on-road decelerations are two to three times larger than chassis decelerations which lead to large kinetic energy difference. Both on-road tests used an attached hauling load to simulate a vehicle weight of 29,484 kgs. Koupal et al. (2021) showed brake temperatures can reach 160 °C when fully loaded for a class 8 vehicle at a weight of ~36,287.4 kg compared to the unloaded scenario of ~17,009.7 kg at 71°C. This agrees with the maximum temperature observed during the long-distance Cruise route, but not the local city route. Discrepancies of the temperature results are discussed in the next section.

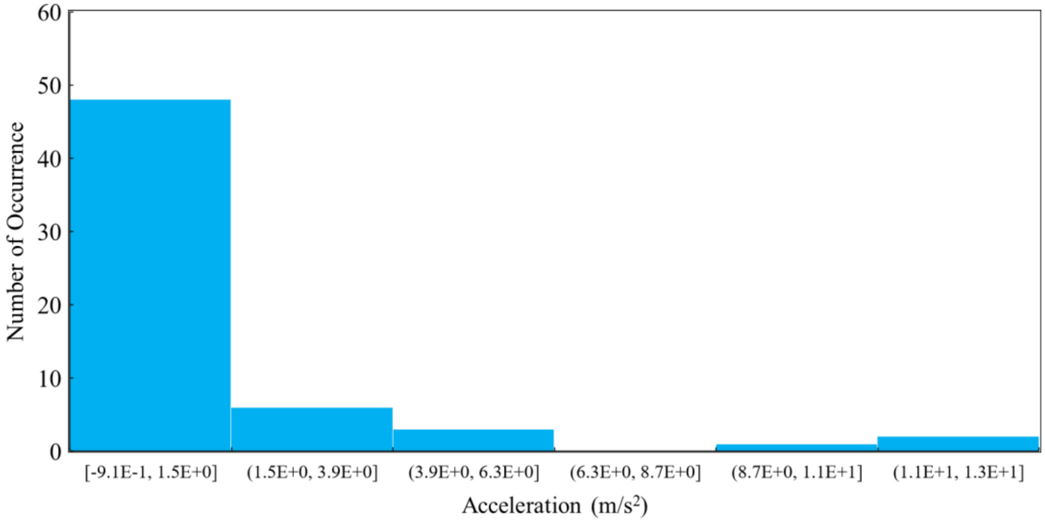

Figure 5-21: Histogram of three second averaged acceleration in m/s^2 during the long-distance Cruise route.

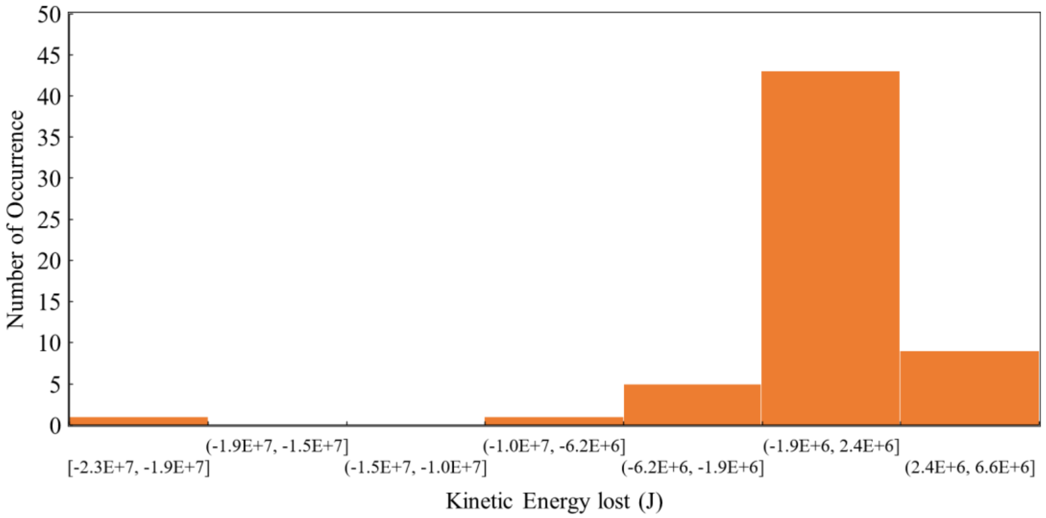

Figure 5-22: Histogram of the kinetic energy lost in Joules of braking events during the long-distance Cruise route.

ERG and Link engineering conducted a CARB and Caltrans co-funded brake dynamometer study to measure brake wear particle emissions in the lab for heavy duty vehicle brake systems. They reported brake wear emissions in terms of PM2.5 mass/stop for the UDDS. Their data ranges from 10 kJ to 1 MJ kinetic energy loss. Kinetic energy loss data has a weak correlation (r^2= 0.35) against brake PM mass data per stop. The brake PM2.5 emissions can be estimated to be about 10 µg/stop at 100kJ and 400µg/stop at 1 MJ kinetic energy loss. They used QCM-MOUDI for real time measurement. The behavior of QCM-MOUDI during emissions testing was not well-known and therefore the values reported by them need to be used with caution.

5.3.2 Bench top testing

A laboratory bench top experiment was set up for the brakes to evaluate temperature measurements recorded during the chassis and on-road tests. The temperature sensor was left intact from the testing conditions and was compared with an exposed tip thermocouple.

A heat source utilizing a 3 inch (=7.6 cm) diameter premixed flame from a camping stove was placed one inch away from the surface of the brake pad. Temperature was recorded at two depths, one being approximately 2 mm from the brake pad surface while the second was approximately 5.2 mm away from the pad surface (Figure 5-23). This allowed an evaluation of the sensor at two depths and to calculate the temperature at the surface of the pads using 1 dimensional Fourier's law.

Figure 5-24 shows lab results for the two different probes and three different depths of 5, 2, and 0 mm from the surface. The exposed tip thermocouple showed a much higher temperature by almost 100 °C compared to the copper capped thermocouple used in the dynamometer and on-road testing. We attribute this to the long copper cap exchanging heat along the linearly decreasing temperature away from the heated surface. The copper capped thermocouple measured a somewhat averaged temperature along the brake pad depth. At the lab test condition where heat flux was relatively constant the difference between the exposed tip and copper probe was about 100 °C to 150 °C. Also, the loss in temperature for the exposed tip thermocouple did not vary as much between 5 and 2 mm which suggests the probe type is more important than probe depth, however, both should be properly controlled.

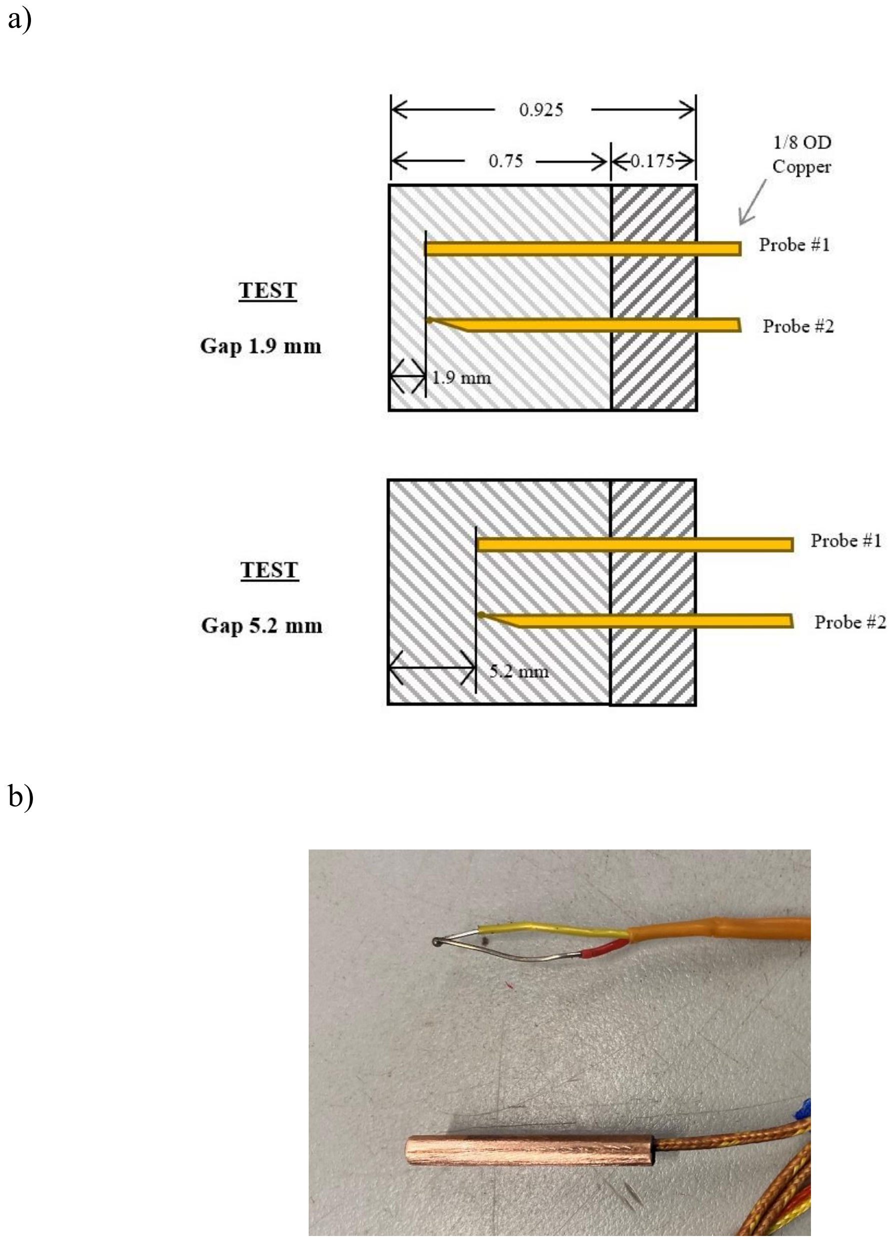

Figure 5-23: a) Cross sectional diagram of the brake shoe backing plate and lining material with installed thermocouples probes with a gap of 1.9 mm and 5.2 mm from the surface. b) Image of the probe tips, one exposed (top) and a second enclosed (bottom), used during bench top tests.

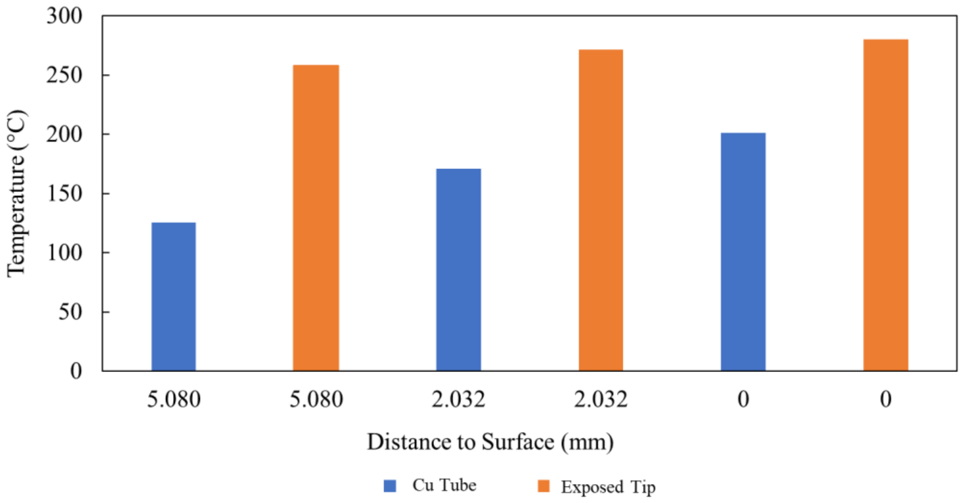

Figure 5-24: Maximum temperature of the copper and exposed probe after 2 minutes of heating exposure.

5.4 Conclusion

Brake activity was measured for two laboratory cycles (CBD and UDDS) and two on-road routes utilizing a heavy-duty vehicle while measuring brake fluid pressure and brake pad temperature. The brake kinetic energy was much higher for the on-road tests compared to the laboratory tests where the on-road activity resulted in ten times higher kinetic energy losses compared to the chassis testing. As such, brake activity from the same heavy-duty vehicle can be more than double due to the route where higher brake temperature are expected with higher hauling weights. Overall brake pressures remained relatively consistent and varied from 135 kPa to 206 kPa during braking events for laboratory and on-road testing. The brake temperatures ranged from 60 °C to 160 °C but it is possible that the true maximum temperatures could be over 260°C if an exposed tip thermocouple probe were utilized. It is recommended to utilize an exposed tip thermocouple to measure brake pad temperature at the targeted depth of two mm. This method can help establish a continuous real-world measurement of brake temperature on other vehicles with different class sizes, vocation, and hauling load. For future work, simultaneous measure of the brake particle emission along with the brake activity can be used to find a relationship between real world braking activity and brake particle emissions.

5.5 References

A. J. Cohen *et al.*, "Estimates and 25-year trends of the global burden of disease attributable to ambient air pollution: an analysis of data from the Global Burden of Diseases Study 2015," *The Lancet*, vol. 389, no. 10082, pp. 1907–1918, May 2017, doi: 10.1016/S0140-6736(17)30505-6.

R. Tong, J. Liu, W. Wang, and Y. Fang, "Health effects of PM2.5 emissions from on-road vehicles during weekdays and weekends in Beijing, China," *Atmos. Environ.*, vol. 223, p. 117258, Feb. 2020, doi: 10.1016/j.atmosenv.2019.117258.

F. Shirmohammadi *et al.*, "The relative importance of tailpipe and non-tailpipe emissions on the oxidative potential of ambient particles in Los Angeles, CA," *Faraday Discuss.*, vol. 189, no. 0, pp. 361–380, Jul. 2016, doi: 10.1039/C5FD00166H.

S. M. S. Wahid, "Automotive brake wear: a review," *Environ. Sci. Pollut. Res.*, vol. 25, no. 1, pp. 174–180, Jan. 2018, doi: 10.1007/s11356-017-0463-7.

T. Grigoratos and G. Martini, "Brake wear particle emissions: a review," *Environ. Sci. Pollut. Res.*, vol. 22, no. 4, pp. 2491–2504, Feb. 2015, doi: 10.1007/s11356-014-3696-8.

N. Bukowiecki *et al.*, "Real-World Emission Factors for Antimony and Other Brake Wear Related Trace Elements: Size-Segregated Values for Light and Heavy Duty Vehicles," *Environ. Sci. Technol.*, vol. 43, no. 21, pp. 8072–8078, Nov. 2009, doi: 10.1021/es9006096.

D. Chan and G. W. Stachowiak, "Review of automotive brake friction materials," *Proc. Inst. Mech. Eng. Part J. Automob. Eng.*, vol. 218, no. 9, pp. 953–966, Sep. 2004, doi: 10.1243/0954407041856773.

B. D. Garg, S. H. Cadle, P. A. Mulawa, P. J. Groblicki, C. Laroo, and G. A. Parr, "Brake Wear Particulate Matter Emissions," *Environ. Sci. Technol.*, vol. 34, no. 21, pp. 4463–4469, Nov. 2000, doi: 10.1021/es001108h.

P. G. Sanders, N. Xu, T. M. Dalka, and M. M. Maricq, “Airborne Brake Wear Debris: Size Distributions, Composition, and a Comparison of Dynamometer and Vehicle Tests,” *Environ. Sci. Technol.*, vol. 37, no. 18, pp. 4060–4069, Sep. 2003, doi: 10.1021/es034145s.

A. Thorpe and R. M. Harrison, “Sources and properties of non-exhaust particulate matter from road traffic: A review,” *Sci. Total Environ.*, vol. 400, no. 1, pp. 270–282, Aug. 2008, doi: 10.1016/j.scitotenv.2008.06.007.

J. K. Gietl, R. Lawrence, A. J. Thorpe, and R. M. Harrison, “Identification of brake wear particles and derivation of a quantitative tracer for brake dust at a major road,” *Atmos. Environ.*, vol. 44, no. 2, pp. 141–146, Jan. 2010, doi: 10.1016/j.atmosenv.2009.10.016.

A. Iijima *et al.*, “Particle size and composition distribution analysis of automotive brake abrasion dusts for the evaluation of antimony sources of airborne particulate matter,” *Atmos. Environ.*, vol. 41, no. 23, pp. 4908–4919, Jul. 2007, doi: 10.1016/j.atmosenv.2007.02.005.

J. Wahlström, L. Olander, and U. Olofsson, “Size, Shape, and Elemental Composition of Airborne Wear Particles from Disc Brake Materials,” *Tribol. Lett.*, vol. 38, no. 1, pp. 15–24, Apr. 2010, doi: 10.1007/s11249-009-9564-x.

C. Agudelo, R. T. Vedula, S. Collier, and A. Stanard, “Brake Particulate Matter Emissions Measurements for Six Light-Duty Vehicles Using Inertia Dynamometer Testing,” *SAE Int. J. Adv. Curr. Pract. Mobil.*, vol. 3, no. 2, Art. no. 2020-01–1637, Oct. 2020, doi: 10.4271/2020-01-1637.

H. Hagino, M. Oyama, and S. Sasaki, “Laboratory testing of airborne brake wear particle emissions using a dynamometer system under urban city driving cycles,” *Atmos. Environ.*, vol. 131, pp. 269–278, Apr. 2016, doi: 10.1016/j.atmosenv.2016.02.014.

J. Koupal, A. DenBleyker, S. Kishan, R. Vedula, and C. Agudelo, “Brake Wear Particulate Matter Emissions Modeling,” Eastern Research Group, LINK Engineering, Final Report CA21-3232, May 2021.

W. Miller, K. C. Johnson, T. Durbin, and P. Dixit, “In-use emissions testing and demonstration of retrofit technology for control of on-road heavy-duty engines,” *Final Rep. South Coast Air Qual. Manag. Dist. Contract*, no. 11612, 2013.

National Automobile Dealers Association, “Class 8 truck manufacturers’ market share in the U.S. as of December 2021 [Graph],” *Statista*, Jan. 2022. https://www.statista.com/statistics/274937/market-share-of-truck-manufacturers-in-the-united-states/ (accessed Jan. 30, 2022).

S. Hill, “Medium- & Heavy-Duty Vehicles: Market Structure, Environmental Impact, and EV Readiness,” *M.J. Bradley & Associates*, Jul. 28, 2021. https://www.mjbradley.com/reports/medium-heavy-duty-vehicles-market-structure-environmental-impact-and-ev-readiness (accessed Feb. 03, 2022).

C. Agudelo, R. T. Vedula, J. Capecelatro, and Q. Wang, “Design of Experiments for Effects and Interactions during Brake Emissions Testing Using High-Fidelity Computational Fluid Dynamics,” SAE International, Warrendale, PA, SAE Technical Paper 2019-01–2139, Sep. 2019. doi: 10.4271/2019-01-2139.

L. Chasapidis, T. Grigoratos, A. Zygogianni, A. Tsakis, and A. G. Konstandopoulos, “Study of Brake Wear Particle Emissions of a Minivan on a Chassis Dynamometer,” *Emiss. Control Sci. Technol.*, vol. 4, no. 4, pp. 271–278, Dec. 2018, doi: 10.1007/s40825-018-0105-7.

6 Chapter 6: Conclusions

Chapter 2 delved into the metal contents and size distributions of brake and tire wear particles dispersed in the near-road environment. The chapter reviews measurement of ambient PM2.5 and PM10 concentrations at near road environments for two major highways in California, I-5 in Anaheim and I-710 in Long Beach. A total of 51 elements were measured from filter samples collected over four-hour intervals for a two-week period in the winter of 2020 before the statewide lockdown by the COVID-19 pandemic. Iron was the most abundant element in ΔPM10 (differences between downwind and upwind sites), contributing to 30% and 24% of total measured elements in ΔPM10 at the I-5 and I-710 locations, respectively. Iron correlated highly with other brake wear markers (e.g., titanium, copper, barium, manganese, zirconium, and zinc) with coefficient of determination (r^2) ranging from 0.67 to 0.90 in both PM2.5 and PM10. Silicon was the second most abundant element, contributing to 21% of total measured elements in ΔPM2.5 and ΔPM10. Silicon showed strong correlations with crustal elements such as calcium (r^2=0.90), aluminum (r^2=0.96), and potassium (r^2=0.72) in ΔPM2.5, and the correlations were even higher in ΔPM10. Barium had a weak correlation with the tire wear marker zinc with r^2 =0.63 for ΔPM2.5 and r^2=0.11 for ΔPM10. Barium showed a positive correlation with crosswind speed and could serve as a good brake wear PM marker. Hourly PM2.5 concentrations of iron and zinc showed cyclic peaks from 0800 to 1000 hours at I-5 during weekdays. Particle mass distributions showed peaks near ~7 μm, while particle number distributions showed peaks near 2.1 μm and 6.5 μm, respectively. This is consistent with brake wear and road dust size ranges previously reported.

Chapter 3 is a continuation of samples collected as discussed in Chapter. Results show that the PM10 concentration is approximately 2-3 times higher than the PM2.5 concentrations at both I-5 and I-710. Minimal differences in the PM concentrations were observed between the upwind and downwind sites and remained below 1-4 $\mu g/m^3$. The low difference is explained to be a result of urban background and wind speed/direction conditions rather than immediate changes in road traffic patterns. The PM concentrations measured showed they were affected more by wind direction and vehicle induced flow, than to the vehicle flow and speeds. From the meteorological data, the nominal downwind sites in this study showed to be true downwind locations outside the early morning hours (0600-1000 LST) even with low wind speeds. The wind direction tends to switch mostly in the middle of the day between 1000-1400 LST. As a result, the afternoon sampling periods of 1000-1400 and 1400-1800 LST represented true upwind and downwind conditions. The gravimetric filter samples were analyzed using XRF analysis to quantify elemental concentrations. Comparison between the element concentrations measured by the Horiba PX-375 and in lab XRF analysis showed strong correlations for Zn (r^2=1), moderate correlation for Fe (r^2 =0.60) and Cu (r^2= 0.68), and weaker correlation for Ti (r^2 = 0.44). This suggests correlations between elements and collected data were consistent with laboratory results.

Chapter 4 covers source apportionment of non-tailpipe emissions to near-road PM2.5 and PM10. The California Air Resources Board EMFAC 2021 model had predicted that the non-tailpipe sources of PM2.5 from on road vehicles will exceed tailpipe emissions by 2020. The EMFAC model also predicts that the non-tailpipe source will continue to be a dominant source. An effective variance-chemical mass balance (EC-CMB) model from source profiles were used to obtain source contribution estimates at the I-5 and I-710 highways in Southern California. Source contributions show the non-tailpipe sources exceed the tailpipe counterparts at the I-5 and are comparable at the I-710. Non-tailpipe contributes 29-30% of PM2.5 mass while tailpipe is at 19-21% at the I-5. A non-tailpipe contribution of 15-17% of PM2.5 mass and 15-19% tailpipe contribution are seen at the I-710 site. In general, the PM10 fraction at both sites accounted for 2-3 times the tailpipe contribution. A higher diesel source contribution and brake (high copper content) was observed at the I-710 indicating an influence of HDVs since the opposite trend was observed at the I-5 (higher gasoline source and low copper brakes). A comparison between the source apportioned upwind and downwind difference ($\Delta PM_{2.5brake}$ and $PM_{10brake}$) showed ratios of 0.37 and 0.14 which are comparable to those reported by prior laboratory results.

Chapter 5 focuses on the development of brake activity measurement. Previous studies have focused on emission measurement from laboratory and track tests. Their findings suggest brake wear PM emission rates are dependent on brake activity. This dissertation used an onboard sensing method to characterize brake emissions by first understanding the real-world brake activity from many different vehicle vocations and driving conditions.

This chapter established a test method and analysis for brake activity measurements of heavy-duty vehicles. In this study, brake fluid pressure and brake pad temperature were measured for a heavy-duty vehicle during chassis and on-road driving tests. The chassis tests consisted of the Central Business District (CBD) cycle representative of a repetitive stop-and-go driving pattern of a bus, and the Urban Dynamometer Driving Schedule (UDDS) cycle representative of urban driving conditions of heavy-duty vehicles. The on-road tests consisted of a local Riverside City route focused on urban roads at low vehicle speeds with frequent braking, while the second route from Riverside City to Victorville focused on highway driving and downhill braking. The brake pad temperature of the triplicate CBD cycle gradually increased linearly with a slope of 2.3°C/min and the temperature per kinetic energy lost during braking increased by 2.3×10^{-5} °C/J for the CBD cycle. The UDDS cycles had the largest kinetic energy loss between 3.2×10^{3} to 3.0×10^{5} J in the histogram. The local Riverside city route brake temperature increased by 2.0°C / min. The kinetic energy loss for the on-road tests were one order of magnitude larger than that of the dynamometer tests due to brake events occurring under higher speeds. A laboratory bench top test of the brake drum and thermocouple revealed that brake temperatures could be higher than what was measured and reach over 260°C. This chapter suggests that utilizing an exposed tip thermocouple should be used at a distance of 2mm below the brake lining surface to establish more accurate results. Future work suggests simulating brake activity along with brake particle emissions.